A UNITED STATES DEPARTMENT OF COMMERCE PUBLICATION

SECTION C

JOURNAL OF RESEARCH

of the NATIONAL BUREAU OF STANDARDS

Volume 74C Nos. 1&2, Jan.-June 1970

Engineering and Instrumentation

U.S. DEPARTMENT OF COMMERCE
National Bureau of Standards

Journal of Research

of the

National Bureau of Standards

C. Engineering and Instrumentation

Jan.–June • 1970

VOLUME • 74C

NUMBERS • 1 and 2

Editor: Martin Greenspan

Associate Editors: G. F. Montgomery, R. V. Smith, A. F. Schmidt

Publication dates: Feb. 15, May 15, Aug. 15, Nov. 15, 1970

J. Res. Nat. Bur. Stand. (U. S.), C
CODEN: JNBCA 74C(1&2) 1–58 (1970)

JOURNAL OF RESEARCH

The National Bureau of Standards Journal of Research reports research and development in the fields of activity shown at right. Also included from time to time are survey articles on topics closely related to the Bureau's scientific and technical program.

The Journal is published in three separate sections as follows:

A. Physics and Chemistry

Contains papers of interest primarily to scientists working in these fields. Issued six times a year. Annual subscription: domestic, $9.50; foreign, $11.75. Single copy, varies.

B. Mathematical Sciences

Presents studies and compilations designed mainly for the mathematician and the theoretical physicist. Issued quarterly. Annual subscription: domestic, $5.00; foreign, $6.25. Single copy, $1.25.

C. Engineering and Instrumentation

Reports research and development results of interest chiefly to the engineer and the applied scientist. Issued quarterly. Annual subscription: domestic, $5.00; foreign, $6.25. Single copy, $1.25.

U.S. DEPARTMENT OF COMMERCE
Maurice H. Stans, Secretary
NATIONAL BUREAU OF STANDARDS
Lewis M. Branscomb, Director

Order all publications from the Superintendent of Documents
U.S. Government Printing Office, Washington, D.C. 20402.
Use of funds for printing this publication approved by the Director of the Bureau of the Budget (June 22, 1968).

JOURNAL OF RESEARCH of the National Bureau of Standards — C. Engineering and Instrumentation
Vol. 74C, Nos. 1 and 2, January–June 1970

Production of Near-Perfect Interferograms of Variable Visibility

J. B. Saunders

Institute for Basic Standards, National Bureau of Standards, Washington, D. C. 20234

(May 20, 1970)

A method is given for producing interferograms of fringes that are straight and equally spaced. The intensity distribution obeys the cosine law. The visibility can be controlled over the entire range from zero to unity. The interferometer is rugged and practically free from vibration effects.

Key Words: Interference fringes, interferograms.

There appears to be considerable need for a method of producing interferograms (sets of interference fringes) of very straight, equally spaced, cosine-distribution fringes whose frequency (width) can be varied over a wide range with minimal change in intensity and with a wide range of controlled visibility. Figure 1 shows a method of accomplishing this. A cube-type [1][1] wavefront shearing prism receives monochromatic light from a point or narrow slit source. Nonlocalized fringes may be observed anywhere in the beam after its emergence from the prism. Fringes localized in the pupil of the lens (shown in fig. 1) may be observed by the eye when it is focused on the lens. The lens serves only as a light collector and need not be of high quality. A discussion of the fringes that appear in the pupil of the lens also applies to those appearing elsewhere.

The fringes may be photographed either by replacing the eye (shown in fig. 1) with a camera or by replacing the lens with a sheet of photographic emulsion.

The relative position of the fringes and their order at any chosen point depend upon the position of the source. A point source produces fringes of unit visibility. Small movements of the point source, parallel to the fringes, cause little or no change either in visibility or order at any chosen point in the field. Consequently, a narrow slit source, parallel to the fringes, also produces unit visibility, with considerable increase in available light.

If the source is moved perpendicular to the fringes, the fringe pattern moves, causing a uniform change in the order over the entire field. Consequently, a rotation or increase in width of the slit causes a decrease in visibility. The visibility is a function of width and orientation of the slit source.

If either a point or narrow slit source is adjusted for unit visibility, the visibility can be varied by the simple rotation of a plate of calcite (cut parallel to one of the cleavage planes), located as shown in figure 1. This provides two mutually noncoherent sources, each of which (when acting alone) produce fringes of unit visibility. A lateral separation of the two sources, produced by a rotation of the calcite plate, causes one set of fringes to become laterally displaced relative to the other. When this displacement equals one-half the fringe width, the visibility of the fringes is zero. When the displacement is zero the visibility is unity. Thus any desired visibility may be obtained.

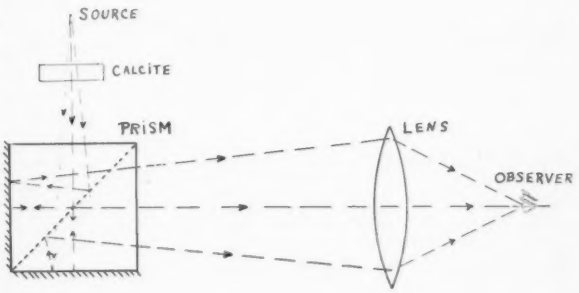

FIGURE 1. *Optics of an interferometer for obtaining straight, equally spaced fringes of variable visibility.*

The thickness of the calcite plate determines the sensitivity of its rotation relative to changes in visibility. The thinner the plate, the less is the change in visibility for a given rotation. However, if the full range of visibility is required then the thickness must be sufficient to provide a change in separation of the two sets of fringes of one-half fringe width.

[1] Figures in brackets indicate the literature references at the end of this paper.

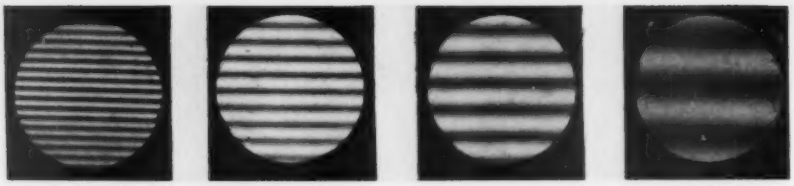

FIGURE 2. *Several interferograms of straight, equally spaced fringes of different widths.*

The width of the fringes, in the pupil of the lens, is

$$W = K(\Phi\rho)$$

where K is a constant, Φ is the angle of shear [2] and ρ the optical path from the source to the lens. Since the optical path, through the calcite plate, is different for the differently polarized images of the source the width of the two sets of fringes are slightly different. This difference, however, may be removed by using two similar calcite plates, cemented together with a 90° relative rotation [3].

The width of the fringes may be varied (fig. 2) by varying either Φ or ρ. Variation of ρ is obtained by varying the distance, from the prism to either the source or the lens. The angle of shear, Φ, can be varied by rotating one component of the prism relative to the other about an axis normal to the beam dividing plane. A more practical method of varying the fringe width is to use several prisms of different shear values and to perform intermediate variations in width by varying ρ.

It should be mentioned that if the angle of divergence of the beam of light, used for the interferogram, is too large, spherical aberration of plane surfaces (both of the calcite plate and the outer faces of the prism) will produce distortion in the fringe pattern.

References

[1] Saunders, J. B., A Simple, inexpensive wave front shearing interferometer, Applied Optics, **6**, No. 9, 1581 (Sept. 1967).

[2] Saunders, J. B., Wave front shearing prism interferometer, J. Res. Nat. Bur. Stand. (U.S.), 74C1&2, (Engr. and Instr.), No. 3, 155–171 (July–Sept. 1968).

[3] Strong, J., Concepts of Classical Optics, p. 133 (W. H. Freeman & Co., San Francisco, 1958).

(Paper 74C1&2–292)

JOURNAL OF RESEARCH of the National Bureau of Standards — C. Engineering and Instrumentation
Vol. 74C, Nos. 1 and 2, January-June 1970

Locked Nuclear Quadrupole Resonance Spectrometer for Pressure Measurements

Ronald C. Frisch and David L. VanderHart

Institute for Materials Research, National Bureau of Standards, Washington, D. C. 20234

(May 18, 1970)

The Nuclear Quadrupole Resonance frequency of a nucleus in a solid is dependent on its local environment and can be quite sensitive to changes in temperature and pressure. A spectrometer capable of locking accurately to the center of a resonance signal is described. The feasibility of using the quadrupole resonance frequency as a transfer gage for precise pressure measurements is discussed using ^{35}Cl resonance in a $KClO_3$ polycrystalline sample. The performance of the instrument implies a limiting accuracy for pressure measurements of 0.7 bar; preliminary results are presented showing frequency versus pressure curves near room temperature. Uncertainties of these measurements are primarily due to inadequate temperature control and the uncertainty of the pressure measurement.

Key words: $KClO_3$ nuclear quadrupole resonance; pressure transducer; spectrometer.

1. Introduction

Many workers in the field of nuclear quadrupole resonance (NQR) have for some time been interested in the temperature and pressure dependence of the NQR frequency. The first theoretical treatment was given by Bayer [1][1] who considered temperature effects in terms of molecular vibrations. Kushida, Benedek, and Bloembergen [2] expanded the theory to take into effect thermal expansion and compressibility. Their results suggest that the NQR frequency might be useful as a sensing device for temperature, and in principle it could also be used to measure pressure. A material suitable for such experiments should be characterized by a strong resonance signal, a relatively narrow line width, and a lack of hysteresis. One such material, which has been considered for an NQR thermometer [2–6], is $KClO_3$. In the early experiments, NQR spectrometers were not locked to the center of the resonance line and the experimental accuracy was of the order of 0.002 K. Volpicelli et al. [7] have described a system for locking the spectrometer to the center of the resonance line. Most recently Utton [8] using a spectrometer locked to the center of the resonance line has been able to measure the temperature in the range 50 to 297 K to an accuracy of ± 0.001 K.

The effects of pressure on the ^{35}Cl NQR frequency in $KClO_3$ [2,2a] are not as great as the temperature variations, i.e., $\left(\frac{\partial f}{\partial T}\right)_P \simeq 5$ KHz/°C at room temperature while $\left(\frac{\partial f}{\partial P}\right)_T \simeq 30$ Hz/bar.[2] Nevertheless, we decided to examine the feasibility of using the pressure dependence of the quadrupole resonance frequency as a method to measure pressure with high precision. If it could be shown that the resonance frequency is a stable, single-valued function of both temperature and pressure, and that its dependence on contamination and crystallinity and other sources of error is below a certain value, then the quadrupole gauge would have one great advantage over other types of transfer gages: once the pressure-temperature dependence of the quadrupole frequency for a particular material had been established, any number of transfer gages could be reproduced and used within established limits of uncertainty without further need for calibration. In contrast all of the transfer gages presently available require initial calibration and frequent recalibration depending on their use.

It is clear from the nature of the application for which this spectrometer was designed, that it must be very stable; in addition, the sensitivity characteristics must be good because of the small sample size dictated by the geometry of the pressure vessel. This paper describes an improved version of the NQR tracking spectrometer used by Utton [8] for temperature studies.

With this system we have been able to track the ^{35}Cl NQR signal in $KClO_3$ and measure the center frequency of the ^{35}Cl resonance to 1 percent of the line width [3] for pressures up to 2 kbar. In constructing a calibration curve

[1] Figures in brackets indicate the literature references at the end of this paper.

[2] 1 bar=10^5 N/m^2.

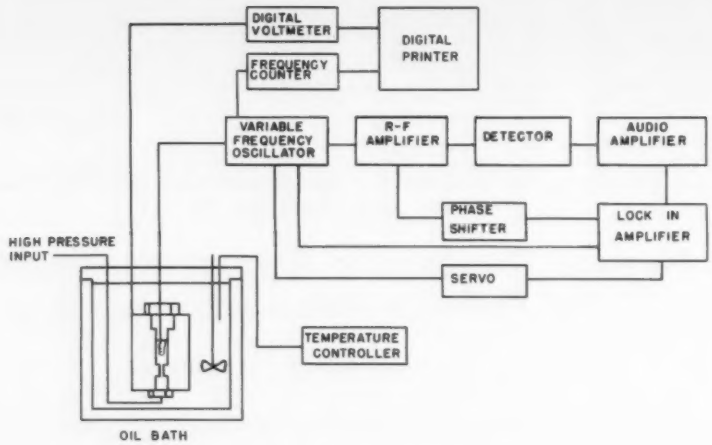

FIGURE 1. *Block diagram of NQR Spectrometer.*

the best pressure uncertainty in the range 0–2 kbar, is at present 0.15 bars at 2 kbars and the percent error is about the same over the range [9]. The fluctuation in the temperature is reflected in the uncertainty of the frequency measurement at each pressure point and would correspond, based on the known temperature coefficient of $KClO_3$, to about 0.25 bars when the sample temperature is held constant to ± 0.001 °C. The uncertainty in the frequency counter is ± 1.0 Hz. or about 0.03 bars. Hence the limiting uncertainty for determining the pressure from a frequency measurement, using such a calibration curve, would be about 0.7 bars.

2. Instrumentation

2.1. Oscillator

A block diagram of the quadrupole spectrometer which was used for the high pressure NQR studies is shown in figure 1. The oscillator detector circuit is given in figure 2. The oscillator detector circuit is a modified version of the circuit described by Pound and Knight [10] and is essentially that used by Utton [8]. The oscillator is of the marginal type and oscillation is maintained by a nonlinear negative resistance provided by the tube feedback circuit [11]. The variable capacitors C_1, C_2 are used for coarse and fine tuning of the oscillator, and the voltage variable capacity diodes (VCD) are used for frequency tracking and frequency modulation. VCD1 can also be used for tuning and will be discussed later. For various applications different values of L can be used to obtain any desired operating frequency. The r-f level at the sample coil can be varied by adjusting the gain control, Rg, or by adjusting the feedback. At 28 MHz, for example, the r-f level is adjustable over the range 0.02–2.20 V.

2.2 R-F Amplifier

The oscillator is followed by a three-stage stagger tuned r-f amplifier. By tuning each stage of an amplifier at slightly different frequencies it is possible to achieve a gain bandwidth product greater than that of synchronously tuned cascade stages. The selectivity curve can also be tailored to fit a prescribed response such as a flat band pass with very good gain [12]. The choice of a flat band pass r-f amplifier is suggested by the operation of the oscillator detector circuit [10]. In the oscillator the level of oscillation is sensitive to the shunt impedance across the tank circuit. As the frequency is varied the corresponding change in the shunt impedance results in a change in the r-f level. This undesirable change in level is compensated for by feeding back part of the r-f rectified voltage in such a way as to control the value of the negative resistance, thereby holding the level of oscillation constant at a level far below natural limiting. In the case where the frequency of oscillation is expected to vary over a large range, as in a tracking spectrometer, it is desirable to have the voltage gain of the r-f amplifier constant over the frequency range of operation. As a result the d-c feedback voltage, which controls the r-f level, is returned to the oscillator essentially independent of frequency within the band pass. The time constant for this feedback loop, of course, is long compared to the modulation frequency, which contains the signal information.

The r-f amplifier used in this spectrometer was designed, using the prescription of Valley and Wallman [12], for a center frequency of 28 MHz and 6 MHz bandpass.

Knowing the bandwidth of each stage and the central frequency one can easily calculate the circuit component values. In figure 3 the a-c equivalent circuit of a typical stage is shown. Given the stage bandwidth, B_i, the loading resistor R_i can be calculated from the relation $B_i = (2\pi R_i C_i)^{-1}$. The capacity C_i is the sum of the output capacity of T_i plus the input capacity of T_{i+1} plus wiring capacity; and the tuning coil, L_i, is wound to resonate with C_i at the appropriate center frequency. An oscilloscope trace of the band pass for this amplifier is shown in figure 4.

In a cascaded linear amplifier without feedback the

[3] Distance between first derivative extrema.

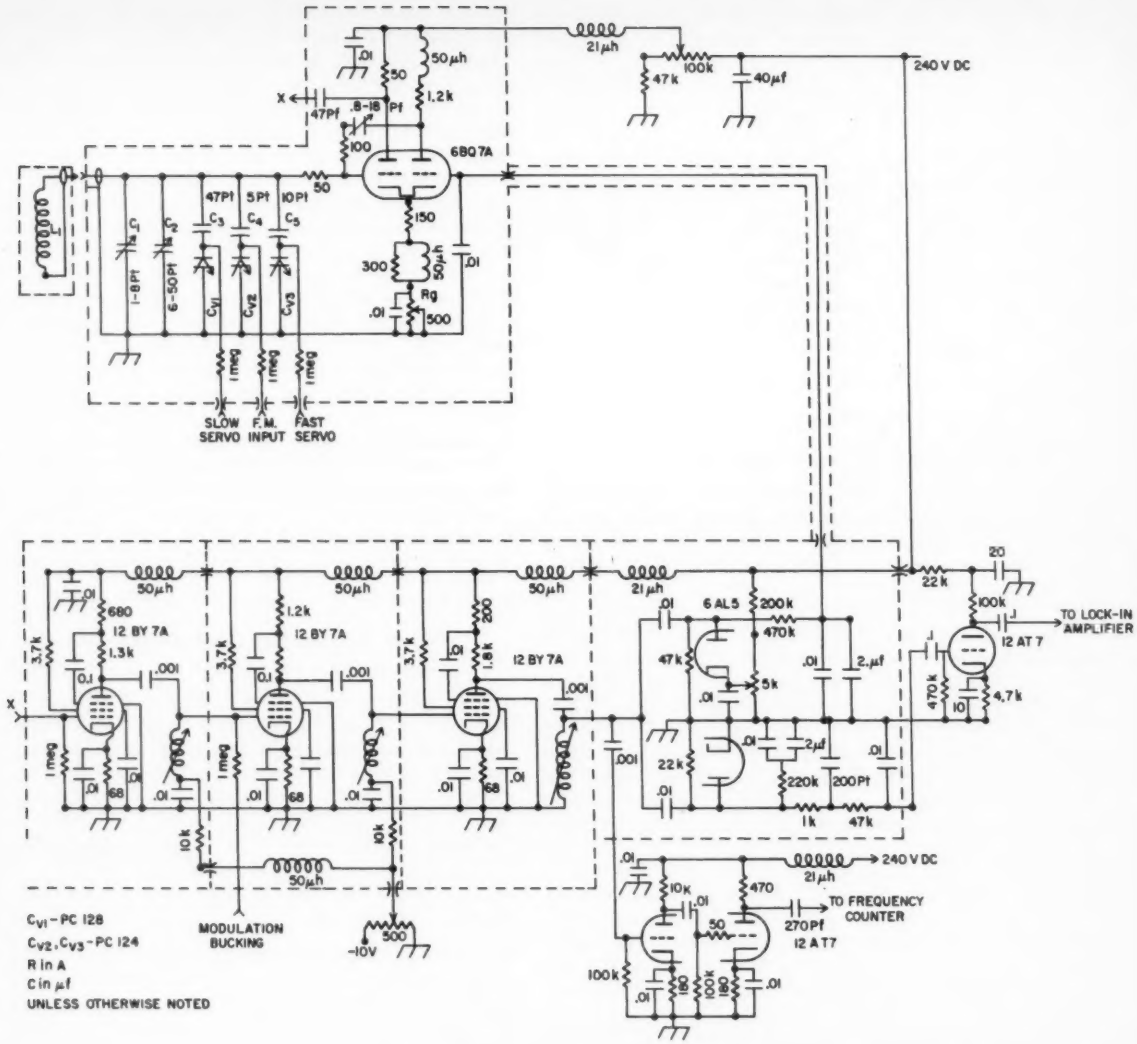

FIGURE 2. *Oscillator detector circuit.*

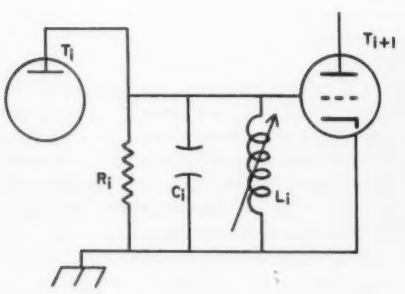

FIGURE 3. *A-C equivalent circuit of a typical stage in rf amplifier.*

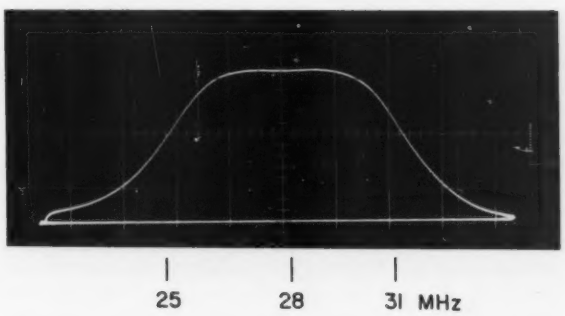

FIGURE 4. *Oscilliscope trace of the band pass of the rf amplifier.*

overall gain at any frequency, f, is the product of the individual stage gains at that frequency. The stage gain is given by

$$G_i(f) = g_{mi} Z_i(f)$$

where $Z_i(f)$ is the impedance function for a single stage. Because of this multiplicative property, if one of the stages has its g_{mi} reduced but its selectivity characteristic, which is determined by $Z_i(f)$, left unchanged, the overall gain is reduced in proportion, whereas the overall selectivity curve is completely unaffected. Consequently, to the extent to which tube capacities and loading do not vary with g_m, it is possible to gain control a stagger-tuned amplifier in any stage or combination of stages [12]. In our case this is accomplished by adjusting the grid voltage on the first two stages.

Following the r-f amplifier the signal is branched; one branch going to a buffer amplifier followed by an electronic frequency counter [13]; the other branch going to the diode detector. The detected signal is then fed into a lock-in amplifier whose output appears as the first derivative of an absorption curve. This is then used to provide the error signal for a servo mechanism which locks the oscillator frequency to the center of the resonance line.

The servo control system is similar to that described by Volpicelli et al. [7] and utilizes two control loops. The fast loop, which responds directly to the error signal and provides a quick response to short-term fluctuations, has a range up to 2 KHz. The second loop has a much slower response and utilizes a commercially available servo amplifier [14] and motor. Tachometer feedback is used and the motor is coupled to a 10-turn potentiometer via a gear box and antibacklash gears giving a total reduction ratio of 1000:1. By coupling the potentiometer shaft to the gear train with a dual magnetic clutch it is also possible to manually adjust the voltage on VCD1 and hence the oscillator frequency, or with the aid of a second motor and gear drive, sweep the frequency. The ability to manually adjust the oscillator frequency greatly facilitates the initial locking of the servo system to the center of the resonance line.

Frequency modulation is provided by varying the voltage on VCD2 at the modulation frequency. As a result of the change in capacity in the tuned circuit the quality factor is also modulated which in turn leads to a modulation of the oscillation level. The result of this incidental amplitude modulation causes a signal to appear at the lock-in detector. The resulting shift in the base line of the NQR signal must be eliminated in order that the lock is at the true center of the resonance line. One method of eliminating this undesirable signal is to introduce a signal of equal amplitude and opposite phase at some convenient point before the input of the lock-in amplifier.

The adjustment of this bucking signal is perhaps the most important one of all and should be checked carefully both above and below the resonance frequency before recording data. Since the oscillator frequency is changing as the NQR signal is tracked, the relative capacity of the tank circuit is also changing which means the bucking signal must be adjusted at each datum point to assure that the measurement is being made at the line center. When the r-f level is relatively high the change in level resulting from a change in frequency is quite small, since the feedback is small, and in this case it is possible to adjust the bucking voltage and phase to produce a relatively stable base line. At low r-f levels, where the feedback is large, the oscillator is most sensitive to the shunt impedance and changes in the relative capacity tend to cause base line drift. Hence the operating point must be such that the r-f level is large enough to ensure a stable base line over a frequency range comparable to the line width and yet small enough to avoid saturation of the nuclear resonance.

In the case of $KClO_3$ we were able to select an operating point which gave the maximum signal-to-noise ratio and, with proper adjustment of the bucking voltage, a stable base line over the line width. In order to carry out the adjustment on the bucking signal it was necessary to unlock the spectrometer and manually shift the frequency, by adjusting the voltage on VCD1, to points on both sides of the resonance. Proper adjustment of the bucking voltage, as evidenced by the output of the lock-in detector, showed no noticeable change in the error voltage at points slightly above and slightly below resonance. The servo is then relocked to the center of the resonance and data recorded.

3. System Performance

The NQR spectrometer described in this paper was designed around the ^{35}Cl resonance in $KClO_3$. As previously mentioned the operating frequency is 28 MHz. The servo system used here to track the NQR signal has a range of about 2.0 MHz. The magnitude of the tracking range is related to the change in capacity of the varicap VCD2, the coupling capacitor C_3, the amplifier bandwidth, and the frequency of operation. If ΔC is the effective change in capacity of the tank circuit, f_0 is the operating frequency, and C_0 is the total tank circuit capacity associated with f_0, then the frequency range is given by $\frac{\Delta f}{f} = \frac{1}{2}\frac{\Delta C}{C_0}$ where the magnitude of ΔC is given by $\Delta C = \frac{\Delta C_v}{(1+C_v/C_3)^2}$. Since C_v and ΔC_v are fixed properties of the varicap and since ΔC_v depends only on the range of bias voltage, Δf will be larger at the higher frequencies. In the case where $C_v/C_3 << 1$ and $C' < C_v$, where C' is the parallel tank circuit capacity excluding C_v and C_3, nearly all of the current passing through L will pass through C_v. This, coupled with the fact that the r-f voltage across both L and C_v is nearly equal, causes the varicap to be the principle frequency controlling element. In addition, the major circuit losses occur in L and C_v and the varicap Q becomes very important in determining the overall circuit Q. This becomes important at the higher frequencies. At the lower frequencies C' is larger than C_v and the varicap Q becomes less important.

Some care should be given to the selection of C_3. If C_3 is large compared to C_v and the resonance line is narrow, small error signals applied to C_v may result in frequency corrections larger than the line width thus causing the

system to lose lock. On the other hand, if C_3 is small compared to C_v the sensitivity of the servo is reduced.

After the spectrometer has been adjusted for maximum signal-to-noise and the bucking voltage properly set, the servo is locked to the center of the resonance line. In $KClO_3$ the signal-to-noise is about 60:1 at room temperature and the line width [9] is about 500 Hz. The phase on the lock-in detector is then adjusted for proper servo control. Depending on the signal to noise it may be necessary to readjust the gain and time constant to stabilize the servo loop gain.

In principle the servo amplifier is capable of tracking over its entire frequency range. In our experiment, however, a large sudden pressure change, corresponding to frequency increments of the order of 30 KHz, would cause the servo to become unlocked from the center of the resonance line, where as a gradual pressure change usually did not affect the lock. On the other hand, if the sample was near thermal equilibrium, the spectrometer, once locked to the resonance, would remain in the locked mode for several hours. The reason for the loss of lock is probably due to inhomogenous broadening of the resonance line associated with the temperature gradients at the sample resulting from the sudden change in pressure $\left(\left(\frac{\partial f}{\partial T}\right)_P = 5 \text{ KHz/°C}\right)$. In those cases where the servo amplifier became unlocked from the resonance signal it could easily be relocked manually to the center of the resonance line after a few minutes.

4. Applications

The NQR spectrometer described thus far could be adapted to any system in which perturbations on the system result in a shift of the NQR frequency. In the case where pressure is used as the perturbation many special problems must also be considered, namely, (1) a low loss feed-through, capable of withstanding high pressure is required in order to get the r-f signal inside the pressure vessel, (2) due to the small working volume, sample size must be kept to a minimum, and (3) depending on temperature sensitivity of the sample, temperature control must be strictly maintained. The latter is perhaps the most difficult problem to deal with.

We have solved some of these problems with reasonable success. The pressure vessel is a commercially available unit [15] and the r-f leads are brought out through a high pressure electrical feedthrough similar to that described by Heydemann [16]. This arrangement has worked satisfactorily for pressures up to 2 kbar. The sample chamber in this pressure vessel is about 25 mm in diameter by 75-mm long and our sample is a cylinder 5 mm in diameter and 10-mm long. By keeping the coil winding diameter small compared to the diameter of the sample chamber the decrease in inductance due to shielding is kept to a minimum.

The temperature dependence of the NQR frequency of ^{35}Cl in $KClO_3$ is considerably larger than the pressure dependence. For this reason we immersed the pressure vessel in a temperature-regulated oil bath. The temperature control was of the order of ± 0.015 °C, measured in the bath, over a 24-hr period corresponding to about 75 Hz or ± 2.5 bars at room temperature.

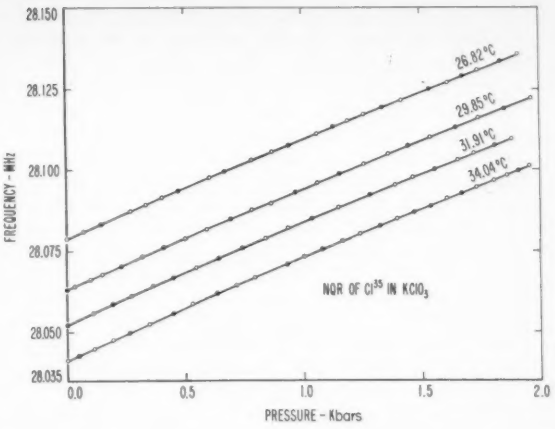

FIGURE 5. *Plot of frequency-pressure-temperature data for* ^{35}Cl *in* $KClO_3$.

The temperature of each curve was determined by comparing the observed NQR frequency at zero pressure with the Spline fitting given by Utton [8]. Open circles indicate increasing values; solid circles, decreasing values.

The stability of the oscillator was determined using a Systron and Donner 1037 frequency counter which was calibrated against an NBS standard frequency. After a 1-hr warm-up period the short term stability of this oscillator, when unlocked, is within ± 3 Hz; the long-term stability is of the order of ± 100 Hz. The stability of the spectrometer when locked to a resonance depends on the stability of the oscillator and on the sample temperature control. The short term stability in the locked mode, with the pressure vessel and sample immersed in the oil bath, is within ± 5 Hz where 5 Hz is the standard deviation of twenty 1-s frequency counts. The long term stability in the locked mode is of the order of ± 45 Hz, although this includes slight temperature drifts.

Samples were prepared by slow recrystallization to improve the sample purity as described by Utton [17]. A plot of the ^{35}Cl NQR frequency as a function of pressure is shown in figure 5. The data shown here are the results of preliminary experiments for the purpose of determining the feasibility of using NQR as a pressure measuring device. The choice of $KClO_3$ as a possible material for pressures less than 6 kbar stems from the good signal-to-noise ratio and narrow line width of the ^{35}Cl resonance, as well as a lack of frequency hysteresis with temperature [8]. $KClO_3$ would not be an acceptable material for a larger pressure range due to a phase transition at 6 kbar [18] at room temperature. The values used for pressure were recorded from a 0–40,000 psi bourdon tube gage [19] and are believed to be accurate to ± 40 psi. The accuracy to which the NQR frequency can be recorded is ± 5 Hz. However, due to the large temperature coefficient in $KClO_3$, and the regulation of the oil bath, ($\pm .015$ °C), the estimated uncertainty due to temperature instability is ± 75 Hz. Hence the total estimated uncertainty in the frequency for a given pressure and temperature is 160 Hz or 5.3 bars. The value of tempera-

ture assigned to each curve was determined by comparing the NQR frequency at zero pressure to the temperature data given by Utton [8]. As previously mentioned this type of temperature measurement is accurate to ±0.001 °C. Since we were interested in small temperature changes, a thermopile consisting of four junctions was used. Fluctuations in temperature were then monitored based on the changes in thermopile EMF. At any temperature the data points, plotted in figure 5, are from both increasing and decreasing pressures. The increasing pressure points are denoted by open circles and the decreasing points by solid circles. For each data point the value of the NQR frequency, pressure, and thermopile EMF, was recorded. The data points shown on the isotherms of figure 4 are normalized to the given temperature which means that although the real data points included small temperature variations, corrections of 4.90 KHz/°C were applied for adjustment; deviations between the line drawn and these values did not exceed 50 Hz. Along the lines of constant pressure the temperature coefficient calculated from the data was found to be 4.93 KHz/°C below 6000 psi and 4.86 KHz/°C at the 2 kbar limit. Qualitatively, this difference agrees with the change in the temperature coefficient with pressure indicated by Benedek et al. [3]. Furthermore, the data shown here demonstrate that $KClO_3$ exhibit no detectable hysteresis in this pressure range.

The results of our preliminary investigation clearly indicate that nuclear quadrupole resonance can be used as a pressure measuring technique. However, substantial progress towards establishing temperature-pressure-frequency curves will depend on more accurate pressure measurements and on controlling temperature more carefully. Experiments are presently in progress towards improving the temperature regulation of the oil bath to ±0.001 °C. We are also considering other materials which have a much smaller temperature coefficient than $KClO_3$. Improving the accuracy of the pressure measurement can only be accomplished by using a more accurate pressure standard such as a piston gage.

We thank Thomas C. Farrar, who suggested this problem, for many helpful discussions. We would also like to thank Peter Heydemann for the use of the pressure vessel and also for constructing the electrical feedthrough; and Daniel Buchalter for his assistance in the fabrication of the high pressure system.

5. References

[1] Bayer, H., Z. Physick **130,** 227 (1951).
[2] Kushida, T., Benedek, G., and Bloembergen, N., Phys. Rev. **104,** 1364 (1956).
[2a] Livingston, R., and Beldes, Mol. Phys. **3,** 501–524, D. Williams, Ed. (1962).
[3] Benedek, G., and Kushida, T., Rev. Sci. Instr. **28,** 92, (1957).
[4] Dean, C., and Pound, R. V., J. Chem. Phys. **20,** 195 (1952).
[5] Vanier, J., Can. J. Phys. **38,** 1397 (1960).
[6] Vanier, J., Metrologia **1,** 135 (1965).
[7] Volpicelli, R. J., Nageswara Rao, B. D., and Baldeschwieler, J. D., Rev. Sci. Instr. **36,** 150 (1965).
[8] Utton, D. B., International Journal of Scientific Metrology **3,** No. 4, 98 (1967).
[9] Heydemann, Peter L. M., Private communication.
[10] Watkins, G., Thesis Howard University, 1952, Pound, R. V., and Knight, W. D., Rev. Sci. Instr. **21,** 219 (1959).
[11] Robinson, F. N. H., J. Sci. Instr. **36,** 481 (1959).
[12] Valley, G. E., Jr., Wallman, H., M.I.T. Radiation Laboratory Series **18,** 166 (1964).
[13] Systron–Donner SD–1037B4D1F.
[14] Honeywell Amplifier #361925.
[15] The pressure vessel was on loan from Dr. P. L. M. Heydemann.
[16] Heydemann, P. L. M., Rev. Sci. Instr. **38,** 558 (1967).
[17] Utton, D. B., J. Res. Nat. Bur. Stand. (U.S.), 71A (Phys. and Chem.), No. 2, 125 (March–Apr. 1967).
[18] Bridgman, P. W., Proc. Am. Acad. Sci. **51,** 55 (1915).
[19] Heise Bourdon Tube Co. Inc., Newtown, Conn.

(Paper 74C1&2–293)

JOURNAL OF RESEARCH of the National Bureau of Standards — C. Engineering and Instrumentation
Vol. 74C, Nos. 1 and 2, January-June 1970

Precise Continuous Optical Attenuator*

G. Ruffino**

(November 17, 1969)

The construction of a precision photometric attenuator is described, which uses linear birefringent polarizers. If properly calibrated, the instrument has relative error not exceeding 2.4×10^{-4} within a relative transmittance range down to 8×10^{-3}. The calibration takes into account stray light, provided the ratio of stray light intensity to total intensity remains constant and low in the whole range. The construction and calibrating procedure apply equally well to the near infrared region.

Key words: Dichroic polarizers; optics; pyrometry; radiometry; relative transmittance factor.

1. Introduction

Very accurate radiometric and pyrometric measurements often require relative transmittance factors to be measured with an accuracy of the order of 10^{-4}. Fixed values of these factors having this order of accuracy may be realized with rotating sectors, where the angular openings of the sector gives the attenuation.

Suitable means for producing a continuously variable relative transmittance factor which may be measured as a function of a mechanical quantity can be constructed with a set of light polarizers. A good arrangement consists of three linear dichroic polarizers lying in parallel planes, the first and third of them having fixed parallel orientation (fig. 1).

The middle polarizer can rotate in its plane, α being the angle between the rotating and fixed axes. R. Clark Jones [1][1] calculated the transmittance of such a train of three birefringent polarizers, which, for the most general case of three nonidentical polarizers, is given by the following expression:

$$T(\alpha)=S_1S_2S_3+D_2(S_1D_3+S_3D_1)\ \cos 2\alpha+S_3D_1D_3\ \cos^2 2\alpha+P_2D_1D_3\ \cos\ \delta_2\ \sin^2 2\alpha \qquad (1)$$

where the coefficients are functions of the two principal transmittances of the polarizers—the subscripts applying to each of them—and δ_2 is the phase retardation of the middle polarizer.

H. E. Bennett [2] described a mechanical arrangement of three polarizers in series for producing optical attenuation. He showed that, if high grade identical polarizers are selected, the relative transmittance factor for the angles α and 0 is given by the simple relation:

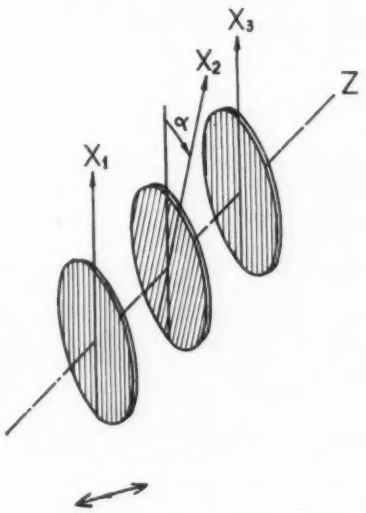

FIGURE 1. *The triple-polaroid optical attenuator.*

$$\frac{T(\alpha)}{T(0)}=\cos^4\alpha. \qquad (2)$$

For this to hold with an accuracy better than 10^{-3}, the principal transmittance ratio of the birefringent polarizers must be $\leq 4 \times 10^{-6}$.

In connection with the development of a photoelectric pyrometer a polaroid attenuator has been constructed, which is basically similar to the one described by Bennett, with provisions for meeting the following major requirements:

(1) the middle polarizer should have the highest resetability;

*An invited paper.

**Present address: Instituto di Metrologia G. Colonnetti, Torino, Italy. Professor Ruffino was a guest worker in the Heat Division, Institute for Basic Standards, National Bureau of Standards, Washington, D. C. 20234, February to July 1969.

[1] Figures in brackets indicate the literature references at the end of this paper.

(2) its rotation angle must be measured with high precision;

(3) the attenuators may be calibrated at a discrete set of points, yielding the coefficients of a function relating the angle with the relative transmittance factor, without any special requirement for the quality of the polarizers.

2. Theory

Equation (1) may be arranged in the following form:

$$T(\alpha)=a-b\sin^2\alpha-c\sin^2 2\alpha \tag{3}$$

with: $a=S_1S_2S_3+D_2(S_1D_3+S_3D_1)+S_3D_1D_3$
$b=2D_2(S_1D_3+S_3D_1)$
$c=D_1D_3(S_3-P_2\cos\delta_2)$.

The transmittance with parallel axes is

$$T(0)=a. \tag{4}$$

Let Φ be the radiant flux of a beam entering the system, Φ_0 the emerging flux with the polaroid set with parallel axes and Φ_α the emerging flux corresponding to the rotation α of the middle polarizer. Then the relative transmittance factor angle α will be:

$$T_r(\alpha)=\frac{\Phi_\alpha}{\Phi_0}=\frac{\Phi_\alpha/\Phi}{\Phi_0/\Phi}=\frac{T(\alpha)}{T(0)}. \tag{5}$$

Referring to (3) and putting $A=\frac{b}{a}$ and $B=\frac{c}{a}$, it is easily seen that

$$T_r(\alpha)=1-A\sin^2\alpha-B\sin^2 2\alpha \tag{6}$$

which gives the relative transmittance factor as a function of α, provided the coefficients A and B are known.

We may expect that not all the incident flux will be attenuated according to eq (3). Then, for every angle, we suppose the incident flux Φ to be divided in two portions: the first Φ^*, which is attenuated according to (3) and the second $\Delta\Phi$ attenuated by a different amount $T'(\alpha)$. We call $\Delta\Phi$ the stray flux, or "stray light."

Now we set two limitations to this stray flux:

(1) it is a small fraction, which will be defined later, of the total flux;

(2) the proportion between stray and total flux is constant for any angle.

The second hypothesis leads to the following expressions for the emerging flux:

$$\Phi_0'=T(0)\ \Phi^*+T'(0)\ \Delta\Phi \tag{7}$$
$$\Phi_\alpha'=T(\alpha)\ \Phi^*+T'(\alpha)\ \Delta\Phi.$$

The transmittance ratio is then:

$$T_r'(\alpha)=\frac{T(\alpha)\ \Phi^*+T'(\alpha)\ \Delta\Phi}{T(0)\ \Phi^*+T'(0)\ \Delta\Phi} \tag{8}$$

$$\cong\frac{T(\alpha)}{T(0)}\left[1+\frac{T'(\alpha)}{T(\alpha)}\frac{\Delta\Phi}{\Phi^*}-\frac{T'(0)}{T(0)}\frac{\Delta\Phi}{\Phi^*}\right]$$

$$=T_r(\alpha)\left[1-\frac{T'(0)}{T(0)}\frac{\Delta\Phi}{\Phi^*}\right]+\frac{T'(\alpha)}{T(0)}\frac{\Delta\Phi}{\Phi^*}.$$

The approximation involved in the second equation is acceptable provided

$$\left|\left[\frac{T'(\alpha)}{T(\alpha)}-\frac{T'(0)}{T(0)}\right]\frac{T'(0)}{T(0)}\left(\frac{\Delta\Phi}{\Phi^*}\right)^2\right|<<1$$

which gives a quantitative expression to the first hypothesis. Putting

$$\frac{T'(0)}{T(0)}\frac{\Delta\Phi}{\Phi^*}=\kappa$$

and taking into account eq (6), eq (8) may be written:

$$T_r'(\alpha)=1-(1-\kappa)\ A\sin^2\alpha-(1-\kappa)\ B\sin^2 2\alpha+\frac{T'(\alpha)\ -T'(0)}{T(0)}\frac{\Delta\Phi}{\Phi^*}. \tag{9}$$

If the last term is

$$\left|\frac{T'(\alpha)\ -T'(0)}{T(0)}\frac{\Delta\Phi}{\Phi^*}\right|<<1$$

then it may be neglected and the transmittance ratio becomes:

$$T_r'(\alpha)=1-(1-\kappa)\ A\sin^2\alpha-(1-\kappa)\ B\sin^2 2\alpha \tag{10}$$

or:

$$T_r^*(\alpha)=1-A^*\sin^2\alpha-B^*\sin^2 2\alpha. \tag{11}$$

Therefore the stray light, at least as defined here, affects only the value of the constant coefficients of the expression of the relative transmittance factor.

The conclusion is that eq (6) yields the relative transmittance factor of a train of three birefringent polarizers in the most general case in which they are not equal, their extinction is not null, and stray flux, under specified conditions, is present in the system.

3. Mechanical Design

An attenuator using sheet polarizers [2] and embodying the above theory has been constructed. A longitudinal section is represented in figure 2. The instrument consists of five principal parts:

(1) A rotor R holds the middle polarizer P_2 and a glass graduated circle C centered on the rotation axis. The latter is divided in degrees and is a component of a precision survey instrument.[3]

[2] Type HN-22, selected to have a principal transmittance ratio $\leq 4\times10^{-6}$.
[3] Made by Salmoiraghi, Italy.

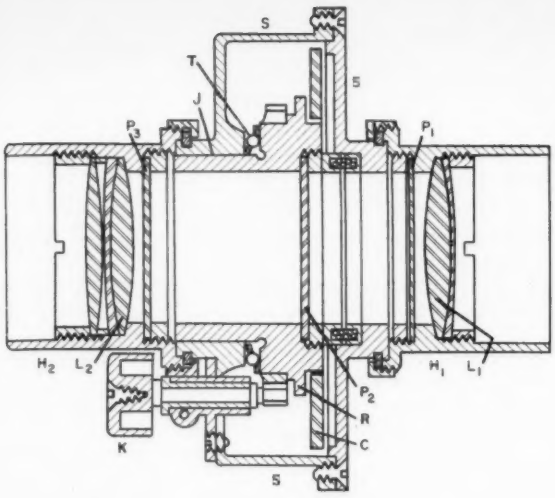

FIGURE 2. *Mechanical design of the attenuator.*

(2) A stator S acts as a support for the instrument and is coupled to the rotor through a journal J, and a thrust bearing T. The journal is made with hardened and ground cylindrical surfaces, which are coupled with a tight tolerance in order to prevent eccentricity and give the highest resetability to the rotor. The thrust bearing consists of two hardened and ground flats, the one in the stator, the other in the rotor, both perpendicular to the rotation axis, holding between them a row of steel balls. A set of springs located in the stator cover presses the rotor against the opposite face. The stator also accommodates a gear train allowing the rotation of the middle polarizer by means of an external knob K. Both stator and rotor are fabricated in hardened steel in order to insure precision coupling. Particular care is required in the choice of the material, which must not be deformed through hardening by an amount which could not be corrected by the precision machining which follows the hardening.

(3) Two tubular pieces, H_1 and H_2, are clamped at the end of the stator, each of them holding one external polaroid P_1 (or P_3) and an objective lens L_1 (or L_2). Each holder, before being clamped, can be independently adjusted for achieving the alinement of the principal optical axes of the polarizers.

(4) A micrometric microscope (not shown in the figure) allows the reading of the scale to be made with the resolution of 0.1 min.

4. Calibration Procedure

The attenuator has been mounted in a photoelectric pyrometer and therefore it was convenient to make use of all parts of the pyrometer for its calibration. Figure 3 represents the optical set up.

The objective lens L_1L_2, embodying the optical attenuator, forms the image of a pyrometric lamp ribbon, acting as a source S, on the slit D_1. A second objective L_3L_4 projects the image of the slit on a plane containing the flat surface of the straight filament of a pyrometer lamp RS.[4] A third objective L_5L_6 forms the image of the filament and of the source on the plane of an oscillating slit D_2. The slit D_1, the filament and the oscillating slit are parallel to each other, the first being 0.15 mm and the latter 0.05 mm wide.

The oscillating slit scans the image of the source, on which is superimposed the filament image. In this way any difference in the radiances of the images gives rise to an alternating component in the radiation flux emerging from the oscillating slit. The radiation flux is detected by a photomultiplier, PM (an RCA type 7265).

The oscillating slit acts as a light chopper and is driven by a cam mounted on the same shaft which actuates synchronous contacts demodulating the output signal of the photomultiplier. In this way the zeroing of this signal reveals the radiance match.

The calibration was performed with an interference filter peaked at 650 nm, with half bandwidth of 10 nm, located between the optical elements of objective L_5L_6.

The flux addition method has been used for calibration [3]. In figure 4 the light beam coming from the source SL (a ribbon lamp) is split by the semireflecting mirror M_1 in two beams which, after reflection in M_2 and M_3, merge in the semireflecting plate M_4, where they are partially superimposed. The two fluxes leaving M_4 are balanced to equality by adjusting the inclination on the optical path of the plates P_1 and P_2. Each of the beams may be intercepted by the shutters D_1 and D_2 and in this way two light fluxes may be produced having a magnitude ratio of two. The fluxes are intercepted by the attenuator and are balanced at the appropriate values of the current of the reference lamp.

The calibration is performed through the following steps:

(1) With parallel polaroid axes ($\alpha=0$) and one shutter closed, the flux Φ_1 is balanced with the reference lamp current I_1. The flux may have any value but must be kept constant within 5×10^{-5} during each step by means of a suitable power supply.

(2) Both shutters are open giving flux $\Phi_2=2\ \Phi_1$ which is matched with I_2.

In this way two values of the reference lamp current are given which correspond to light fluxes having a given ratio. Experience has shown that, after careful degassing of the lamp, and with low filament temperature (about 1300 K), the flux ratio corresponding to current I_1 and I_2 remained appreciably unchanged during several weeks of operation. The same ratio holds when the flux adder is removed, only the absolute values of Φ_1 and Φ_2 being changed.

(3) The flux $\Phi_2=2\ \Phi_1$ is balanced with current I_1 and an appropriate angle α_1 of the middle polarizer. This angle gives the relative transmittance factor, 1/2.

(4) With the attenuator set at the angle α_1 the source radiance is raised until it is balanced with current I_2. Setting now the current at I_1, the attenuator is turned to balance at the angle α_2, which corresponds to the relative transmittance factor 1/4.

The same procedure is repeated, generating in this

[4] The setup described is the one which was in use during calibration. However there are many advantages in interchanging the position of systems $L_1P_1P_2P_3L_2$ and L_3L_4.

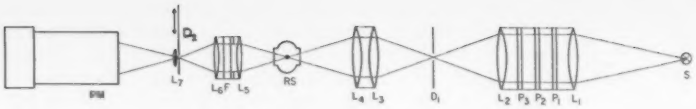

FIGURE 3. *Optical setup.*

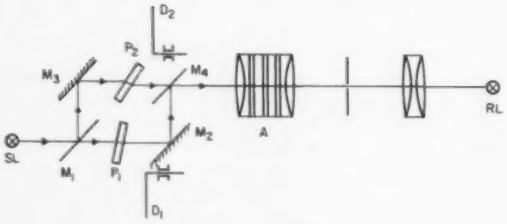

FIGURE 4. *The calibration arrangement.*

way a geometric series of values of the relative transmittance factors having seven terms.

The actual calibration was performed by sweeping the entire relative transmittance range seven times, proceeding stepwise from the lowest value, allowing due time for stabilization, and always using the same two values of the reference currents. For each point two readings were made so that for each nominal value of the relative transmittance factor a total of 14 readings were taken. Table 1 reports, in successive columns, the nominal values of the relative transmittance factor, the mean value of the angle, the estimated standard deviation of a reading and the estimated standard deviation of the mean.

TABLE 1

T_r	$\bar{\alpha}$	s	s_m
2^{-1}	32° 48.44′	0.54′	0.16′
4^{-1}	45° 5.70′	.50′	.14′
8^{-1}	53° 40.32′	.41′	.11′
16^{-1}	60° 14.11′	.32′	.09′
32^{-1}	65° 28.42′	.25′	.07′
64^{-1}	69° 46.04′	.29′	.08′
128^{-1}	73° 21.55′	.22′	.07′

5. Treatment of Calibration Data

The constant coefficients of eq (6) now may be determined through the least squares method on the basis of the calibration data. But first two remarks have to be made:

(1) The first attenuation step, T_{r1}, is affected by an error which is mainly due to inequality of the two fluxes which are added to create the ratio 1/2. Any other value of the attenuation is generated by multiplying the preceding one by T_{r1}, expressed as

$$T_{ri}=T_r^i{}_1 \qquad (12)$$

in which i is the serial number of the step. Obviously the multiplication by T_{r1} propagates the error by which it itself is affected.

(2) The transmission ratio decreases rapidly with increasing angles. Therefore equal deviations of their calculated values from the experimental ones may lead to enormous relative errors for the lowest transmittance ratios. This must be avoided.

On this basis the coefficient A and B are determined according to the following procedure.

(1) We form a series of relative transmittance factors, each term being formed according to eq (12). Giving to the first term T_{r1} values which are closely and equally spaced around the expected value, for each of them we form a series of relative transmittance factors. Then, for each series, we minimize the function:

$$\Phi\ (A,B)=\sum_{i=1}^{7}\left[\frac{T_{ri}-(1-A\sin^2\alpha-\mathrm{B}\sin^2 2\alpha))}{T_{ri}}\right]^2. \qquad (13)$$

Each term of this function is the square of the relative deviation, which is the difference between experimental and computed values divided by the experimental value. Each value of T_{r1} yields a value of A and of B.

(2) With each set of values of A and B the following quantities are computed:

(a) $T_{rc}=1-A\sin^2\alpha-B\sin^2 2\alpha$

(b) $\varepsilon_c=T_r-T_{rc}$

(c) $\eta_c=\dfrac{\varepsilon_c}{T_r}$

(d) $\varepsilon_e=\dfrac{dT_{rc}}{d\alpha}s_m$ (experimental absolute error)

(e) $\eta_e=\dfrac{\varepsilon_e}{T_r}$ (experimental relative error).

(3) Finally, among the ensemble of the groups of T_{rc}, A and B values, the one is chosen for which $\varepsilon_c<\varepsilon_e$. In this way the errors of the relative transmittance factor given by the fitting formula lies within the uncertainty of the experimental values. A program embodying this procedure has been put in a computer and the results of the best fit are collected in table 2.

The equation of the relative transmittance factor for the polaroid train tested is

$$T_r=1-0.999655\sin^2\alpha-0.246799\sin^2 2\alpha \qquad (14)$$

TABLE 2

α	T_r	T_{rc}	ε_c	η_c	ε_e	η_e
32° 48.44′	0.50175	0.50181	-5.8×10^{-5}	-1.2×10^{-4}	6.0×10^{-5}	1.2×10^{-4}
45° 5.70′	.25175	.25172	3.5×10^{-5}	1.4×10^{-4}	4.1×10^{-5}	1.6×10^{-4}
53° 40.32′	.12632	.12630	1.4×10^{-5}	1.1×10^{-4}	2.2×10^{-5}	1.7×10^{-4}
60° 12.11′	.063380	.063377	0.2×10^{-5}	0.4×10^{-4}	1.1×10^{-5}	1.8×10^{-4}
65° 28.42′	.031801	.031805	$-.4 \times 10^{-5}$	-1.3×10^{-4}	0.5×10^{-5}	1.7×10^{-4}
69° 46.04′	.015956	.0159560	0	0	$.4 \times 10^{-5}$	2.4×10^{-4}
73° 21.55′	.0080059	.00080057	$.2 \times 10^{-6}$	0.2×10^{-4}	$.2 \times 10^{-5}$	2.4×10^{-4}

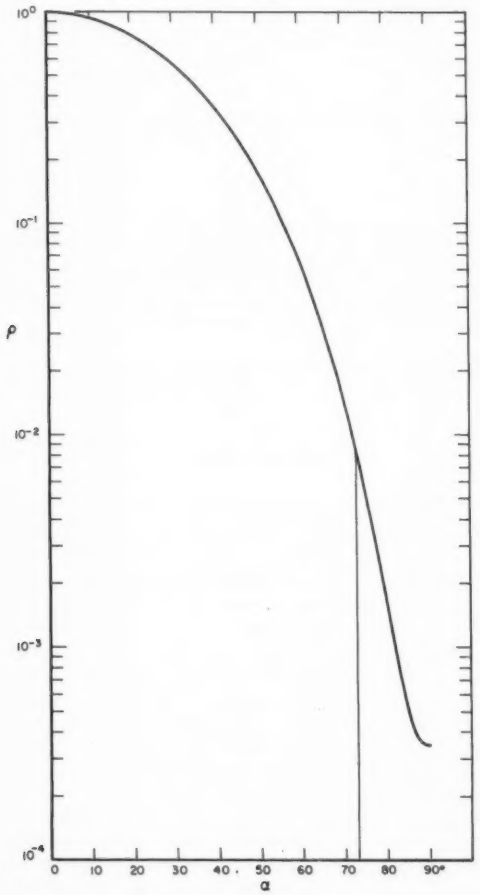

FIGURE 5. *Optical attenuation versus angular setting.*

which is plotted in figure 5 (the vertical line in the diagram represents the upper limit of calibrated range).

6. Discussion

From the last column of table 2 it is apparent that the optical attenuator here described may be calibrated in the range from 1 to 8×10^{-3} of the transmission ratio, with a maximum random error of 2.4×10^{-4}. From the calibration data are computed the constant coefficients of the theoretical interpolating equation, which gives the intermediate values well within the experimental errors. Very important is the fact that the formula giving the attenuation as a function of the angle, under certain general conditions, takes into account the stray light.

From the operation and the calibration procedure of the instrument it is apparent that its precision is subject to a few limitations:

(1)—Unfortunately the transmittances and their ratio in birefringent polarizers are not wavelength independent. Polarizer sheets are manufactured to have roughly constant parameters over the entire visible radiation band and in the near infrared. Therefore, for the highest precision, they must be calibrated within a narrow bandwidth at each wavelength for which they are intended to be used.

(2)—It is well known that several sources, such as incandescent lamps, emit partially polarized radiation. In this case the present device attenuates the polarized component according to the angle between the polarization plane and the optical axis of the outer polarizers. This fact is not objectionable when the instrument is used for generating different flux values from a constant source, since the relative transmittance factor is independent of the polarization state of the entering radiation.

(3)—The attenuator has been calibrated with a parallel radiation beam. Since the transmittance and the retardation depend on the propagation direction of the radiation through the polarizing sheets, calibration precision will be assured only if the attenuator is operated with plane waves. Therefore the target area should have small dimensions and the source should be placed in the focal plane of the front lens of the instrument.

On the other hand, this device has an important advantage in the fact that the interpolating equation does not make any assumption about the ratio between the principal transmittances of the birefringent polarizers. This means that an accurate calibration may be performed even when that ratio is rather high, which opens the way to the use of accurate optical attenuators in the near infrared.

The author is grateful to A. Rosso and G. Canta of the Colonnetti Institute of Metrology for the skillful construction of the instrument and for the help which the former gave in its testing.

7. References

[1] Clark Jones, R., J. Opt. Soc. Am. **46,** 528 (1956).
[2] Bennett, H. E., Appl. Opt. **5,** 1265 (1966).
[3] Gordov, A. N., Lapina, E. A., Exp. Techn. **5,** 544 (1958); Bojarski, L. A., Proc. Verb. Com. Int. Poids Mes. **26A,** T150 (1959); Erminy, D. E., J. Opt. Soc. Am. **53,** 1448 (1963); Lee, R. D., Metrol. **2,** 150 (1966).

(Paper 74C1&2–294)

JOURNAL OF RESEARCH of the National Bureau of Standards — C. Engineering and Instrumentation
Vol. 74C, Nos. 1 and 2, January-June 1970

An A–C Resistance Thermometer Bridge

Robert D. Cutkosky

Institute for Basic Standards, National Bureau of Standards, Washington, D. C. 20234

(December 16, 1969)

A 400 Hz bridge designed specifically for measuring the resistances of platinum thermometers is described. When used in conjunction with a conventional 25 ohm thermometer, the instrument can resolve a resistance change of 2 micro-ohms or less, or about 20 microdegrees. It is believed to be in error by no more than 3 micro-ohms throughout the useful temperature range of a conventional thermometer. The instrument features an automatic phase angle balance, and extensive use is made of multistage transformers and operational amplifiers.

Key words: Automatic phase balance; bridge; multistage transformers; operational amplifiers, resistance bridge; resistance thermometry; temperature measurement.

1. Introduction

A number of new resistance thermometer bridges have been described in the last several years [1, 2, 3, 4].[1] The incentive behind this rash of activity has been to take advantage of recent advances in bridge networks and null detectors, in order to provide a measurement accuracy closer to the limit set by thermal agitation noise in the thermometer than had been possible using the older technology. Most of the new resistance thermometer bridges, including the design described here, utilize alternating current rather than direct current, because of the resultant freedom from errors due to changing thermal emf's, and because of the availability of low noise a-c amplifiers. At the present time, inexpensive amplifiers with optimum noise figures smaller than one dB are only available for frequencies higher than a few hundred hertz. For this reason in part, the thermometer bridge described here was designed to operate at 400 Hz.

Factors which were considered in the choice of the measuring frequency for the bridge were, in addition to amplifier noise, the existence of the technology involving precision decade inductive dividers and multistage transformers, and the technology involving operational amplifiers. Both technologies can be used to full advantage at 400 Hz. Some problems might be expected due to the unavoidable frequency dependence of the resistance thermometer, but our measurements indicated that the resistance at the triple point of water of the particular thermometer used in our experiments did not change by more than 1 part per million (ppm) from dc to 400 Hz. The frequency dependence of the thermometer is in any case unimportant if it is both calibrated and used at the same frequency. It may, however, be necessary to select a standard frequency for use in resistance thermometry.

Early in the design of a resistance thermometer bridge it is necessary to choose a specific configuration for the leads and terminals to be used with the thermometer. The most reliable and most precisely defined lead arrangement available at this time is the so-called four-terminal-pair system [5], in which each of the four leads of the standard is provided with a coaxial shield.

We have elected to retain the usual four-terminal lead configuration, but modify our thermometers to accept a pair of coaxial cables. One cable constitutes the "current" terminals of the thermometer, and the other constitutes the "potential" terminals. This decision greatly simplifies the design of the bridge, and is acceptable in this case because the principal uncertainty introduced thereby is only in the phase angle of the resistor, which is of no importance in resistance thermometry.

A disadvantage of the two-pair system is that the cable admittances appear in parallel with the thermometer, but tests have shown that the shunt conductance of 15 meters of RG 58/U cable changes the apparent resistance at 400 Hz of a conventional 25 Ω thermometer by less than two parts in 10^8. The cable capacitance causes a substantial phase angle under these conditions, but this can be readily handled.

A key part of the circuit described below is a three-stage transformer. A three-stage transformer is similar to the well known two-stage transformer [6, 7], but contains three high-permeability cores rather than two. The construction of a three-stage transformer begins with a

[1] Figures in brackets indicate the literature references at the end of this paper.

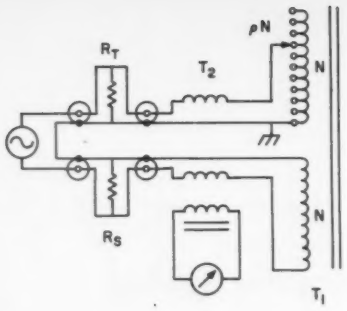

FIGURE 1. *Elementary bridge circuit.*

winding called the first stage winding on a single core. In a circuit diagram it is helpful to label this core "inside." The second core is then placed next to the completed first stage, and another winding called the second stage winding is wound around both cores. This assembly is a two-stage transformer. Following this, the third core is placed next to the two-stage transformer and the final winding, called the third stage winding, is wound around all three cores. The relative positions of the cores and windings can be duplicated on the circuit diagram starting with the labeled inside core. This provides a visual picture of the construction of the transformer, from which its operation can be easily inferred. A three-stage transformer is an obvious extension of a two-stage transformer, and its behavior can be calculated using the methods described in the publications cited above.

2. Bridge Circuitry

The general plan of the bridge is given in figure 1, which shows the resistance thermometer R_t in series with a standard resistor R_s and a current generator. A precision adjustable transformer T_1 of very high input impedance is connected to the potential leads of the two resistors via a three winding detector transformer, T_2. If the input impedance of T_1 is sufficiently high, the detector will register a null when $R_t = \rho R_s$, where ρ is the ratio of T_1.

In order to maintain a high accuracy in the presence of lead and winding impedances which may be as large as several ohms, without the necessity for separately balancing these impedances, the input impedance of T_1 must be at least 10^8 Ω. The easiest way to achieve this is by constructing T_1 as a two-stage transformer. The first stage of T_1 could then be excited by connecting it directly in parallel with the generator supplying current to R_t and R_s, provided that the total number of turns were continuously adjusted to equal $N(1+\rho)$ by ganged switching. This method of excitation was rejected because we wanted to be able to use the bridge not only with $R_s = 100$ Ω and a standard 25 Ω resistance thermometer, but also with $R_s = 0.1$ Ω and a special 0.025 Ω thermometer designed for measurements at the gold point. In the latter case, the very large potential drops in the current leads of the resistors would have resulted in an incorrect excitation of the first stage of T_1.

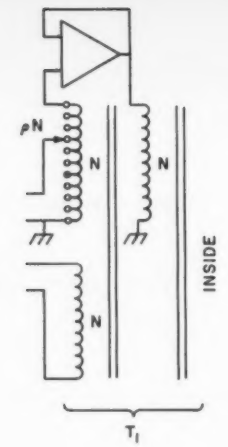

FIGURE 2. *Excitation of a two-stage transformer with a voltage follower.*

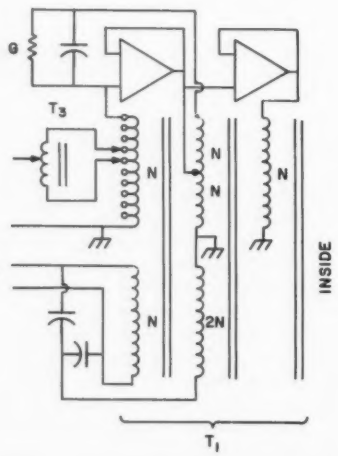

FIGURE 3. *Excitation of a three-stage transformer with two voltage followers.*
The technique used for compensating the interwinding capacitance of the third stage is also shown.

Figure 2 shows how an operational amplifier connected as a voltage follower can be used to automatically supply the correct excitation to the first stage of a two-stage transformer, and yield a high input impedance as viewed at the second stage. This circuit is inherently highly stable, and is much less prone to oscillate than alternative circuits based on the permeability multiplier developed by D. L. H. Gibbings [8]. The actual circuit used for T_1 contains two voltage followers and a three-stage transformer as shown in figure 3. Additional windings were put on the second stage as shown to provide a means of compensating the interwinding capacitances of the third or outer stage. Small resistors (not shown) were added in series with the compensating capacitors to suppress high

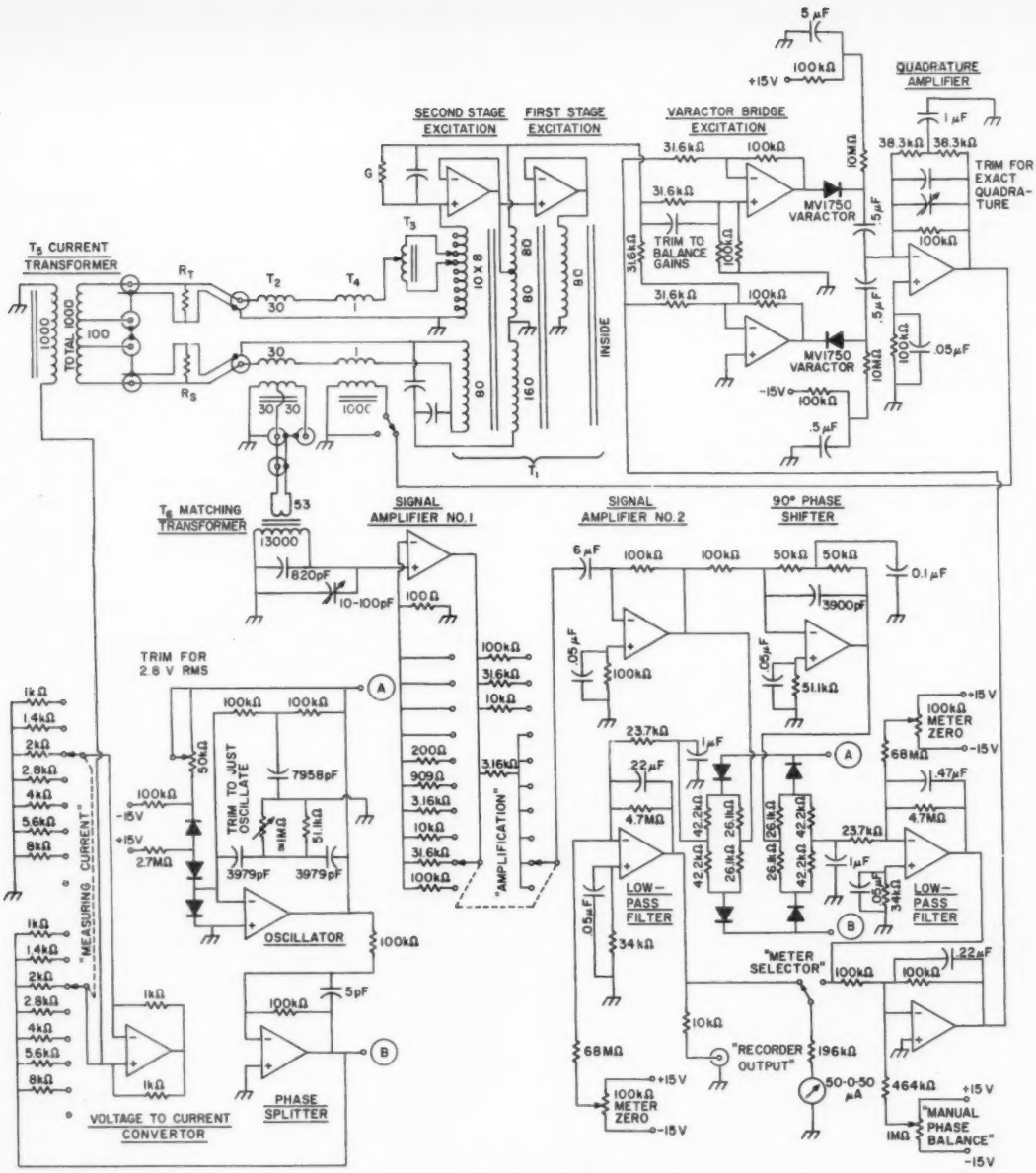

FIGURE 4. *Complete circuit of the a-c resistance thermometer bridge.*
The numbers associated with each transformer winding indicate the number of turns.

frequency oscillations. The third stage was constructed with polytetrafluoroethylene insulated wire to minimize the shunt conductance between the windings.

Only the first decade of T_1 was specially constructed, the lower seven decades being obtained from a commercial inductive divider T_3, which bridges adjacent taps on T_1. The equivalent shunt resistance of T_3 is about 10^6 Ω, and its effect on the input impedance seen across a fixed winding on the third stage of T_1 is independent of ρ. The conductance labeled G in figure 3 is selected to eliminate the potential lead current that would otherwise result. A resistor of about 10^8 Ω was required.

The detector system used with the bridge contains a matching transformer, an amplifier with an optimum source impedance of 6×10^6 Ω and a noise figure of 0.2 dB, and two phase-sensitive detectors followed by low pass filters. The first phase-sensitive detector is adjusted so that it responds to a resistive unbalance in the

bridge. Its output is passed through a filter with a 1 s time constant, and displayed on a panel voltmeter and an optional external recorder. The second phase-sensitive detector responds to a phase angle unbalance. Its filtered output is used to control the level of a quadrature voltage added in series with the detector transformer, T_2, to provide an automatic phase angle balance.

The quadrature balance voltage was obtained by amplifying the output of the voltage follower driving the second stage of T_1, and applying this voltage to a bridge involving a pair of varactor diodes. The d-c output of the second phase-sensitive detector determines the biases on the two varactor diodes, and hence controls the short circuit current at the varactor bridge detector junction. This current is 90° out of phase with the input voltage, since the varactor diodes behave like capacitors. An operational amplifier connected as a current to voltage converter then produces an output voltage proportional to this a-c current, and the voltage is inserted in series with T_2. A very similar automatic phase balance system using a balanced mutual inductor rather than varactor diodes has been developed by A. M. Thompson [4].

The behavior of the feedback loop sketched above is somewhat difficult to calculate, since the effective loop gain depends not only upon the gains of a series of a-c and d-c amplifiers, but also upon the excitation current applied to the resistance bridge. The bandwidth of the feedback loop is limited principally by the low pass filter following the second phase-sensitive detector, but also by the finite bandwidth of the tuned matching transformer preceding the detector amplifier. In order to avoid low frequency instabilities due to excessive phase shifts, the Q of the matching transformer must be kept small.

The complete circuit of the resistance thermometer bridge is shown in figure 4. In addition to the features described above, it includes a constant current generator with switch-selectable output currents to excite the bridge, so that the measuring current is independent of the temperature of the thermometer. Provisions are also made for changing the ratio of the current transformer driving the bridge and the ratio of the detector matching transformer to accommodate either a 25 Ω or a 0.025 Ω resistance thermometer. A liberal use of mu-metal shielding was required, not only to avoid interactions between various parts of the bridge, but also to prevent saturation of the detector by harmonics of the 60 Hz power supply.

3. Performance

When R_s is a 100 Ω standard, a change of one step in the last decade of the bridge corresponds to a resistance change of 1 μΩ, or about 10 μdeg when R_t is a conventional 25 Ω platinum thermometer. With a measuring current of 1 mA, a bridge unbalance of 2 μΩ can be resolved throughout the useful temperature range of the thermometer. Tests have been made which indicate that the bridge reading is in error by no more than 3 μΩ over the entire range of 0 to 100 Ω, provided that the RG 58/U thermometer cables are no longer than 15 m.

When R_s is a 0.1 Ω standard and R_t is a 0.025 Ω platinum thermometer, and with a measuring current of 0.028 A, the bridge will resolve a temperature change of 100 μdeg. This relatively large uncertainty greatly exceeds that which would be produced by thermal agitation noise in the thermometer, and is caused principally by thermal agitation noise in the winding resistance of the commercial inductive divider, T_3. For the time being, a resolution of 100 μdeg is adequate for the measurements to be made at the gold point.

The accurate calibration of the bridge was greatly simplified through the use of a special two-stage inductive divider constructed and made available by Wilbur C. Sze of the NBS Electricity Division, High Voltage Section. The reliability of the bridge was verified through an exhaustive series of measurements made by John L. Riddle and William R. Bigge of the NBS Heat Division, Temperature Section. The special 0.1 Ω standard resistor for use with a thermometer designed for operation at the gold point was constructed of a gold-chromium alloy by James L. Thomas while serving as a consultant to the NBS Electricity Division. The 0.025 Ω platinum thermometer is currently under development by L. A. Guildner and R. L. Anderson of the NBS Heat Division, Temperature Section, who provided much of the stimulus for the work reported here.

4. References

[1] Hill, J. J., and Miller, A. P., An A. C. double bridge with inductively coupled ratio arms for precision platinum resistance thermometry, Proc. I.E.E. **110,** No. 2 (1963).

[2] Automatic Systems Laboratories, Ltd., Precision Resistance Bridges (Brochure) Leighton Buzzard, Beds., England.

[3] Kusters, N. L., and MacMartin, M. P., National Research Council, Ottawa, Canada (private communication).

[4] Thompson, A. M., National Science Laboratory, Sydney, Australia (private communication).

[5] Cutkosky, R. D., Four-Terminal-Pair Networks as Precision Admittance and Impedance Standards, Communication and Electronics, **70** (Jan. 1964).

[6] Brooks, H. B., and Holtz, F. C., The Two-Stage Current Transformer, AIEE Trans. **41,** 383 (1922).

[7] Cutkosky, R. D., Active and Passive Direct Reading Ratio Sets for the Comparison of Audio Frequency Admittances, Nat. Bur. Stand. (U.S.), 68C (Eng. and Instr.) No. 4, 195–322 (Oct.–Dec. 1964).

[8] Gibbings, D. L. H., A Circuit for Reducing the Excitation Current of Inductive Devise, Proc. I.E.E. **108B,** 339–343 (1961).

(Paper 74C1&2–295)

JOURNAL OF RESEARCH of the National Bureau of Standards — C. Engineering and Instrumentation
Vol. 74C, Nos. 1 and 2, January-June 1970

On the Flow Induced by a Maxwell–Chartoff Rheometer

Elliot A. Kearsley

Institute for Materials Research, National Bureau of Standards, Washington, D. C. 20234

(May 5, 1970)

The Maxwell-Chartoff rheometer does not supply the surface tractions necessary to maintain the flow customarily assumed. This can be seen from considerations of the energy balance.

Key words: Normal stresses; rheology; rheometer; viscoelasticity.

Most steady-state rheometers in use today utilize some form of viscometric flow, i.e., a flow which is dynamically equivalent to a plane steady simple shearing motion [1].[1] Recently, there has been a great deal of interest in extending rheological studies to nonviscometric flows, such as the flow in a Maxwell-Chartoff rheometer [2–5]. This apparatus is basically a pair of parallel plates rotating steadily and in the same sense about noncoincident axes perpendicular to the plates. The test sample is placed between the plates and rotates with them and must consequently undergo some shearing.

A flow has been proposed [4] which is supposed to take place in the Maxwell-Chartoff rheometer, and which has been studied in considerable detail along with its rheological consequences [5, 6]. In this proposed flow the material particles travel within planes parallel to the confining planes and describe circles about a center on the straight line connecting the centers of rotation of the confining planes. Thus, the material forms a cylinder whose cross section perpendicular to its generators is an ellipse. This flow can be described by the following deformation

$$\begin{aligned} x(t-s) &= X\cos\Omega s + (Y-\Psi Z)\sin\Omega s \\ y(t-s) &= -X\sin\Omega s + (Y-\Psi Z)\cos\Omega s + \Psi Z \\ z(t-s) &= Z \end{aligned}$$

where X, Y, Z are the coordinates of a material particle at time t and x, y, z are the coordinates of the same particle at any previous time, $t-s$. The angular velocity of the confining planes is Ω and Ψ is the tangent of the angle between the axis of rotation and the line connecting the centers of rotation.

Because this deformation is a linear mapping, the relative deformation gradient history is the same throughout the sample. For an incompressible isotropic simple fluid (in which the extra stress is an isotropic function of the history of the relative deformation gradient) the stress must also be a constant throughout the sample. Thus, the divergence of the stress is zero within the sample (ignoring any inertial forces), and the flow is dynamically possible if suitable surface tractions are supplied at the boundaries. This flow is a member of the class called controllable,[2] for which the necessary surface tractions can be supplied by geometrical constraints on the boundaries *without reference to the properties of the material.* On the plane boundaries, these tractions are supplied by the reaction forces of the rotating planes. A consideration of the symmetries of the situation is enough to establish that these forces do no work since there are no net displacements and no net torques. It is clear, however, that whatever power is consumed by the assumed flow must be supplied by the surface tractions on the cylindrical boundary, since they are the only external forces which do work. The power input from the surface tractions on the cylindrical boundary is proportional to the volume of the sample, and, of course, it cannot be made ignorable by decreasing the thickness of the sample.

Although the rotating plates of the Maxwell-Chartoff rheometer are physically equivalent to the confining planes of this flow, this rheometer does not control the sample surfaces between the plates, and one must expect the resulting flow to depend on the properties of the material being sheared. Crude experiments in our laboratory showed several different flows for different materials, none of which resembled the flow of the above equations. It is clear that the flow induced by the Maxwell-Chartoff rheometer can approximate that assumed above only to the extent that the test material dissipates a negligible amount of energy. It is interesting that the Maxwell-

[1] Figures in brackets indicate the literature references at the end of this paper.

[2] More exactly, this flow is controllable [6] (ignoring inertia) for simple incompressible isotropic fluids. Controllable flows are of particular rheological interest because they offer the possibility of producing a known flow in a material with unknown properties. Then, if stress measurements are taken simultaneously, rheological information may be developed.

Chartoff rheometer seems to have been a direct outgrowth of a device used by Mooney [7] to study the stored energy in vulcanized rubber cylinders.

Modifications of the Maxwell-Chartoff rheometer to supply the necessary constraints, such as the addition of an elastic cylindrical confining wall around the sample, are conceivable, but not without considerable design problems.

References

[1] Coleman, B. D., Markovitz, H., and Noll, W., Viscometric Flows of Non-Newtonian Fluids (Springer, 1966).

[2] Maxwell, B., and Chartoff, R. P., Studies of a polymer melt in an orthogonal rheometer, Trans. Soc. Rheol. **9**, 41 (1965).

[3] Blyler, L. L., Jr., and Kurtz, S. J., Analysis of the Maxwell orthogonal rheometer, J. Appl. Poly. Sci. **11**, 127 (1967).

[4] Bird, R. B., and Harris, E. K., Jr., Analysis of steady state shearing and stress relaxation in the Maxwell orthogonal rheometer, A.I.Ch.E. Jour. **14**, 758 (1968).

[5] Huilgol, R. R., On the properties of the motion with constant stretch history occurring in the Maxwell rheometer, Trans. Soc. Rheol. **13**, No. 4, 513 (1969).

[6] Pipkin, A. C., Nonlinear phenomena in continua, Div. Appl. Math., Brown University, Tech. Rep. #2, 69 (1969).

[7] Mooney, M., Stress-strain curves of rubbers in simple shear, J. Appl. Phys. **35**, 23 (1964).

(Paper 74C1&2–296)

JOURNAL OF RESEARCH of the National Bureau of Standards — C. Engineering and Instrumentation
Vol. 74C, Nos. 1 and 2, January-June 1970

Mechanical Compliance Measurements of Single–Edge–Notch Tension Specimens*

Mary Jane Orloski

Institute for Basic Standards, National Bureau of Standards, Washington, D. C. 20234

(June 12, 1970)

This paper describes the mechanical compliance measurement of a 15 × 3-in single-edge-notch (SEN) specimen, effective gage length greater than twice specimen width, and a 7 × 3-in SEN specimen, effective gage length less than twice specimen width, both of ¼-in-thick 7075–T6 aluminum. The 15 × 3-in specimen was chosen to provide experimental values of $EW\mathcal{G}/P^2$ for comparison with the theoretical stress function solutions of Srawley and Gross. Results obtained are in good agreement with the theoretical values. The 7 × 3-in specimen was chosen as proportional to a practical size SEN specimen that has been widely used. Comparisons of experimental values of $EW\mathcal{G}/P^2$ for this specimen were made with these theoretical stress function solutions.

Key words: Compliance; crack-toughness; fracture; single-edge-notch specimen.

Glossary

a	crack length
B	thickness of specimen
$C, \frac{d\delta}{dP}$	compliance
δ	displacement
E	Young's modulus
$\mathcal{G}$	strain energy release rate with crack extension
L	gage length, effective length of specimen
P	load per unit thickness
W	width of specimen

1. Introduction

Improvement of design criteria for high-strength materials, particularly metals, depends on a better understanding of their fracture properties. Compliance measurement is a technique frequently used in attempting to isolate the causes of brittle fracture experimentally. One of a family of compliance specimens, the single-edge-notch (SEN) specimen, is especially well suited to plate or sheet materials. Compliance measurements of a fracture toughness SEN specimen produce the experimental analog (sometimes referred to as a compliance "calibration") of the theoretical stress function solution of the axially loaded notched elastic plate. This paper describes mechanical compliance measurements of a 15 × 3-in SEN specimen (with an effective gage length greater than twice the specimen width) and a 7 × 3-in SEN specimen (with an effective gage length less than twice the specimen width), both of ¼-in-thick 7075–T6 aluminum. For convenience, the specimens will be referred to hereafter as "long" and "short" respectively.

We chose a long specimen to provide experimental values, derived from compliance measurements, for comparison with the theoretical stress function solutions of Srawley and Gross [1].[1] We chose a short specimen to determine compliance also for a practical size SEN specimen that has been widely used in determination of the long-term environmental effects, principally radiation, on the crack-toughness properties of materials.

2. Specimens

The specimens were fabricated from 7075–T6 aluminum, a metal well suited to the study of fracture because of its low toughness and long elastic range. Nominal specimen dimensions are given in figure 1. The specimens were heat treated to remove residual stresses and were ground to minimize variations in thickness. Measurements of the specimens are given in table 1.[2]

*The work covered in this publication was supported in part by National Aeronautics and Space Administration under contract No. R–09–022–042.

[1] Figures in brackets indicate the literature references at the end of this paper.

[2] English units are used throughout this paper since these are the units most frequently used in fracture toughness work in the United States. Conversion to SI units can be made by use of the relationships found in NBS Handbook 102 (ASTM Metric Practice Guide).

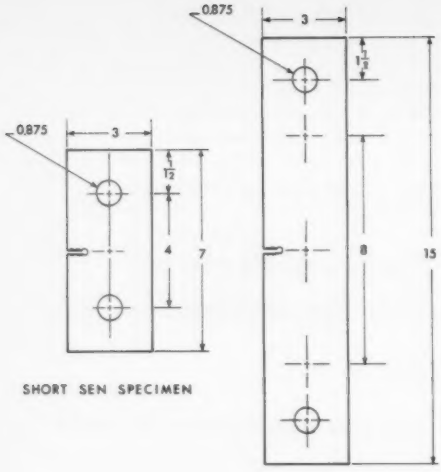

FIGURE 1. *Nominal dimensions in inches.*

TABLE 1. *Specimen dimensions*

Dimension	Long		Short	
	Measurement	Std. dev.[a]	Measurement	Std. dev.[a]
	in	*in*	*in*	*in*
B, thickness	0.22947	0.00010	0.23910	0.00007
W, width	2.9982	.0016[b]	2.9952	.0006
L, effective length	8.0011	.0007[b]	4.0327	.0001
a, crack length	0.1544	.0018 (avg)	0.1643	00014 (avg)
	.2905		.3083	
	.4432		.4448	
	.5995		.5966	
	.7528		.7516	
	.9023		.9004	
	1.0545		1.0464	
	1.2059		1.2078	
	1.3541		1.3463	
	1.5059		1.4978	

[a] The standard deviations included uncertainties in the uniformity of the specimen dimensions and also limitations in the measurement process. The predominant factor was the variability in specimen dimensions.

[b] These measurements were made at the beginning of this work. The measurement technique was refined for L and W of the short specimen.

The gage length of the short specimen is defined as the distance between the load bearing edges of the specimen holes minus ½ the diameter of each pin. The crack length (notch length) of both specimens is the distance from the edge of the specimen to the bottom of the hole. These dimensions are illustrated in figure 2.

The notch in the specimen was made in the following way. A hole was drilled with a 0.019-in drill, 0.150 in from the edge of the specimen at its midlength. Then, a wire was slipped into the hole and a cut was made with a 0.013-in-wide jeweler's saw from the edge of the specimen to the wire. The notch was increased in steps of 0.150 in so that after the tenth cut, the notch was halfway across the specimen.

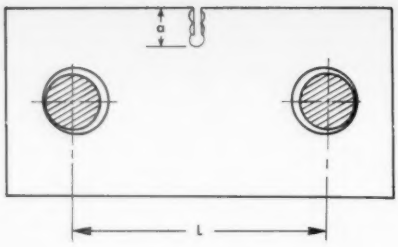

FIGURE 2. *Specimen notch depth, a, and short specimen effective length, L.*

3. Apparatus

The instruments used in the experimental work are listed in table 2.

TABLE 2. *Instruments and utilization*

Instrument	Resolution	Utilization
Gage block and null indicator	0.00005 in	*B*, thickness
Micrometer	.0001 in	*W*, width *d*, pin diameter
Toolmakers' microscope	.00005 in	*a*, crack length
Optical comparator	.00003 in	*L*, effective length
Length extensometer		δ, displacement
Load cell and indicator	.2 lbf	Load

A 10,000-lbf capacity load cell was used to measure the load. The cell was mounted in series with the specimen in a 100,000-lbf capacity screw-powered testing machine. The estimated errors in the load measurement did not exceed 0.15 percent of load.

The displacement was measured by means of an extensometer, developed by J. R. Houghton especially for this kind of work and described in Appendix A. A linear-variable-differential-transformer (LVDT) of 0.1-in range is the sensing element in the extensometer. With this instrument it is possible to resolve extensions of less than 1 μin.

For our tests the extensometer was modified to use nylon bushings to replace the flexures centering the LVDT cores in their transformer bodies, a brass thumb screw spring loaded against the active LVDT core to replace the micrometer-screw adjustment of the core, and minor changes in the electrical circuitry [2]. A 2-in gage length Tuckerman strain gage equipped with a 0.4-in lozenge [3] was used to calibrate the extensometer in an extensometer comparator. Random errors in calibration over the seven-month period on the short specimen ranged from 1.4 to 2.9 μin.

Support pins for the long specimen were of different design than those for the short specimen. As the long-specimen pins were tightened in their clevises, the pins were expanded to a tight fit in the specimen holes by means of split bushings around the pin midsections, figure 3. The short specimen pins, simple cylinders, had a sliding fit in the specimen holes, as shown in figure 4. The long-specimen pins, supported by roller bearings in the

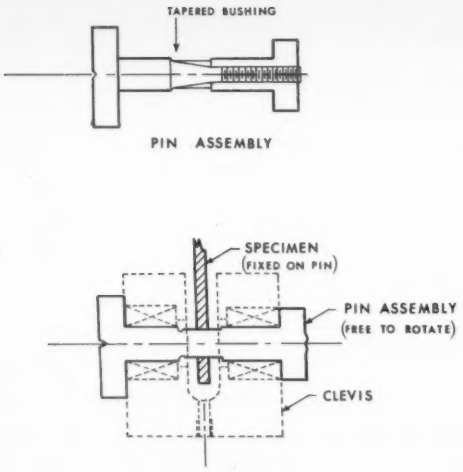

FIGURE 3. *Long specimen fixtures.*

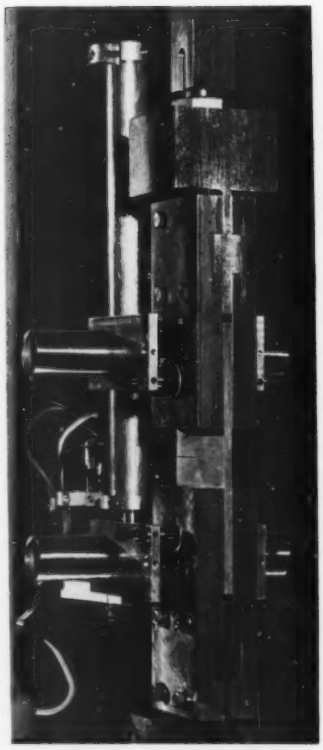

FIGURE 4. *Short specimen fixtures.*

clevis, were free to rotate as load was applied. The pins could also be locked with respect to the clevis. The short-specimen pins were not fixed with respect either to the clevis or the specimen.

4. Plan of Experimental Work

Compliance ($d\delta/dP$) was determined for both specimens for crack length/specimen width (a/W) = 0.0 to 0.5. Six load-displacement runs were made at each value of a/W on the long specimen and three on the short specimen. The first three runs on the long specimen were made with the pins free to rotate and the second three with the pins locked. With the long specimen, the extensometer was not disturbed until the six test runs had been completed, since the extensometer was attached directly to the specimen. In the case of the short specimen, the extensometer and the specimen were removed and replaced between runs to randomize errors due to attachment of the extensometer to the pins.

The extensometer was calibrated (three runs per calibration, averaged) over a range of 8000 μin before and after the test series on each specimen. In addition, because maximum accuracy and precision were desired for the short specimen, the extensometer was calibrated for each of the notch lengths of this specimen. The load cell and indicator were calibrated by dead weights before the long-specimen test series and before and after the short specimen test series.

After all tests were concluded on the long and short specimens, three load-displacement runs were made on a short, unnotched steel specimen in the short specimen fixtures. The purpose of these tests was to estimate the deflection of the pins under load from the known ratio of the stiffness of aluminum to that of steel. Finally, three load-displacement runs were made on a 7075–T6 aluminum reduced cross-section specimen to determine the value of modulus for use in evaluation of the experimental data. This specimen had dimensions similar to the standard plate type specimen, figure 6 of ASTM E 8–68, except that the ends were for pin-ended connections.

5. Test Procedure

The specimen was installed in the grips in the testing machine. (The pins for the short specimen were lubricated with a high-pressure lubricant before being inserted into the clevis and specimen. The short specimen was centered in its grips by means of 0.003-in shims to prevent contact between the specimen faces and the clevis surfaces.) The assembly was oscillated or lightly tapped to aline it properly prior to loading.

An initial load, 60 lbf for the long specimen and 1000 lbf for the short specimen, was applied (and the short specimen shims were removed) to eliminate slack and nonlinear motion in the grips. The extensometer was attached and then set to an initial reading which was the same for all the tests on one specimen. After a 15-min stabilization period, three preloads were applied to an average stress level of about 12,000 lbf/in^2, based on specimen area at the notch.

After each preload, the load was reduced to zero for the long specimen and to 1000 lbf for the short specimen.

The loading rate was approximately 100 lbf/min. Loading was continuous during a test run, the indicated load being read from the load cell at extensometer-extension intervals of 400 up to 7600 μin. At the end of a test run

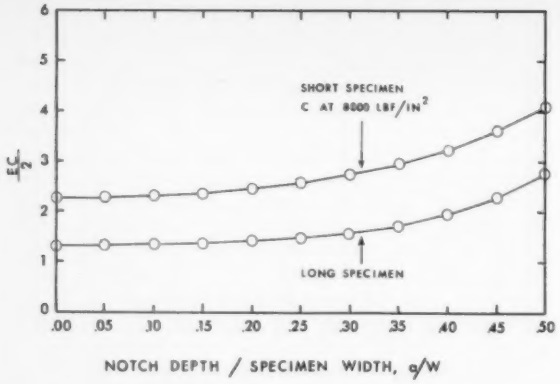

FIGURE 5. *Normalized compliance for short and long specimens.*

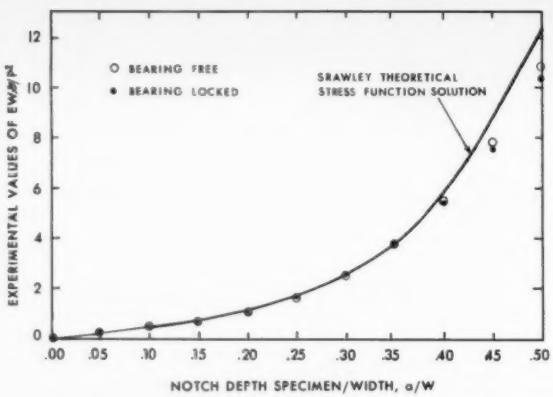

FIGURE 6. *Experimental values of* $EW\mathcal{G}/P^2$ *versus* a/W *for 8-in gage-length SEN specimen.*

on the long specimen, the load was reduced to zero. Whenever possible, the next of the six test runs was made immediately (without preloads). At the end of a test run on the short specimen, the load was brought down to 1000 lbf. At this time the extensometer was removed; then the load was brought down to zero and the specimen removed. When the specimen was reinstalled in the grips, the entire test procedure (with preloads) as described above was repeated for another test run.

6. Reduction of Data

In line with the practice followed by other investigators, we wished to work with the compliance, or the slope $(d\delta/dP)$, of the load-displacement relationship. It is convenient to express the experimental compliance measurements in terms of Srawley's stress function solution, EWG/P^2, which is related to the compliance by [4]:

$$\frac{d(EC/2)}{d(a/W)}=\frac{EW\mathcal{G}}{P^2}. \qquad (1)$$

This expression was derived by boundary collocation of the Williams stress function which requires that plane strain conditions exist on the specimen. It is recognized that the compliance of the short specimen also included deformation at the contact points and the deformations of the pins. See figure 5.

A linear fit by the method of least squares was sufficient to describe the load-displacement relationship for the long specimen. For the short specimen, however, the measurements indicated slight curvature in the relationship that was inadequately described by a linear fit. A third-degree fit reduced the standard deviation by 8 to 1 and was selected for fitting the short specimen data. Short specimen compliance was evaluated at average stress levels, based on the area of the specimen at the notch, of 5000, 6000, 7000, and 8000 lbf/in². In fitting curves to the data from both specimens, data below 1000 lbf load were dropped to minimize computer round-off errors. The data from both specimens were normalized to a specimen of nominal length 8 in and 4 in, respectively, and a thickness of 1 in.

TABLE 3. *Stress function solutions and experimental values of* $EW\mathcal{G}/P^2$ *for 7075–T6 aluminum SEN specimen of 8-in effective length and 3-in width*

Notch depth (a)	Notch depth-to-width ratio (a/W)	Stress function solutions			
		Bearing free	Bearing locked	Theoretical (Srawley)[a]	Experimental (Srawley)[b]
in					
0.00	0.00	0.000	0.000	0.000	0.000
.15	.05	.261	.228	.204	.314
.30	.10	.459	.427	.445	.556
.45	.15	.687	.675	.758	.816
.60	.20	1.037	1.051	1.180	1.180
.75	.25	1.601	1.633	1.768	1.735
.90	.30	2.470	2.500	2.603	2.571
1.05	.35	3.737	3.728	3.813	3.775
1.20	.40	5.492	5.397	5.596	5.436
1.35	.45	7.829	7.587	8.826	7.641
1.50	.50	10.839	10.373	12.399	10.447

[a] Reference [1].
[b] Reference [5].

Values of $EC/2$ for the different crack length ratios a/W were fitted by the method of least squares to a fourth-degree polynomial of the form:

$$EC/2=B_1+B_2(a/W)^2+B_3(a/W)^3+B_4(a/W)^4. \qquad (2)$$

This particular form of the equation was chosen so that the derivative of $EC/2$ is forced through zero at $a/W=0$, a condition imposed by the fact that EWG/P^2 is zero in the unnotched specimen. Srawley's stress function solutions were then evaluated for both specimens as:

$$EW\mathcal{G}/P^2=2B_2(a/W)+3B_3(a/W)^2+4B_4(a/W)^3. \qquad (3)$$

7. Results and Discussion

Long specimen results both with the clevis bearing locked and unlocked are given in table 3. Theoretical [1] and experimental [5] values from the work of Srawley are also given for comparison. Comparison of our values

TABLE 4. *Values of coefficients of polynomial fit, long specimen*

$$\frac{d(EC/2)}{d(a/W)} = EW\mathscr{S}/P^2 = 2B_2(a/W) + 3B_3(a/W)^2 + 4B_4(a/W)^3$$

	Bearing free	Bearing locked
B_2	3.22	2.69
B_3	−10.26	−7.15
B_4	30.62	26.10

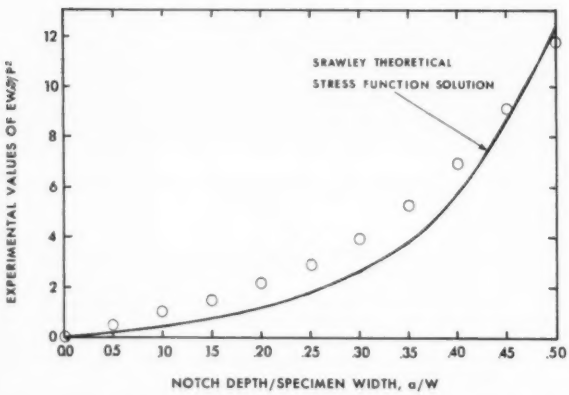

FIGURE 7a. *Experimental values of* EW$\mathscr{S}$/P² *versus* a/W (C *evaluated at 5000 lbf/in²) for the short specimen.*

with the theoretical values of Srawley is also shown in figure 6. Values of the coefficients of the polynomial fit are given in table 4.

The differences between our results with the pin-assembly free to rotate and with it locked average 0.023 for a/W ratios up to 0.35. This seems to indicate that limiting the motion of the assembly does not affect the results significantly. There is good agreement, in general, with the Srawley theoretical stress function solutions, particularly for small notches.

Short specimen results evaluated at four average stress levels (as discussed in the previous section) are given in table 5. Theoretical values of the Srawley [1] theoretical stress function solutions and the experimental values of Sullivan [6] are given for comparison. Our results at 5000 and 8000 lbf/in² are shown in figures 7a and 7b along with the Srawley theoretical stress function solutions.

Derived for specimens having an L/W ratio of at least 2, the theoretical stress function solutions may not be completely applicable to a specimen such as our short specimen having $L/W = 1.3$. Also, see remarks in reference [1], pp. 8–9. In addition, deformation measurements made by connection through the pins introduce effects such as the deformation around the holes not contained in Srawley's theoretical treatment. We estimate the contribution of the bending of the pins to be about 2 percent of the measured compliance value for the short specimen. This estimate was based on the compliance measurement

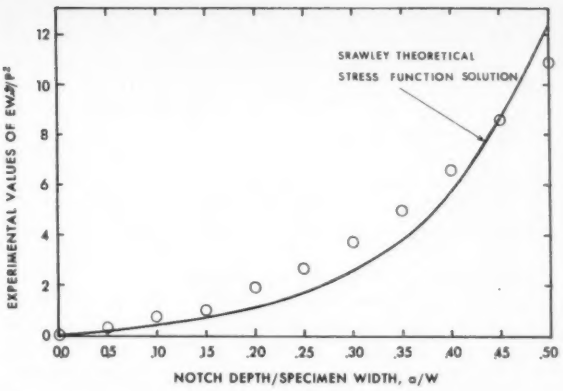

FIGURE 7b. *Experimental values of* EW$\mathscr{S}$/P² *versus* a/W (C *evaluated at 8000 lbf/in²) for the short specimen.*

TABLE 5. *Stress function solutions and experimental values for* EW$\mathscr{S}$/P² *for 7075–T6 aluminum SEN specimen of 4-in effective length and 3-in width*

Notch depth (a)	Notch depth-to-width ratio (a/W)	Experimental				Experimental [a] (Sullivan)	Theoretical [b] (Srawley)
		5000 [c]	6000 [c]	7000 [c]	8000 [c]		
in							
0.00	0.00	0.000	0.000	0.000	0.000	0.00	0.000
.15	.05	.532	.513	.463	.384	.35	.204
.30	.10	1.024	.998	.924	.804	.60	.445
.45	.15	1.543	1.517	1.438	1.035	1.00	.758
.60	.20	2.159	2.133	2.058	1.934	1.40	1.180
.75	.25	2.941	2.909	2.841	2.736	1.95	1.768
.90	.30	3.959	3.906	3.840	3.758	2.75	2.603
1.05	.35	5.280	5.188	5.109	5.045	4.20	3.813
1.20	.40	6.974	6.815	6.705	6.644	6.20	5.596
1.35	.45	9.111	8.852	8.681	8.601	8.90	8.826
1.50	.50	11.759	11.359	11.093	10.961	12.40	12.399

[a] Reference [6].
[b] Reference [1].
[c] Stress level at which evaluated, lbf/in².

of a short steel and a short aluminum specimen in the same fixtures and considering the modulus of the respective materials.

From the range of the stress function values in the individual runs, the estimated standard deviations of the data for notch depths up to 1.05 ranged from 0.20 at the 5000 lbf/in² level to 0.13 at the 8000 lbf/in² level. For notch depths of 1.20 and greater, the estimated standard deviations increased to a maximum of 2.4 at 5000 lbf/in² and 1.1 at 8000 lbf/in². As indicated previously, the specimen was removed and replaced between runs so that, in effect, each run was an independent determination for the specimen. The individual runs for 5000 and 8000 lbf/in² are shown in figures 7c and 7d.

Lack of correlation between our data and those of Sullivan, who measured the compliance of a proportionally smaller specimen, is probably due to the different points of attachment of the extensometer. The extensometer in

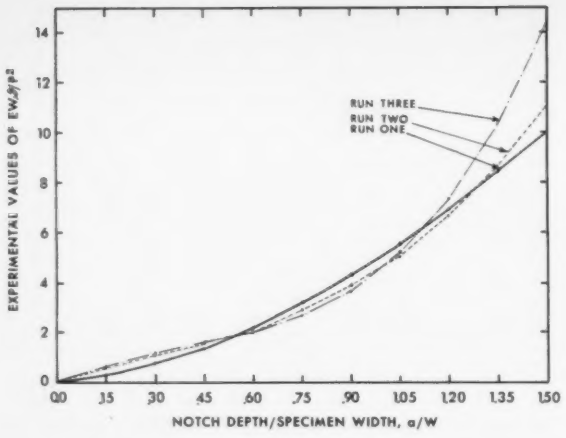

FIGURE 7c. *Experimental values of* EW/P² *versus* a/W (C *evaluated at 5000 lbf/in²) for short specimen first, second, and third runs.*

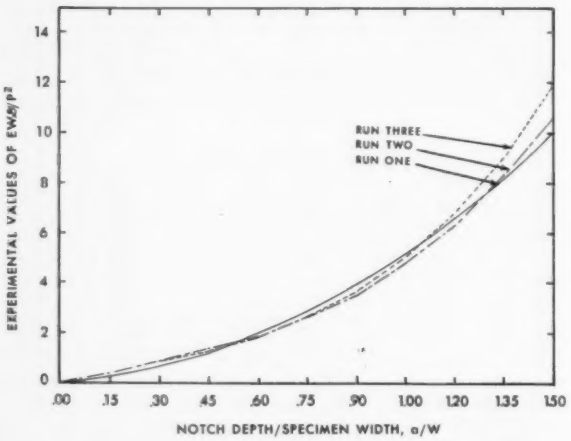

FIGURE 7d. *Experimental values of* EW/P² *versus* a/W (C *evaluated at 8000 lbf/in²) for short specimen first, second, and third runs.*

our case is attached across the pins, while it was attached across the grips for Sullivan's work. The complex loading configuration of these specimens does not permit direct comparison. We found, for example, that to obtain reproducible results in the setup on the short specimen, the angle between the loading area of the specimen hole and the specimen face had to be off from the perpendicular by not more than 0.002 radian. Attachment of the extensometer to the specimen would permit workers in different laboratories to compare results obtained from identical specimens directly and meaningfully.

The small random errors, on the order of 7 μin, in the extensometer calibrations over the test period on the short specimen indicate good stability. A modification of this extensometer that could be considered in the future to facilitate transfer between setups is the incorporation of a lock providing both a fixed initial gage length and fixed reference point on the LVDT.

8. Summary

The SEN long specimen results are in good agreement with the Srawley theoretical stress function solution and with his experimental work on SEN specimens of $L/W = 8/3$. Differences in our experimental stress functions values for the long specimen with the pin assembly free and with it locked in its clevis are small and indicate that the ability of the assembly to move is not important.

The precision of the results obtained on the short specimen would be improved, in our opinion, if the extensometer were attached to the specimen. This practice would also permit workers in different laboratories to compare results obtained from identical specimens directly and meaningfully.

I thank Douglas R. Tate for his many helpful suggestions.

9. References

[1] Srawley, J. E., and Gross, B., Stress-intensity factors for a single-edge-notch specimen by boundary collocation of a stress function, Nat. Aeron. Space Admin. Tech. Note D–2395 (1964).
[2] Houghton, J. R., Voltage ratio detector for millivolt signals, Nat. Bur. Stand. (U.S.) Tech. Note 266 (1965).
[3] Wilson, B. L., Characteristics of the Tuckerman strain gage, Proc. ASTM **44**, 1017 (1944).
[4] Srawley, J. E., and Brown, W. F., Jr., Fracture toughness testing, Nat. Aeron. Space Admin. Tech. Note D–2599 (1965).
[5] Srawley, J. E., Jones, M. H., and Gross, B., Experimental determination of the dependence of crack extension force on crack length for a single-edge-notch tension specimen, Nat. Aeron. Space Admin. Tech. Note D–2396 (1964).
[6] Sullivan, A. M., New specimen design for plane-strain fracture toughness tests, Materials Res. and Stds. **4**, 1, 20–24 (Jan. 1964).

Appendix A

A. 1. Features of the Prototype Extensometer

A prototype extensometer developed at the National Bureau of Standards by J. R. Houghton to meet certain design criteria is shown in figure 8, disassembled. The design criteria are listed in table A.1. An aluminum tube and an aluminum column are the chief structural members. Spring-loaded bearings contact the inside of the tube to guide the lower column and minimize friction during axial motion and limited rotation.

TABLE A.1. *Design Criteria for prototype extensometer*

Sensitivity	1 division per 1 μin (0.025 mm)
Range	0.015 in (0.38 mm)
Gage length	1 to 12 in (25 to 305 mm)
Mechanical amplification factor	1.0
Readout	Electrical

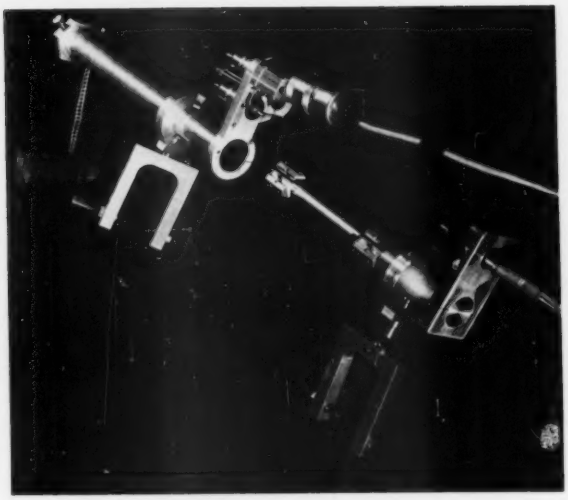

FIGURE 8. *Prototype extensometer disassembled.*

Two linear-variable-differential-transformers (LVDT's) are located at the base of the tube. The LVDT coupled with extensometer motion is mounted so that the core moves with the column while the transformer coil moves with the tube. Small adjustments in the position of this core may be made by means of a micrometer screw. A similar LVDT having a fixed core is mounted adjacent to the displacement-sensing LVDT. The cores of both LVDT's are centered in their transformer bodies by means of flexure plates.

The voltage outputs of the secondary coils of the LVDT's were compared by means of a voltage-ratio detector. This voltage-ratio detector can resolve voltage differences as small as 10 ppm [3].

One set of gage points is mounted on the tube and one set on the column. The gage length may be set from 2 to 12 in without changing the extensometer calibration. The adjustment is made by moving the upper set of gage points up or down the tube.

A. 2. Modification of the Prototype

Houghton modified the prototype extensometer to replace the inner spring-loaded bearing column by a rod supported on flexure plates to provide parallel motion. He designed the present extensometer gage points, adjustable for specimen widths up to 6 in. He also designed the support fixtures that were used for our long specimen.

(Paper No. 74C1&2–297)

JOURNAL OF RESEARCH of the National Bureau of Standards — C. Engineering and Instrumentation
Vol. 74C, Nos. 1 and 2, January-June 1970

Effect of Notch Geometry and Temperature on the Creep–Rupture Behavior of a Titanium Alloy

William D. Jenkins and William A. Willard

Institute for Basic Standards, National Bureau of Standards, Washington, D. C. 20234

(June 9, 1970)

Creep-rupture tests were made on circumferentially notched Ti–8Al–1Mo–1V specimens at temperatures of 600, 800, 1000, and 1200 °F (588, 699, 811, and 921 K) with stresses to produce rupture times ranging from 1 min to several thousand hours. A comprehensive study was made to determine the effects of notch geometry (angle, depth, root radius) on creep, rupture, and ductility characteristics of the alloy. Although a limited first stage and well-defined second and third stages of creep were observed, neither rupture times nor reduction of area values were predictable from extension-time behavior. Rupture time and ductility appeared to be affected more by the initial root radius at the base of the notch than by notch depth. Differences in mechanical behavior between specimens of different notch geometries were less as the temperature was increased or the stress decreased. A limited number of tests indicated that prior strain history had a marked effect on subsequent creep-rupture behavior at 1000 °F.

Relative amounts of alpha and beta constituents, the number of observed internal cracks, and the mode of fracture were affected by notch geometry and test temperatures.

Key words: Creep; elevated temperature; engineering design; notch geometry; stress concentration; stress-rupture; titanium alloy.

1. Introduction

Notch sensitivity of metallic materials is one of the most important factors to be considered in the selection and use of metals in design of engineering components. Notches in metals may, in general, be classified as metallurgical (grain boundaries, precipitates, lattice defects, inclusions, etc.) or geometrical (screw threads, scratches, cracks, dents, etc.). Research at the National Bureau of Standards has been directed towards evaluating the factors influencing the mechanical behavior of metals by using specimens whose notch geometery was known [1, 2, and 3].[1] The majority of the NBS data was obtained from short-time tests at low or elevated temperatures. A number of other researchers have made experiments, designed to evaluate the notch sensitivity of metals in elevated temperature creep-rupture tests, but these have been confined mainly to materials for use in specific products [4]. It is recognized that, at low temperatures, hexagonal close-packed (hcp) metals are less notch sensitive than body-centered cubic (bcc) metals. The phenomenon has been investigated only to a limited extent at elevated temperatures with alloys in which the two structures (hcp and bcc) coexist [4,5]. The purpose of the present research is to study the effects of notch geometry, temperature, and stress on creep behavior, rupture time, ductility, and microstructural changes of a titanium alloy, initially heat-treated to produce an alpha (hcp) and beta (bcc) structure.

[1] Figures in brackets indicate the literature references at the end of this paper.

2. Material, Specimens, and Experimental Procedures

The experimental program consisted of creep-rupture tests at 600, 800, 1000, and 1200 °F (588, 699, 811, and 921 K) on notched cylindrical specimens of a duplex-annealed Ti–8Al–1Mo–1V alloy. This alloy was selected for the research as it is one of the candidate materials for aerospace applications in components used at intermediate temperatures (up to 1000 °F). Furthermore, its short-time tensile notch behavior and long-time creep properties on unnotched cylindrical specimens have been extensively investigated at the National Bureau of Standards [3, 6].

Test specimens were prepared from bars obtained from the same heat of material as that used in the previous investigations. The chemical composition of the alloy is given in table 1.

TABLE 1. *Chemical composition (percentage by weight) of the alloy used* [a]

Titanium	90.4
Aluminum	7.7
Molybdenum	1.0
Vanadium	0.7
Iron	.08
Carbon	.01
Hydrogen	.0094
Oxygen	.0628
Nitrogen	.0022

[a] Analysis made at the National Bureau of Standards.

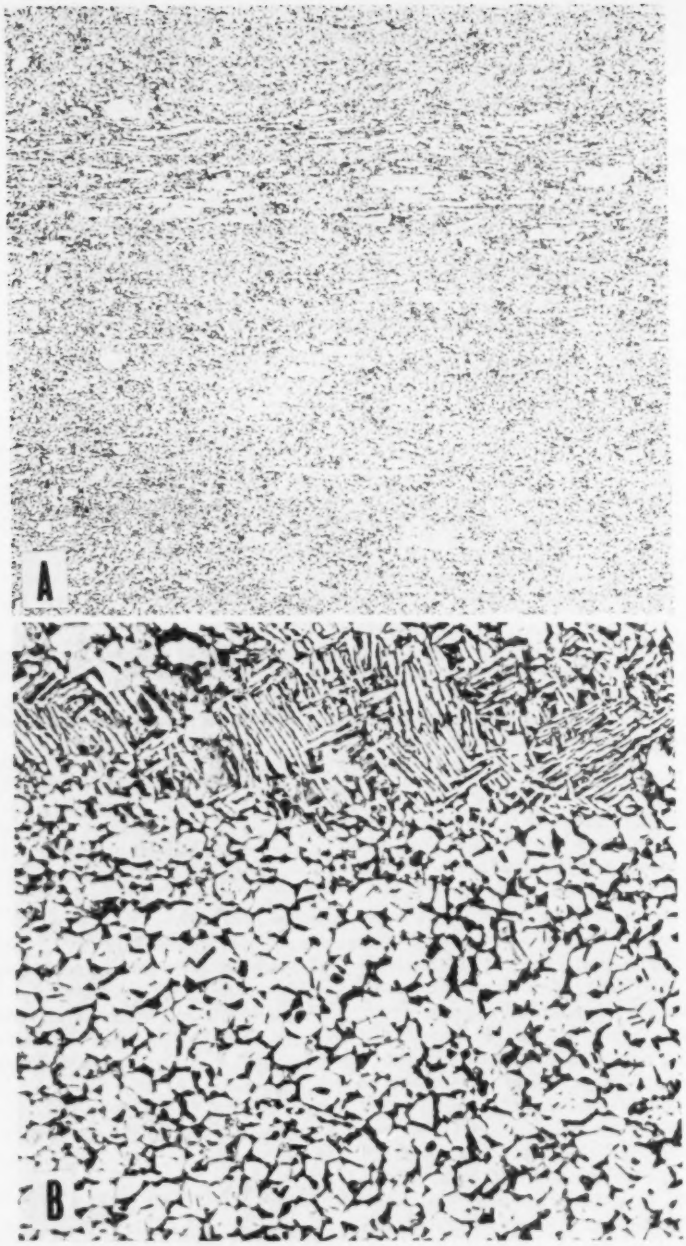

FIGURE 1. *Microstructure of the* Ti–8Al–1Mo–1V *alloy after duplex-annealing.* Longitudinal sections. Etched in a solution containing 3 ml HF, 6 ml HNO_3, and 100 ml H_2O. A, ×100. B, × 500.

Bars were received in the hot-rolled and annealed condition and were cut into 6.5-in lengths before subsequent annealing at 1750 °F (1226 K) for 1 hr, and air cooling. This was followed by a stabilizing anneal at 1050 °F (838 K) for 8 hr. This heat-treatment was used to cause the coexistence of alpha (hcp) and beta (bcc) structures in the alloy as shown in figure 1. The light areas are alpha and the dark areas are beta.

Each of the specimens had a circumferential V-notch. The notch geometries and elastic stress concentration factors [7] of the specimens are shown in table 2. The minimum diameter of each specimen was 0.357 in.

TABLE 2. *Notch geometry and elastic stress concentration factors of specimens used*

Notch angle	Notch depth [a]	Root radius	Elastic stress concentration factors [b]
deg	*%*	*in*	
60	70	0.01	4.2
60	50	.01	3.9
60	50	.5	1.1
Unnotched	–	–	1.0

[a] Notch depth $= \frac{D^2 - d^2}{D^2} \times 100\%$

where D = reduced diameter
d = diameter at root of the notch.

[b] Elastic stress concentration factor is equal to the ratio of the maximum normal stress to the nominal normal stress. It is directly proportional to the notch depth and inversely proportional to the notch angle and root radius.

The numerical values for elastic concentration factors were derived from Peterson [7].

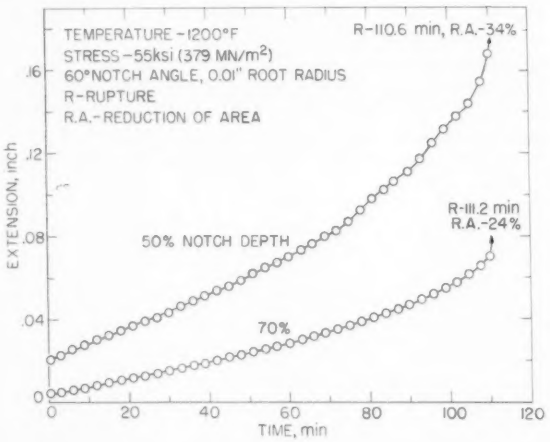

FIGURE 2. *Effect of notch depth on extension-time curves of two specimens tested in creep at 1200 °F (921 K) with a stress of 55 ksi (379 MN/m²).*

Prior to testing, each creep-rupture specimen was heated in air in a tube furnace to the desired temperature and equilibrated at temperature for 16 hr. It was tested at this temperature under constant load in a multi-lever creep-rupture machine equipped with motorized jack to alleviate shock loading. The loading time was 1 to 2 min. Test temperatures were controlled to an accuracy of ± 2 °F. Extension-time data were obtained from electric contact follow-up type extensometers attached to the shoulders of the specimens.

Metallographic examinations were made on selected ruptured specimens to ascertain the effects of notch geometry, temperature, and rupture time on micro- and macrocracking and changes in microstructure.

3. Results and Discussion

Test data obtained in the present investigation are shown in figures 2 through 10. Extension-time curves

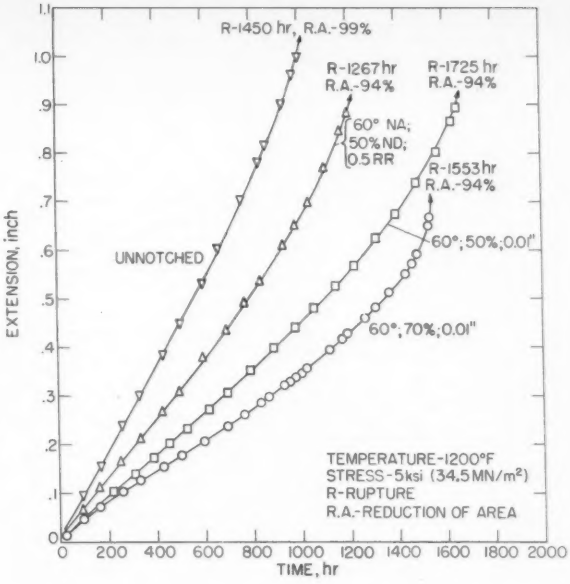

FIGURE 3. *Effect of notch geometry on extension-time curves for specimens tested in creep at 1200 °F (921 K) with a stress of 5 ksi (34.5 MN/m²).*

NA, notch angle in degrees; *ND*, notch depth in percent; *RR*, root radius in inches.

were constructed for all the specimens tested to complete fracture. It was observed that the curves for the notched specimens had the same general shape as those usually associated with creep of unnotched specimens. Each exhibited first stage (decreasing creep rate), second stage (constant rate), and third stage (increasing rate). The first stage is not evident in figures 2 and 3 as it lasted only a very short time as compared to the total test time. As might be expected for tests run at the same temperature and stress, the total strain decreased with increase in notch depth and decrease in root radius. However, as indicated in figures 2 and 3, rupture times and reduction of area values could not be predicted from strain-time data.

A number of investigators [4] have predicted that a linear relation exists between stress-rupture time, stress-log rupture time, or log stress-log rupture time. Data obtained in the present investigation were plotted in each manner, and linear relations were observed only over limited ranges of stresses at each temperature except 600 °F. At this temperature, little or no creep was apparent even at stresses in excess of 95 percent of the short-time tensile strength. Difference in behavior may be due in part to (1) the relaxation of stress concentration at the root radius of the notch as a result of plastic yielding, (2) time at temperature, (3) formation of a compound such as Ti_3Al, or (4) the healing of internal voids. Stress-log rupture time curves for some of the Ti–8Al–1Mo–1V specimens are shown in figure 4. In general, the relative positions of the curves are affected by notch geometry more at low temperatures and high stresses than at high temperatures and low stresses. For example, at 1200 °F and very low stresses, notch geometry appeared to have no

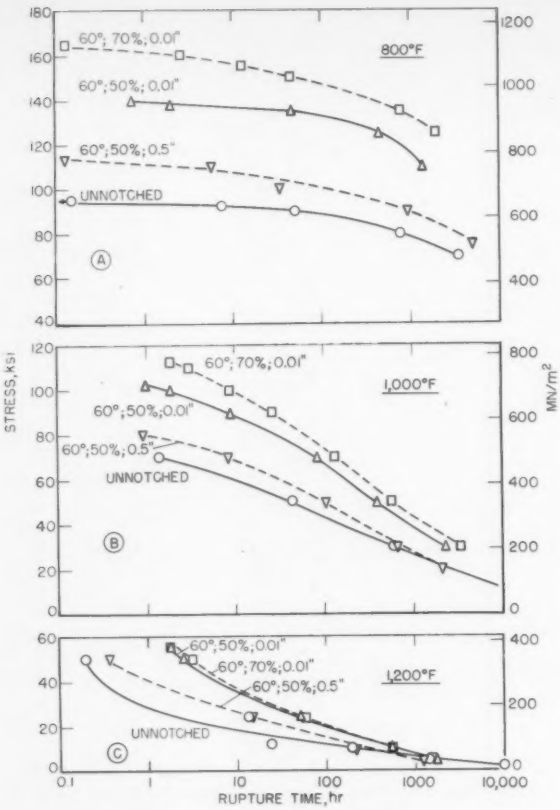

FIGURE 4. *Effect of notch geometry on stress-rupture time relations for specimens tested at 800, 1000, and 1200 °F (699, 811, and 921 K).*

Numbers adjacent to curves indicate notch angle in degrees, notch depth in per cent, and root radius in inches.

effect on the stress-rupture time relations. At 800 °F, an inflection point must occur at stresses below those used in these tests or the stress could be zero for extremely long rupture times. Conversely, at 1200 °F, an inflection point must occur for stresses higher than those shown in figure 4. At 1000 ° F, the inflection points are clearly shown, and the time of their occurrence appears to be affected by notch geometry.

According to elastic theory, root radius has a more dominating influence on the stress concentration at the base of the notch than does the notch depth. The influence of each of these variables on rupture times at different stresses is shown in figures 5 and 6 for the present tests. Although no exact equivalence between notch depth and root radius could be established for the specimens (table 2), each of these variables had a marked effect on the rupture behavior. The effect of each is more apparent at the low temperatures and high stresses than at the high temperatures and low stresses.

Engineering design curves, showing stress-temperature relations to produce rupture of the specimens in 1, 10, 100, and 1000 hr, are presented in figure 7. Within the range of temperatures used in the tests, no inflection points are evident in the 1-hr and 10-hr curves (figs. 7A and 7B). Obviously, these points must occur at higher values of temperature than those used in this investigation or the specimens would have to rupture in 1 or 10 hr at zero stress. As indicated in figures 7C and 7D, the

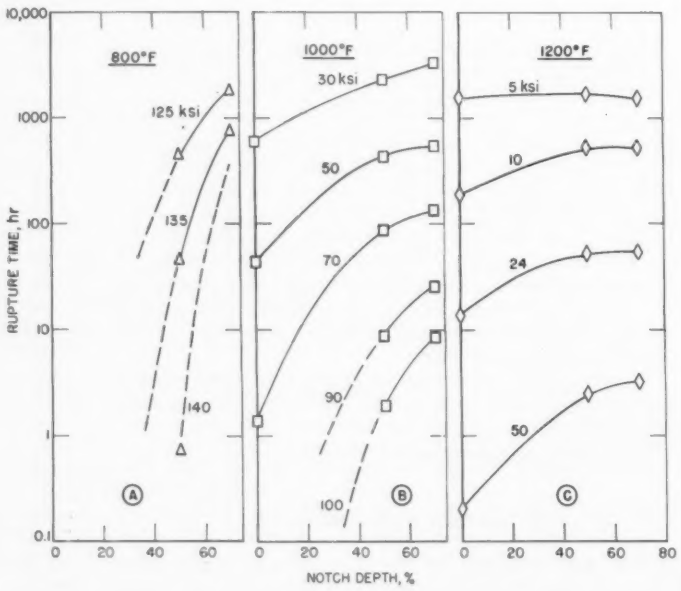

FIGURE 5. *Effect of notch depth on rupture time of specimens tested at different temperatures and with different stresses.*

Dashed curves indicate extrapolated data. Zero notch depth indicates unnotched specimens. Notched specimens have 60° notch angle and 0.01 in root radius.

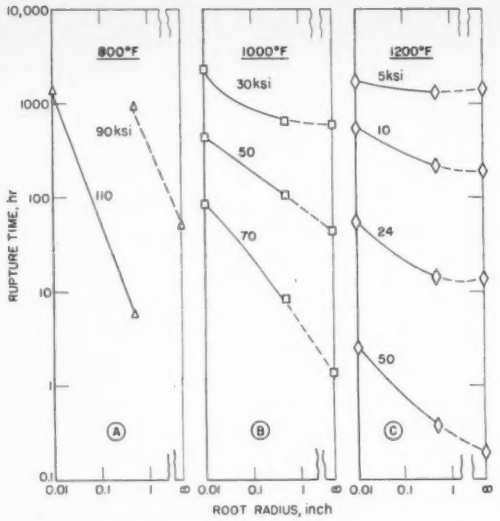

FIGURE 6. *Effect of root radius on rupture time of specimens tested at different temperatures and with different stresses.*
Infinite root radius indicates unnotched specimens. Notched specimens have 60° notch angle and 50 percent notch depth.

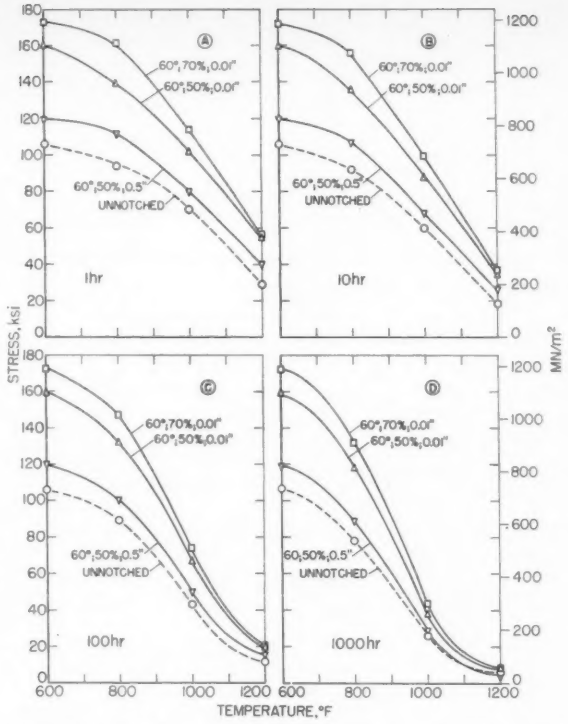

FIGURE 7. *Variation of stress with temperature required to cause rupture at various times, of specimens with different notch geometries.*
Numbers adjacent to curves indicate notch angle in degrees, notch depth in percent, and root radius in inches.

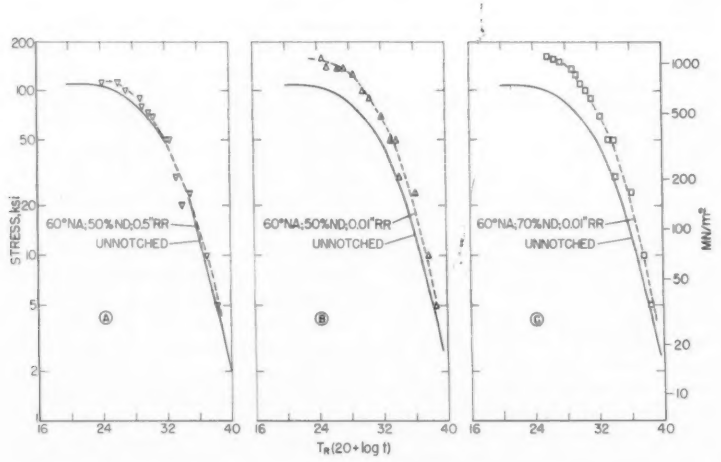

FIGURE 8. *Relation between stress and a temperature-time parameter for specimens having various notch geometries.*
Numbers adjacent to curves indicate notch angle in degrees, notch depth in percent, and root radius in inches.
T_R = temperature in degrees Rankine divided by 1000.
t = rupture time in hours.

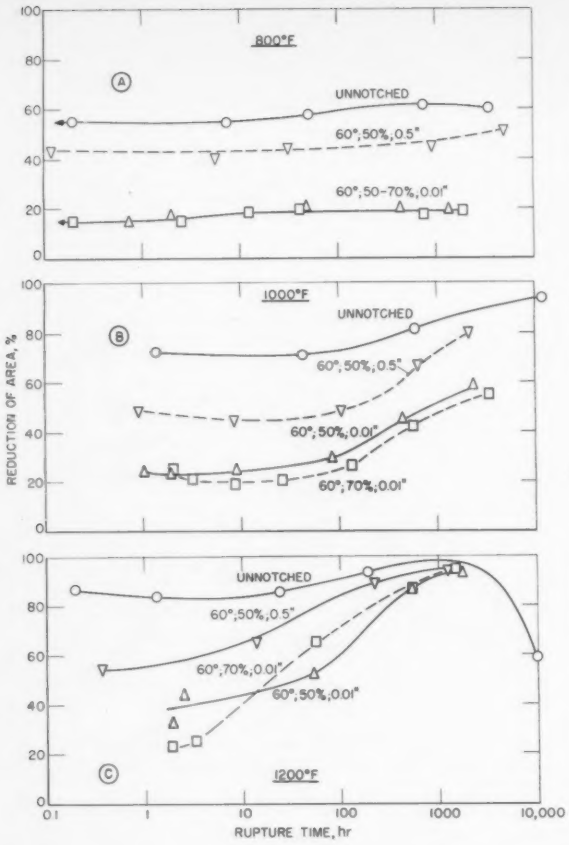

FIGURE 9. *Relation between rupture time and reduction of area values for specimens having various notch geometries and tested at 800, 1000, and 1200 °F (699, 811, and 921 K).*
Numbers adjacent to curves indicate notch angle in degrees, notch depth in percent, and root radius in inches.

occurrence of these inflection points is affected both by notch geometry and test time.

A number of "parametric" expressions have been developed to evaluate creep-rupture data for specific materials over wide ranges of stresses and temperatures [4]. It was previously shown that creep data for the unnotched specimens of this Ti–8Al–1Mo–1V alloy [6] could be described by a single curve. The time-temperature parameter used was derived by Larson and Miller [8]. As shown in figure 8 for the present tests, a single curve can also describe stress-"parameter" relations for each group of notched specimens; however, no simple translation was available to cause all the curves to coincide. The difference in the shape of these curves from those previously shown [6] is due to the fact that the stress values in figure 8 are plotted on a log instead of a linear basis. This method of analysis is recommended for comparing and storing engineering data obtained over wide ranges of test conditions, even though the theoretical significance of the relations is suspect.

The relation between reduction of area values and rupture-time is shown in figure 9. Rupture time had little or no effect on ductility, as defined by reduction of area values, at 800 °F (fig. 9A), whereas a large effect was observed at 1000 and 1200 °F (figs. 9B and 9C). Although, at the latter two temperatures, the ductility appeared to increase with increase in rupture time, inflection points and a reversal in one ductility-time curve are shown. One point at 1200 °F and 1450 hr was omitted for the unnotched curve as it nearly coincided with the notched data. These indicate the possibility of a change in the mode of deformation. Introduction of a notch tended to lower reduction of area values below those of the unnotched specimens. Moreover, decreasing the root radius caused the reduction of area values to decrease even more. However, increasing the notch depth from 50 to 70 percent had little effect on reduction of area.

The influence of prior thermal-strain history on creep-rupture behavior of specimens tested at 1000 °F with a stress of 30 ksi (207 MN/m^2) is shown in figure 10. Although the number of tests are limited, several general observations can be made concerning the effect of prestraining. (1) The rate of extension is significantly changed from that of the unstrained material. (2) Reduction of area values were not seriously affected. (3) Rupture times were decreased by prestraining at temperatures above and below 1000 °F. (4) Prestraining at 1200 °F relieved the stress at the root of the notch to such an extent that the rupture time was increased above that of the metal strained at 800 °F (curves 10B and 10C). This occurred even though the amount of prestraining at 1200 °F was greater than that at 800 °F.

4. Metallography

Metallographic examinations were made on a number of selected specimens after rupturing in creep. Little or no difference in microstructure from that observed in short-time tensile tests [3] was apparent for specimens tested at 600 or 800 °F. This was not totally unexpected since it was indicated, in figure 9 of the present paper, that the reduction of area values for specimens tested at 800 °F were independent of rupture time. Photomicrographs of several specimens tested to rupture at 1000 and 1200 °F are shown in figures 11 through 14. Specimens, shown in figures 11 and 12, were lightly etched to remove any surface effects due to metallographic preparation of the samples. At 1000 °F, increasing the root radius from 0.01-in (figs. 11A and 11B) to 0.5-in (fig. 12A) tended to cause an increase in the number of internal cracks that did not link up to become a part of the main fracture surface. At 1200 °F, however, no significant differences in the number of internal cracks were observed for the specimens even though the increase in elastic stress concentration factor (from 1.1 to 3.9) appeared to cause an increase in the tendency toward surface cracking (figs. 11C and 11D and 12B, 12C, and 12D). Increasing the temperature from 1000 to 1200 °F increased the number and size of cracks in regions away from complete fracture. However, the relation between the number or size of cracks and test time was different at 1000 from that at 1200 °F. At 1000 °F, tendency to form

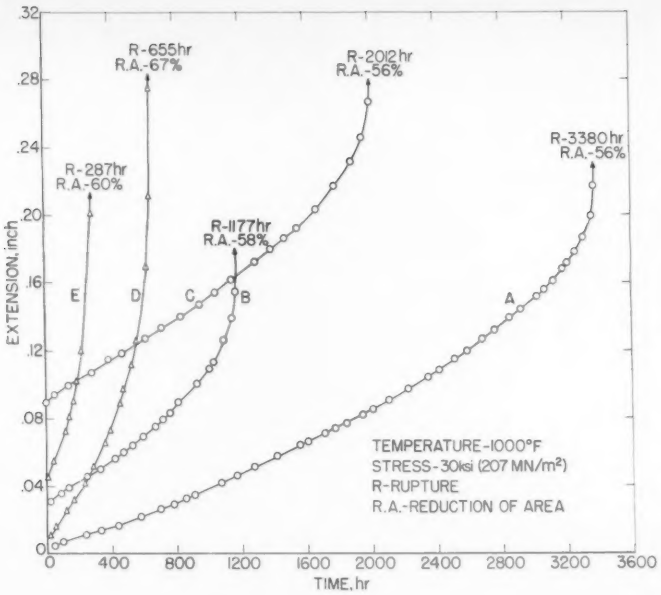

FIGURE 10. *Effect of prior thermal-strain history on extension-time relations of specimens tested at 1000 °F with a stress of 30 ksi (207 MN/m²).*

Curve	Notch angle	Notch depth	Root radius	Prestrain	
				Temp.	Time
	deg	*%*	*in*	*°F*	*hr*
A	60	70	0.01	None	None
B	60	70	.01	800	2350
C	60	70	.01	1200	403
D	60	50	.5	None	None
E	60	50	.5	800	1539

cracks increased with increase in test time (figs. 11A and 11B) while at 1200 °F the opposite was observed (figs. 11C and 11D).

In order to find a solution to some of the anomalies associated with the previous observations, a metallographic examination was made by deep-etching the specimens (figs. 13 and 14), and attempts were made to relate changes in microstructure to changes in mechanical behavior and fracture characteristics of the alloy. Previously, it has been shown that at high temperatures in short-time tensile tests [3] and in some creep tests made by Soltis [9] on another similar alloy that voids could be initiated at alpha boundaries in the vicinty of beta particles. In addition, Seagle and Bartlo [10] have indicated that an intermediate ordered phase (Ti_3Al) can form in titanium alloys containing 5 percent or more of aluminum at temperatures less than 1300 to 1500 °F. They also showed that elongation and short-time tensile strength increased with decrease in cooling rate. As shown in figure 13A for a short-time creep-rupture test, the microstructure appeared to be nearly unchanged from the starting material (fig. 1). Apparently, as the test time was increased, recovery caused a weakening of the grain boundaries and a reduction in the number of beta particles located at the alpha grain boundaries (figs. 13B and 14B). Good ductility, associated with these specimens, can be attributed to relief of stress by plastic deformation at the root of the notches. The presence of some beta and weakening of the grain boundaries could contribute to the increase in the number of internal cracks, previously shown in figures 11 and 12, as the test time was increased. Microstructures of specimens tested at 1200 °F also indicated that the amount of beta decreased as the test time increased (figs. 13C and 13D and 14B, 14C, and 14D). Apparently, an additional reaction also occurs and results in the formation of a new phase (possibly Ti_3Al) at this temperature. The relative amounts of this phase increased with increase in test time and with increase in root radius at the base of the notch (figs. 13 and 14). Decrease in beta and increase in the amount of this new constituent could contribute to increased ductility, a decrease in the number of internal cracks, and the presence of inflection points in the stress-temperature curves.

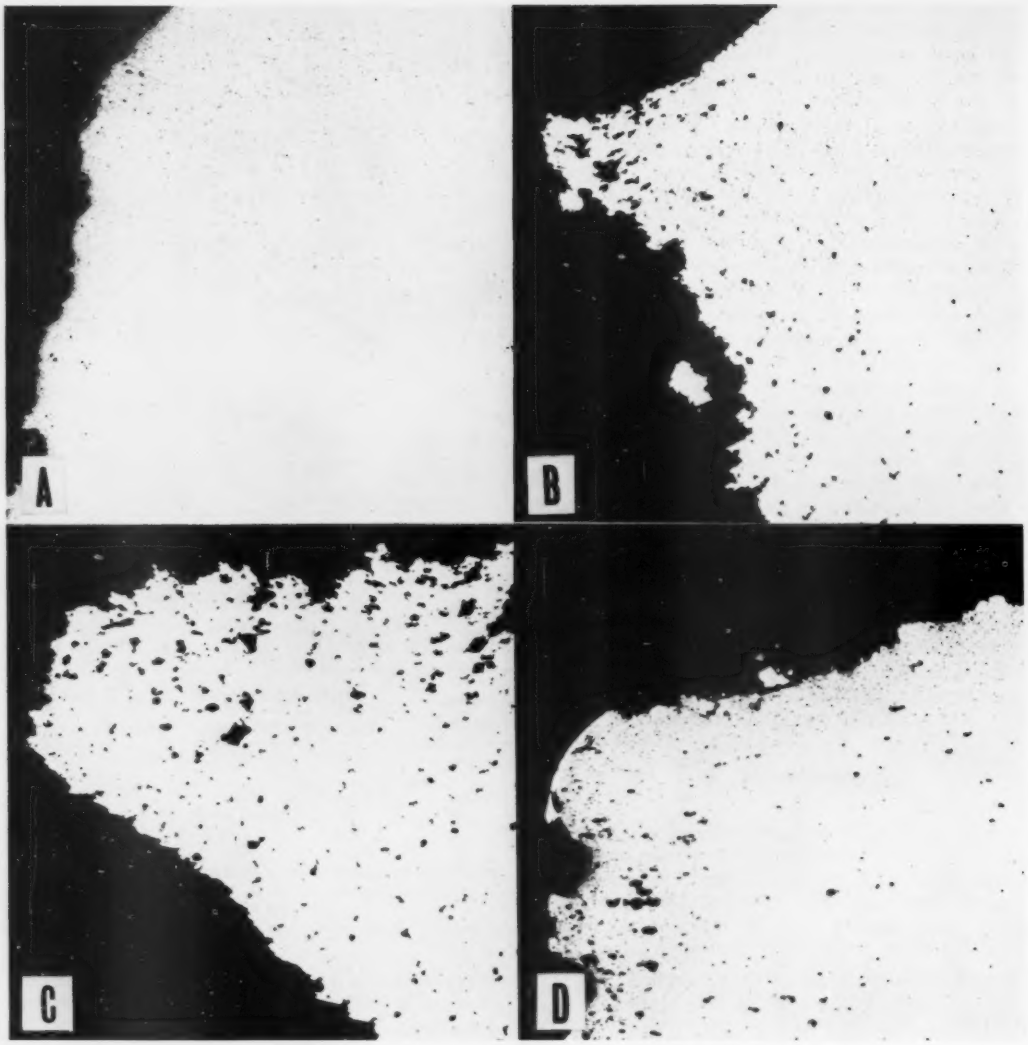

FIGURE 11. *Photomicrographs of sections of fractured specimens after testing to complete rupture in creep.*
Initial notch geometry—60° notch angle, 50 percent notch depth, and 0.01-in root radius. Longitudinal sections near outer surface near fracture. Lightly etched in a solution containing 1.5 ml HF, 3.5 ml HNO_3, and 95 ml H_2O. × 40.

Specimen	Test		Reduction of area
	Temperature	Time	
	°F	*hr*	%
A	1000	9	24
B	1000	2311	58
C	1200	52.5	52
D	1200	1725	94

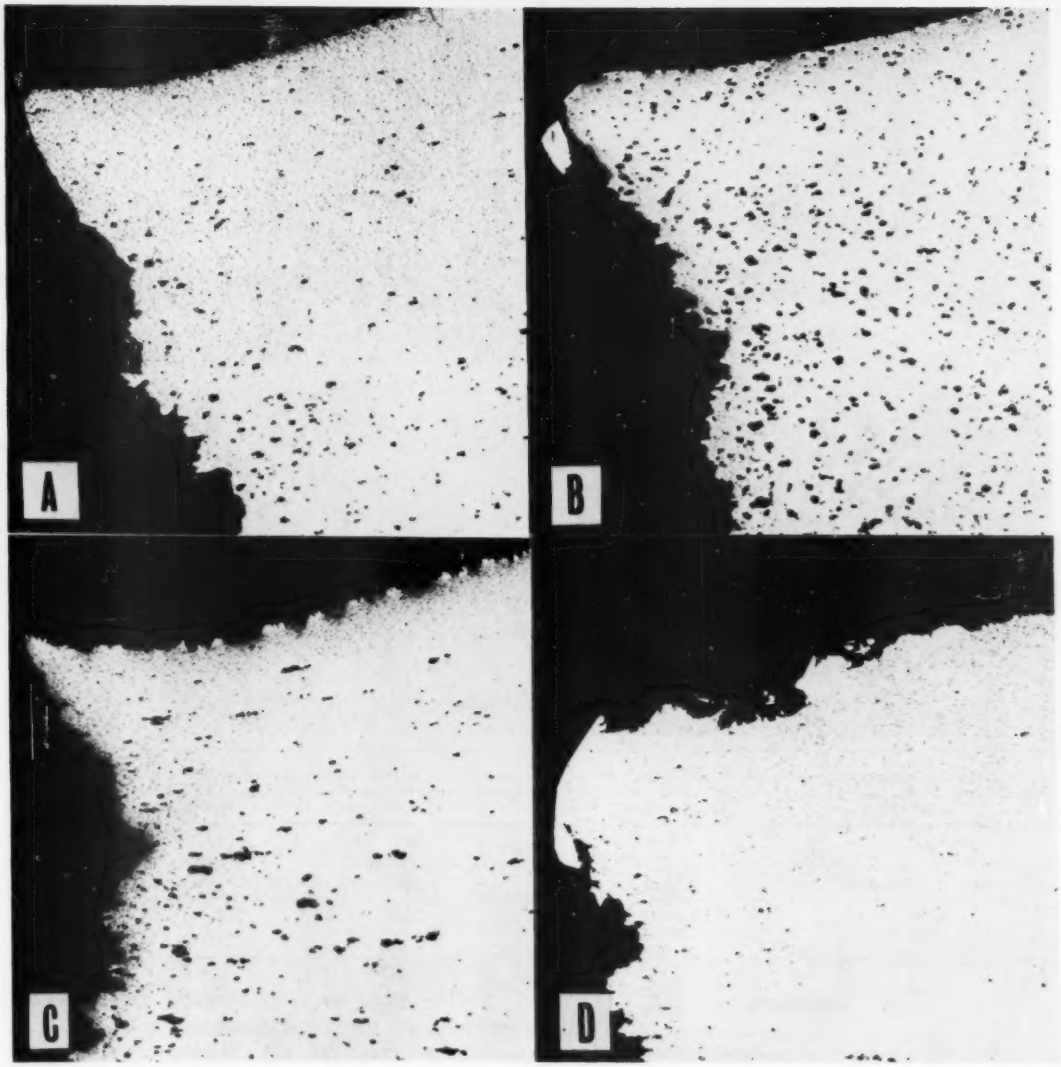

FIGURE 12. *Photomicrographs of sections of fractured specimens after testing to complete rupture in creep.*
Initial notch geometry—60° notch angle, 50 percent notch depth, and 0.5-in root radius. Longitudinal sections near outer surface near fracture. Lightly etched in a solution containing 1.5 ml HF, 3.5 ml HNO_3, and 95 ml H_2O. × 40.

Specimen	Test		Reduction of area
	Temperature	Time	
	°F	*hr*	%
A	1000	655	67
B	1200	14	65
C	1200	222	89
D	1200	1267	94

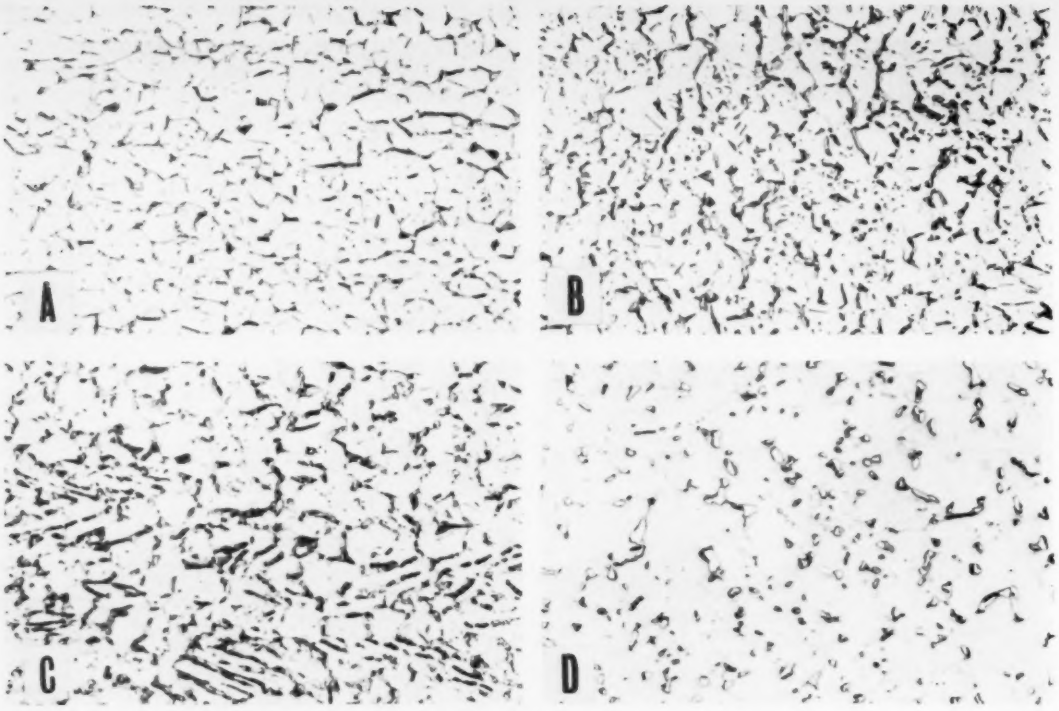

FIGURE 13. *Photomicrographs of sections of fractured specimens after testing to complete rupture in creep.* Initial notch geometry—60° notch angle, 50 percent notch depth, 0.01-in root radius. Longitudinal sections near axis, 0.1 in from fracture. Etched in a solution containing 3 ml HF, 6 ml HNO_3, and 100 ml H_2O. × 500.

Specimen	Test		Reduction of Area
	Temperature	Time	
	°F	*hr*	%
A	1000	9	24
B	1000	2311	58
C	1200	52.5	52
D	1200	1725	94

5. Summary

A. Creep-rupture tests were made to determine the effects of notch geometry on the creep-rupture behavior of duplex-annealed Ti–8Al–1Mo–1V alloy at temperatures of 600, 800, 1000, and 1200 °F (588, 699, 811, and 921 K).

B. When specimens were tested at the same temperature and stress, the total extension at any given time decreased with increase in notch depth and with decrease in root radius. However, no accurate predictions of rupture time or reduction of area values could be made on the basis of extension-time data.

C. The slopes of the stress-log rupture time curves decreased with decrease in stress at 800 °F, whereas the opposite behavior was observed at 1200 °F. At 1000 °F, inflection points in the curves were observed at intermediate stresses.

D. At constant load, rupture times generally increased with increase in notch depth and decrease in root radius. This phenomenon was more apparent at high stresses and low temperature than at low stresses and high temperatures.

E. The elastic stress concentration factor was a consistent index for predicting rupture times.

F. The shape of the "engineering design" curves indicate that extrapolations should not be made to temperatures higher than those used in determining stress-temperature relations.

G. A single curve was used to describe the stress temperature, rupture-time relations for each group of specimens having the same notch geometry. However, no single curve could describe all the data.

H. With few exceptions, reduction of area values increased with increase in temperature and decrease in elastic stress concentration factor.

I. Creep-rupture behavior was markedly affected by prior strain history.

J. Microstructures of specimens after fracture were greatly influenced by initial notch geometry and test conditions. Decrease in the amounts of beta structure and the formation of a compound (probably Ti_3Al) was evident in microstructures of specimens tested at 1200 °F. The amount of the compound increased and the number of internal cracks decreased as the rupture time increased.

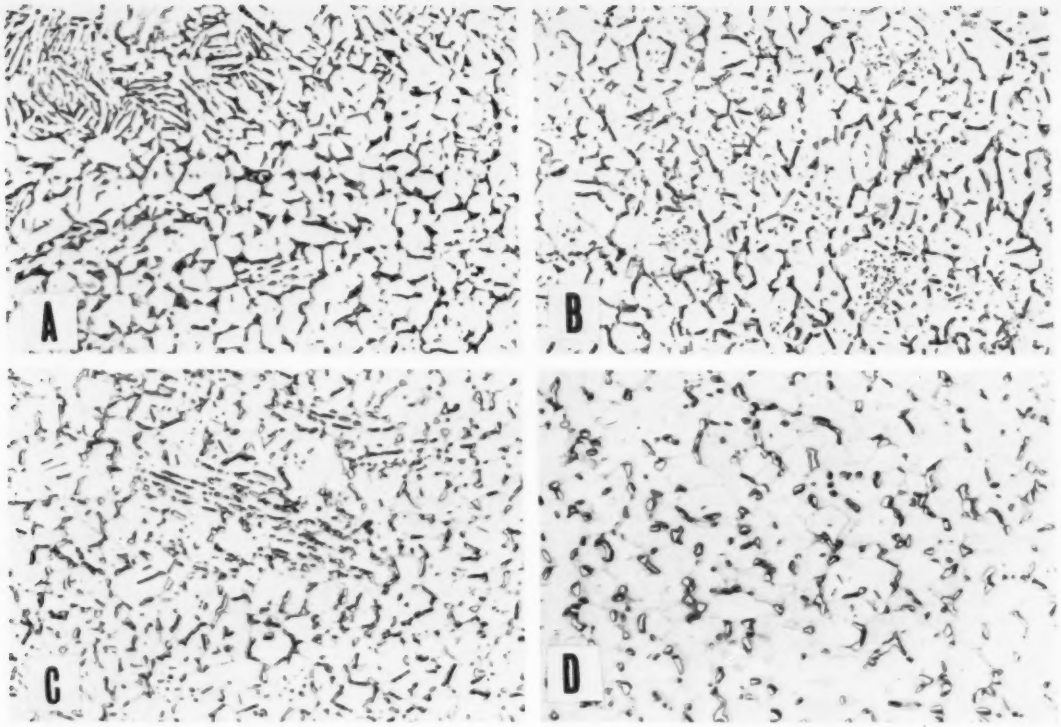

FIGURE 14. *Photomicrographs of sections of fractured specimens after testing to complete rupture in creep.*
Initial notch geometry—60° notch angle, 50 percent notch depth, 0.5-in root radius. Longitudinal sections near axis, 0.1 in from fracture. Etched in a solution containing 3 ml HF, 6 ml HNO_3, and 100 ml H_2O. × 500.

Specimen	Test		Reduction of area
	Temperature	Time	
	°F	*hr*	%
A	1000	655	67
B	1200	14	65
C	1200	222	89
D	1200	1267	94

The authors gratefully acknowledge the helpful discussions with G. W. Geil and the excellent technical assistance of D. E. Harne and L. C. Smith during this investigation.

6. References

[1] Geil, G. W., and Carwile, N. L., Effect of notch geometry on tensile properties of annealed titanium at 100, 25, −78, and −196°C, Proc. Am. Soc. Testing Materials **59,** 985 (1959).

[2] Geil, G. W., and Carwile, N. L., Fracture characteristics of notched tensile specimens of titanium and a titanium alloy, Materials Res. and Stds. **1,** No. 1, 16 (1961).

[3] Jenkins, W. D., and Willard, W. A., Effect of temperature and notch geometry on the tensile behavior of a titanium alloy, J. Res. Nat. Bur. Stand. (U.S.) **70C** (Eng. and Instr.), No. 1, 5 (Jan.–March 1966).

[4] Joint International Conference on Creep, New York and London, 1963 Papers, Inst. Mech. Engrs. (1963).

[5] ASM Metals Eng. Q. **8,** No. 3 (Aug. 1968).

[6] Jenkins, W. D., and Willard, W. A., Creep-rupture properties of Ti–8Al–1Mo–1V alloy, J. Res. Nat. Bur. Stand. (U.S.) **72C** (Eng. and Instr.), No. 2, 167 (Apr.–June 1968).

[7] Peterson, R. E., Stress Concentration Design Factors, (John Wiley & Sons, Inc., New York, N. Y. (1953)).

[8] Larson, F. R., and Miller, J., A time-temperature relationship for rupture and creep stresses, Trans. Am. Soc. Mech. Engrs. **74,** 765 (1952).

[9] Soltis, P. J., Instability and evidence of ordering in Ti–8Al–1Mo–1V alloy, Trans. Met. Soc. AIME **233,** 903 (1965).

[10] Seagle, S. R., and Bartlo, L. J., Physical metallurgy and metallography of titanium alloys, Met. Engr. Quart. **8,** 1 (1968).

(Paper No. 74C1&2–298)

JOURNAL OF RESEARCH of the National Bureau of Standards — C. Engineering and Instrumentation
Vol. 74C, Nos. 1 and 2, January-June 1970

Publications of the National Bureau of Standards*

Selected Abstracts

Astin, A. V., **Management and the metric system,** *Defense Management J.* **5,** *No. 2, 27–34 (1969).*

Key words: Accommodation; adaptation conversion; customary units (U.S.); economic costs; interchangeability; international cooperation; metric system; SI units.

A decision on whether or not the United States will convert to the metric system may be facilitated by a current Congressionally authorized study of the problem, described here by NBS Director Astin. Scientific, military, industrial, economic, trade, and educational considerations are discussed in detail, with illustrative material drawn from the experience of U.S. industries as well as those in foreign countries. Attention is focused on three kinds of interaction which would be involved in a metric changeover: accommodation, adaptation, and conversion.

Arp, V., **Properties and preparation of high-purity aluminum,** *Proc. 1968 Summer Study on Superconducting Devices and Accelerators, Brookhaven National Laboratory, Upton, N. Y., June 10–July 19, 1968, Part III, BNL 50155 (C–55), pp. 1095–1114 (Clearinghouse for Federal Scientific and Technical Information, Springfield, Va., Apr. 1969, $3.00).*

Key words: Aluminum; resistivity; impurity; skin effect; thermal conductivity.

The potential economy of using aluminum magnets operating at cryogenic temperatures was suggested by Post and Taylor in 1959, before the advent of high field superconductivity. A liquid hydrogen-cooled aluminum magnet was built and operated not long thereafter (Purcell and Payne, 1963), but by this time superconducting magnets seemed to be generally more attractive. Nevertheless, a small effort was carried on, since for some low duty cycle conditions aluminum appears to be more attractive than superconductors (Arp, 1965). We have continued a study of the properties of aluminum which are related to this type of application, and a major part of this paper summarizes this study and knowledge in a tutorial fashion. The final and minor section of the paper reports the current status on the availability of high-purity aluminum in technologically useful quantities.

Bates, R. G., Editor, **Electrochemical Analysis Section, summary of activities July 1968 to June 1969,** *Nat. Bur. Stand. (U.S.), Tech. Note 503, 99 pages (Aug. 1969), $1.00.*

Key words: Acidity; analysis; conductivity; electrochemical analysis; electrochemistry of solutions; ionic activity; ion-selective electrodes; pD measurements; pH measurements; medium effects; solvent effects; standard reference materials.

This survey of the activities of the Electrochemical Analysis Section, Analytical Chemistry Division, covers the period July 1968 to June 1969. An attempt is made to summarize a year's progress on the technical projects of the Section, to indicate the composition and capabilities of the unit as a whole, and to stress the Section's role in the mission of the Institute. Brief summaries of several lines of work under way are given. The concept of a broad program on acidity measurements is outlined, and new efforts to provide assistance in clinical acid-base measurements are summarized. Progress toward reference standards for the calibration of ion-selective electrodes is reported. Equilibrium data for phosphoric acid in heavy water, for piperazinium ion in 50 wt % methanol-water, and for hydrochloric acid in a solvent composed of 2-methoxyethanol (80 wt %) and water (20 wt %) have been obtained. Considerable effort has been devoted to the development of new standard reference materials, including standards for conductivity measurements. Lists of publications, talks, and committee assignments of staff members are given.

Bates, R. G., **Inner reference electrodes and their characteristics, Chapter in Glass Microelectrodes,** Lavallee, M., Schanne, O. F., and Hebert, N. C., Eds., pp. *1–24 (John Wiley & Sons, Inc., New York, N.Y., 1969).*

Key words: Glass electrode; inner solutions; pH measurement calomel electrode; reference electrodes; silver-silver chloride electrode; temperature coefficients of e.m.f.

The principles governing the selection of the most suitable electrodes and inner solutions for making electrical contact with the reference side of the glass electrode are set forth. Particular attention is given to choice of the best electrode and solution composition to minimize, or even to nullify, the temperature variation of the standard e.m.f. of the pH cell. Temperature coefficients of the e.m.f. of glass electrode pH cells of various designs are listed and other useful characteristics of inner electrodes and inner solutions are summarized.

Bates, R. G., **Medium effects and pH in nonaqueous solvents, Chapter in Solute-Solvent Interactions,** Ritchie, C. D., and Coetzee, J. F., Eds., *pp. 45–96 (Marcel Dekker Inc., New York, N. Y., 1969).*

Key words: Acidity; pH; medium effect; nonaqueous solvents; ion activity; thermodynamics.

The nature of acidity in nonaqueous solvents of various types is discussed and the implications of acid-base behavior on the feasibility of establishing useful scales for experimental pH and acidity measurement are considered. The Brønsted concept provides a useful approach to the quantitative expression of acid-base potential in many solvent media with some acidic or basic character but is of doubtful value in aprotic or inert solvents. A general scale of acidity or electrode potential applicable to more than one solvent requires a knowledge of the medium effect of the proton or the free energy of transfer of the proton from one solvent to another. Various methods of determining medium effects for ions are considered and shown to be inadequate at the present time. The role of dielectric constant and solvation phenomena in the medium effect are discussed, and suggestions are made for the practical measurement of acidity in deuterium oxide and alcohol-water solvents.

Berger, M. J., Seltzer, S. M., Chappell, S. E., Humphreys, J. C.,

Motz, J. W., **Response of silicon detectors to monoenergetic electrons with energies between 0.15 and 5.0 MeV,** *Nucl. Instr. Methods* **69,** *No. 2, 181–193 (Apr. 1969)*

Key words: Detector response function; electron absorption; electron backscattering; electron transmission; silicon transmission detector.

By means of measurements as well as Monte Carlo calculations, response functions have been obtained which describe the pulse-height distributions produced by monoenergetic electrons incident perpendicularly on silicon detectors. Generally good agreement has been found between experimental and Monte Carlo results at energies of 0.25, 0.50, 0.75, and 1.00 MeV for detectors with thicknesses of 0.061, 0.105, 0.191, 0.530, 1.0, and 3.0 mm. Additional calculated results have been obtained as follows: (1) response functions at fifteen energies between 0.15 and 5.0 MeV for detectors with ten thicknesses between 0.05 and 10.0 mm; (2) response functions for arrangements in which the silicon detector is shielded partially or completely by other detectors operating in anticoincidence; (3) reflection, transmission and absorption coefficients of electrons for plane-parallel silicon targets.

Berger, M. J., Seltzer, S. M., Chappell, S. E., Humphreys, J. C., Motz, J. W., **Table of response functions for silicon electron detectors,** *Nat. Bur. Stand. (U.S.), Tech. Note 489, 62 pages (Aug. 1969), 60 cents.*

Key words: Electron; energy absorption; electron back-scattering; electron transmission; detector response function; silicon detectors.

Calculated response functions are presented which describe the pulse-height distributions produced by monoenergetic electrons incident on silicon detectors. It is assumed that the direction of incidence is perpendicular, and that the detectors are wide enough so that lateral leakage of energy is insignificant. The validity of the calculations has been confirmed experimentally for incident energies between 0.25 MeV and 1.0 MeV and detectors with thicknesses between 0.061 mm and 3.0 mm. The calculated response functions cover a wider range of conditions, including fourteen energies between 0.15 MeV and 5.0 MeV and ten detector thicknesses between 0.05 and 10.0 mm. At energies $\geq$ 1 MeV, response functions are given not only for bare detectors but also for an arrangement in which the detectors are shielded on the transmission side by another detector operating in anti-coincidence.

Blanford, J. M., Bensing, P. L., **Book, Testing Programs for the Apparel Industry. Evaluation of Material and Components,** *Part I, 31 pages (Oct. 1, 1968); Part II, 222 pages (Apparel Research Foundation, Inc., Washington, D. C., Oct. 1, 1968).*

Key words: Apparel materials; equipment; fabric defects; fabrics; physical properties; programs; test methods; testing equipment; textile; textile equipment; textile testing.

This publication presents the details of minimum, intermediate, and advanced textile testing programs for evaluating the appearance and performance properties of materials and components used by the apparel industries. Tabulations give testing equipment, properties its use may determine, testing procedures and evaluation materials employed, and sources of supply and approximate prices of the equipment and evaluation materials.
Included are: 1). sections on the significance of a textile testing program, conditioning for testing textiles, performance requirements for textile fabrics ((USA) Standard L22), and the availability of short laboratory training courses for apparel company employees; 2). reprints of the fifty-nine referenced test methods.

Boone, T. H., Skoda, L. F., Cullen, W. C., **Laboratory-field comparisons of built-up roofing membranes,** *Roofing Siding Insul. Mag.* **46,** *No. 4, 28–33 (Apr. 1969).*

Key words: Bituminous adhesive; bituminous built-up membranes; engineering properties; laboratory-field comparison; strength-thickness.

The values of breaking load, elongation and thermal expansion of nine bituminous built-up membranes prepared by roofing contractors under field conditions and by technicians in the laboratory were measured at subfreezing temperatures. The data indicated that the field-prepared specimens agreed favorably with laboratory-prepared specimens, although the samples from the field frequently reflected higher values for thermal-shock resistance than did their laboratory-prepared counterparts. The higher values were attributed to the smaller amounts of bitumen used between the plies of the field specimens. The results appeared to support the validity of the application of the "strength-thickness rule" to bituminous built-up membranes.

Bowen, R. L., Cleek, G. W., **X-ray-opaque reinforcing fillers for composite materials,** *J. Dental Res.* **48,** *No. 1, 79–82 (Jan.–Feb. 1969).*

Key words: Barium fluoride; composite materials; dental restorations; refractive index; reinforcing fillers; x-ray opaque.

Clear, colorless glasses designed for use as part of the reinforcing fillers for composite dental restorative materials were prepared. They were formulated by melting together materials such as silica, boric oxide, alumina, barium oxide, and barium fluoride. Barium made the glasses radiopaque, fluoride lowered the refractive index, and alumina tended to stabilize the glasses.

Broadhurst, M. G., **The dielectric properties of leaves, sticks, and dirt at radio and microwave frequencies,** *Proc. 1968 Annual Report Conf. Electrical Insulation and Dielectric Phenomena, Oct. 21–23, 1968, Buck Hill Falls, Pa., pp. 146–152 (Natl. Acad. Sci.-Natl. Res. Council, Washington, D. C., 1969).*

Key words: Dielectric constant; dielectric loss; dielectric measurements; soil, vegetation.

The dielectric constant and loss of a variety of fresh leaves were measured at room temperature from 0.1 MHz to 4.2 GHz. A water displacement method was used with a single thickness of leaf in a coaxial line. Capacitance and conductance were determined with a bridge up to 250 MHz and a slotted line above 250 MHz. The leaf is a high admittance shunt in the line and both the real and imaginary components of the admittance could be measured within a few percent accuracy. The accuracy of the dielectric constant and loss values is limited to about 10% mainly by uncertainties in the sample thickness measurements. The main features of the data are a Maxwell-Wagner type relaxation at about 10 MHz with a tan δ maximum of about 2. Both κ' and κ'' rise to about 10,000 at 0.1 MHz with a second relaxation at lower frequencies apparent in the tan δ curve. About 100 MHz, κ' levels off at about 50 and above 10^9 Hz a third relaxation—presumably due to the dipolar relaxation in water—appears. The results are surprisingly consistent among all varieties of leaves measured. Measurements were also made with reduced precision on twigs and clay at various moisture contents. The measurement techniques, and evaluation of errors of the method will be described together with the data.

Brower, W. S., Robbins, C. R., **Growth of $CaTiSiO_5$ by the Czochralski method,** *J. Crystal Growth* **5,** *233–234 (1969).*

Key words: $CaTiSiO_5$; crystal growth; Czochralski method; single crystals.

Crystals of $CaTiSiO_5$ suitable for physical property measurements have been grown by the Czochralski method. Best results were obtained with relatively high rotation rates (100–150 rpm) and a linear growth rate of 0.15 cm/hr. The crystals are monoclinic with space group $P2_1/n$, the symmetry previously observed for anhydrous synthetic $CaTiSiO_5$, as compared with space group $C2/c$ reported for natural sphene (titanite) minerals of general formula $CaTiSiO_4(O,OH,F)$.

Brown, P. J., **Human factors research in motor vehicle occupant restraint systems,** *IEEE Trans. Man-Machine Systems* **MMS–9,** *No. 3, 88–89 (Sept. 1969).*

Key words: Highway safety; human factors research; motor vehicle restraint; systems highway safety.

The national program in highway and motor vehicle safety has provided a new stimulus to human factors research by agencies of

the Federal Government. An important area included in their list was the protection of occupants of a motor vehicle from injury during a crash. This paper will describe some results of human factors research in motor vehicle occupant restraint systems by the Office of Vehicle Systems Research in the National Bureau of Standards.

Bullis, W. M., Editor, **Methods of measurement for semiconductor materials, process control, and devices. Quarterly report January 1 to March 31, 1969,** *Nat. Bur. Stand. (U.S.), Tech. Note 488, 44 pages (July 1969), 50 cents.*

Key words: Carrier lifetime; die attachment; electrical properties; gamma detectors; germanium; gold-doped silicon; indium antimonide; metallization; methods of measurement; microelectronics; nuclear radiation detectors; resistivity; semiconductor devices; semiconductor materials; semiconductor process control; silicon; thermal resistance; thermographic measurements; wire bonds.

This quarterly progress report, third of a series, describes NBS activities directed toward the development of methods of measurement for semiconductor materials, process control, and devices. Principal emphasis is placed on measurement of resistivity, carrier lifetime, and electrical inhomogeneities in semiconducting crystals; evaluation of wire bonds; and measurement of thermal properties of semiconductor devices. Other tasks involve: study of infrared measurement methods, deep-lying impurities in InSb, gold in silicon, and high field effects; establishment of a processing facility; evaluation of aluminum metallization and wafer die attachment; review of NASA measurement methods; and measurement of Hall effect in semiconductor crystals, second breakdown in transistors, and noise in microwave diodes. Related projects on silicon nuclear radiation detectors and specification of germanium are also described. Supplementary data concerning staff, committee activities, technical services, and publications are included as appendixes.

Cameron, J. M., **The statistical consultant in a scientific laboratory,** *Technometrics* **11,** *No. 2, 247–254 (May 1969).*

Key words: Consulting; statistical consultation; statistics.

The responsibilities of the statistical consultant who is a regular staff member of a scientific institution are discussed. The effects of the continuing nature of his association with the organization, and of the fact that extended collaboration with the individual scientists is the rule, not the exception, are described. The importance of the statistician's educational role in providing lectures, courses, manuals, etc., which are tailor made for the needs of his organization is emphasized, along with the duty to provide computer aids for statistical analysis and data handling designed for the convenience of the using scientist.

Chang, S. S., **Switch arrangement and power averaging in constant current calorimetric heating,** *Rev. Sci. Instr.* **40,** *822–825 (1969).*

Key words: Constant current power supply; calorimetry; energy measurement; power averaging; switch contact arrangement; transient.

In order to minimize the transient effect associated with switching a constant current power supply to different loads, a break-before-make type of switch contact arrangement is shown to be preferable to a make-before-break type of arrangement. Series resistance in the load circuit may be required for low current applications.
With a constant heater current, the average heater power for the entire heating period can be precisely determined as the product of the current and the mean value of two particular potential readings. These two readings, symmetrical about the mid-point of the heating period, should be taken at specified intervals as determined by the exponential heat conduction characteristics of the calorimeter assembly.

Christ, B. W., Giles, P. M., **On the detection of retained austenite in high-carbon steels by Fe^{57} Mössbauer spectroscopy, with appendix,** *Trans. Met. Soc. AIME* **242,** *1915–1925 (Sept. 1968).*

Key words: Chemical shift; hyperfine peaks; Mössbauer spectra; 10105 steel; retained Austenite; singlet center peak; x-rays.

Mössbauer effect measurements have been made on 1-mil-thick foils of commercial 1 wt pct C steel and Fe-2 wt pct C alloy. The experimental method required about 3 to 5 vol pct of a phase in the multiphase steel sample for detection. Room-temperature Mössbauer patterns obtained on austenitized and quenched samples exhibit fifteen, and possibly twenty-one, lines. A sharp paramagnetic singlet and a quadrupole doublet, poorly resolved from the singlet, are attributed to austenite. Remaining lines are due to martensite. Accurate evaluation of austenite line parameters is not feasible if significant amounts of other phases such as carbides or martensite occur simultaneously with austenite. This is demonstrated by comparison of hyperfine interactions determined for austenite in multiphase high-carbon samples with those reported for Fe-C austenite in a nearly 100 pct austenitic sample. Lines from carbides are incompletely resolved from austenite lines, as demonstrated by comparison of austenite line positions with carbide line positions calculated from published values of hyperfine interactions. One martensite line overlaps an austenite line in the pattern for commercial 1 wt pct C steel. Results of this study suggests that the usefulness of Fe^{57} Mössbauer spectroscopy for quantitative analysis of austenite in bulk samples of quenched and tempered high-carbon steels is restricted by poor resolution. Use of Mössbauer spectroscopy for phase identification and for evaluation of atomic and electronic structures appears quite feasible.

CODASYL COBOL, Journal of Development 1968, *Nat. Bur. Stand. (U.S.), Handb. 106, 344 pages (July 1969), $2.75.*

Key words: COBOL; CODASYL; journal.

This document is a report to the COBOL community from the Conference on Data Systems Languages (CODASYL) Common Business Oriented Language (COBOL) Programming Language Committee. It is an official report documenting the development activities of CODASYL through July 1968.

Coleman, J. A., Love, D. P., Trainor, J. H., Williams, D. J., **Effects of damage by 0.8 MeV–5.0 MeV protons in silicon surface-barrier detectors,** *NASA Rept. No. x-611-68-221, 38 pages (National Aeronautics and Space Administration, Goddard Space Flight Center, Greenbelt, Md., June 1968).*

Key words: Detector; proton; semiconductor; silicon.

Changes in the performance of silicon surface-barrier detectors after irradiation with protons at energies between 0.80 MeV and 5.00 MeV have been investigated for fluences up to 10^{17} protons cm^{-2}. Irradiations of the front, surface-barrier contacts and the rear, ohmic contacts of these transmission detectors were performed. In general, the detector current and noise increased with fluence. When the rear, ohmic contact was irradiated with protons which stopped within the detector, the changes in the current and noise after irradiation were several orders of magnitude smaller than after a similar irradiation of the front contact. For protons with energies greater than about 1 MeV, the detector capacitance decreased at low reverse biases and increased at high biases with increasing fluence. The results indicate that a significant reduction in the increase of detector current and noise can be obtained if the density of radiation-produced defects in the region of the junction is minimized.

Coriell, S. R., Hardy, S. C., **Morphology of unstable ice cylinders,** *J. Appl. Phys.* **40,** *No. 4, 1652–1655 (Mar. 1969).*

Key words: Crystal growth; cylinder; ice; morphological stability; morphology; water.

The wavelengths of sinusoidal perturbations in the shape of ice cylinders growing in supercooled water have been measured as a function of the experimental variables, primarily bath supercooling. The experimental results are in good agreement with theory.

Cutkosky, R. D., **A varactor null detector for audio frequency capacitance bridges,** *IEEE Trans. Instr. Meas.* **IM–17,** *No. 4, 232–238 (Dec. 1968).*

Key words: Audio amplifier; capacitance bridge detector; noise reduction; null detector; parametric amplifier; varactor amplifier.

A two-varactor, double sideband up-converter pumped at 30 MHz has been constructed. Operated at room temperature with a signal frequency of 10^4 radians per second, the device has an optimum source resistance of 10^5 ohms and a minimum noise figure of 0.01 dB. Immersed in liquid N_2, minimum noise figures below 0.001 dB referred to a room temperature source have been measured. The device is particularly useful as a null detector for audio frequency capacitance bridges. At 10^4 radians per second, a signal current of 10^{-14} A through a capacitance of 1000 pF can be detected in less than one second with this instrument. Techniques for suppressing microphonics and other extraneous sources of noise are described.

Deslattes, R. D., Paretzkin, B., **A small set of reference crystals for double-crystal topography,** *J. Appl. Cryst.* **1,** *Part 3, 176–178 (Sept. 1968).*

Key words: Crystal perfection; silicon; topography.

A set of six reference crystals of silicon with planes ranging from 220 to 422 makes possible double crystal topography in the grating space range of 1–2 Å with Cu $K\alpha_1$ radiation.

DeRis, J. N., **Spread of a laminar diffusion flame,** *Proc. Conf. Twelfth Symp. (International) on Combustion, Poitiers, France, July 17, 1968, pp. 241–252 (Combustion Institute, Pittsburgh, Pa., 1969).*

Key words: Combustion; conduction; diffusion flames; flame spread; heat transfer; integral equations; mass transfer; radiation; reaction kinetics; thermal properties.

This work considers the problem of a gas-phase laminar diffusion flame spreading against the wind over a solid or liquid fuel bed. Both a thin sheet and a semi-infinite fuel bed are considered. The burning process is described as follows. The hot flame heats the unburnt fuel bed, which subsequently vaporizes. The resulting fuel vapor reacts with the oxygen supplied by the induced air; thus producing the heat which maintains the flame spreading process.

A simplified model is formulated and subjected to mathematical analysis. This model treats the combustion as a diffusion flame for which the reaction kinetics can be ignored. The model includes the effects of gas-phase chemical combustion, gas-phase conductive heat transfer, radiation, mass transfer, fuel vaporization, and fuel bed thermal properties.

The calculated flame spread formulas are consistent with available experimental data. These results reveal much of the physics involved in a spreading flame. For instance, the reaction chemistry affects the flame speed only through the adiabatic stoichiometric flame temperature. While most of the fuel bed thermal properties are very important to the flame spread, the parallel fuel bed conductivity does not significantly affect the flame speed.

DeWit, R., **Differential geometry of the nonlinear continuum theory of dislocation** *(Proc. IUTAM Conf. Stuttgart, Germany, Aug. 28–Sept. 2, 1967), Chapter in Mechanics of Generalized Continua, pp. 251–261 (Springer-Verlag, Berlin, Germany, 1968).*

Key words: Affine connection; continuum; deformation defect; dislocation; nonlinear; non-Riemmannian geometry.

The differential geometric aspects of the limited nonlinear continuum theory of crystal dislocations are developed in terms of a non-Riemmannian geometry with vanishing Riemann-Christoffel curvature. The emphasis is on a general notation and a covariant formulation of the theory. Comparisons are made with the works of KRÖNER and ERINGEN. The drawback of non-distant parallelism in passing to the general theory with non-vanishing curvature are discussed.

Diamond, J. J., Editor, **Bibliography on the high temperature chemistry and physics of materials, April, May, June 1969,** *Nat. Bur. Stand. (U.S.), Spec. Publ. 315-2, 74 pages (July 1969), 75 cents.*

Key words: Bibliography; high temperature; chemistry, high temperature; high temperature chemistry; materials properties; research at high temperatures; thermophysical properties.

The bibliography consists of references to research involving temperatures above 1000 °C, which were noted by the Contributors during the above three-month period. Since this is intended primarily as a current-awareness bibliography, there is no cross-referencing or indexing. This issue contains about 700 references roughly grouped under fifteen subject headings.

Dickson, R. W., Wachtman, J. B., Jr., Copley, S. M., **Elastic constants of single crystal Ni_3Al from 10 to 850 °C,** *J. Appl. Phys.* **40,** *No. 5, 2276–2279 (Apr. 1969).*

Key words: Aluminum; elastic constants; elastic moduli; nickel; single crystals; superalloy.

The elastic constants of single-crystal Ni_3Al were determined 10 to 850°C by a resonance technique. The values of the compliance and their standard errors at 25°C are $s_{11} = 0.927 \pm 0.015$, $s_{44} = 0.825 \pm 0.027$ and $s_{12} = -0.319 \pm 0.050$ in units of 10^{-11} m²/N.

DiMarzio, E. A., Guttman, C. M., **Separation by flow,** *J. Polymer Sci. Polymer Letters* **7,** *267–272 (1969).*

Key words: Chromatography; gel permeation chromatography; polymer fractionation.

It is proposed that the separation in Gel Permeation Chromatography is due in part to the fact that polymer molecules of different volumes entertaining Brownian motion flow down capillary tubes with different mean velocities. The velocity of the polymer, v_p, for each position in the tube is found to be a linear function of the fluid's velocity at the polymer's center of mass. The average velocity of the polymer is then the average of v_p over those positions in the tube available to the polymer's center of mass. If one assumes a model in which a column is viewed as a bundle of capillary tubes then agreement with experiment is obtained. It is suggested fine capillary tubes or a bed of impermeable beads could be used to fractionate polymers.

Dise, J. R., **Significance of the test for normal consistency of hydraulic cement,** *Am. Soc. Testing Mater. Spec. Tech. Publ.* **441,** *Cement, Comparison of Standards and Significance of Particular Tests, pp. 3–15 (Aug. 1968).*

Key words: Autoclave soundness; hydraulic cement; normal consistency; tensile strength; time of setting.

The Vicat Test for Normal Consistency was devised in France approximately 150 years ago and has been in use as a standard ASTM method of test for hydraulic cements since 1904. Much has been learned about the relationship between normal consistency and various other properties of these materials from the numerous studies of related questions that have been carried out over the years. A summation of the information that has been developed concerning time of setting, autoclave soundness and tensile strength tests, and other subjects of potential interest to those engaged in the development of specifications and methods of test for cements, is presented in this review.

Domen, S. R., **Heat loss compensated calorimeter,** *Nature* **222,** *No. 5198, 1061 (June 14, 1969).*

Key words: Absorbed dose; calorimeter; heat loss compensation; heat flow theorem.

A new calorimetric design and measuring technique are proposed for reducing uncertainties caused by temperature gradients. A theoretical analysis revealed a mathematical theorem concerning heat transfer among the calorimetric elements.

Durst, R. A., **Determination of fluoride by analate additions potentiometry,** *Mikrochim. Acta, pp. 611–614 (1969).*

Key words: Analate additions potentiometry; fluoride; fluoride ion selective electrode; potentiometry.

A novel direct potentiometric technique called analate additions potentiometry has been applied to the determination of fluoride using a fluoride ion selective indicator electrode. As expected, the analytical results are comparable to those obtained by the standard additions technique. An error of less than 1 part in 1000 and a precision of about 0.5% was achieved. The technique should be most useful in the determination of small sample volumes which cannot be done by the standard additions method without prior dilution.

Edelman, S., Roth, S., Grisham, L., **Electrical generation of motion in elastomers,** *Shock and Vibration Bull.* **39,** *Part 2, 18 pages (Shock and Vibration Information Center, Naval Research Laboratory, Washington, D. C., Feb. 1969).*

Key words: Elastomers, electrets; electrically controlled dampling; electrostriction; piezoelectricity; polymers; vibration generation.

Motion occurring in response to an applied electrical signal was studied in a number of elastomers. Motion at double the exciting frequency (electrostriction) was common. Linear response was found in a few materials. A few showed linear response in their original condition. Treatment with heat and intense electric fields caused linear response to appear or to increase in others. Superposition of a d.c. bias on the driving signal linearized the double frequency response and increased the linear response.

Ehrlich, M., **Personal dosimetry: methods other than T.L.D.,** *Proc. First Intern. Congress Radiation Protection, Rome, Italy, Sept. 5–10, 1966, Part 1, pp. 69–76 (Pergamon Press Inc., New York, N. Y., 1968).*

Key words: Calibration; data processing; evaluation; gamma rays; intercomparison; performance; personnel dosimetry; phosphate glass; photographic film; radioactive sources; thermal neutrons; x rays.

This is the rapporteur paper that was presented by the author on September 5, 1966, at the First International Congress of the International Radiation Protection Association, in Rome, Italy. The following eight papers were covered: Photographic dosimetry; beta-gamma calibration, M.P. Olivares, S. Perez-Modrego (Spain); Transportable calibration facility for film dosimetry of X-rays by means of radioactive sources. V. Paič (Yugoslavia); A new concept in film badge design, J. D. Eastes, M. L. Maurer, F. L. Paschal (U.S.A.); A phosphate glass dosimeter adapted to the requirements of health physics applications. W. Buttler, R. Maushart, E. Piesch (Federal Republic of Germany); Personnel film monitoring in Poland: organization, method, results, T. Musiałowicz (Poland); Practical personnel dosimetry of thermal neutrons, D. Nachtigall (Switzerland), E. Rose (Federal Republic of Germany); Automatic data processing of a film badge service, W. Benari, M. Schatz, G. Ben-David (Israel); Expérience pratique de dosimétrie comparée dans les six pays d'Euratom (premiers résultats), M. Collet, P. Recht (Euratom).

Ehrlich, M., **Proposed National Bureau of Standards Program for the calibration of instruments used in high-energy electron and x-ray beams,** *(Proc. Conf. High-Energy Radiation Therapy Dosimetry, New York, N. Y., June 1967), Annal. N. Y. Acad. Sci.* **161,** *No. 1, 139–145 (July 3, 1969).*

Key words: Absorbed dose; calibration; electrons; ferrous-sulfate system; graphite calorimeter; interim program, ~1 to 50 MeV, photons; transfer standard; uniformity checks.

The NBS Radiation Physics Division plans to develop services for calibrating suitable measuring instruments in terms of absorbed dose in low-atomic number materials, for use with electrons and photons in the energy range from approximately 1 to 50 MeV. As the standard instrument, NBS plans to use a graphite calorimeter, surrounded by a graphite block. For use in routine calibrations, a stable transfer instrument will be developed which requires less exacting measurements than the calorimeter.

Since the absorbed-dose calibration services based on calorimetry will not be immediately available, an interim program has been initiated for uniformity checks of high-energy electron-beam calibrations. Starting in July 1967, NBS will prepare and mail ferrous-sulfate solutions in sealed radiation-resistant spectrophotometer cells. A minimum of four cells will be supplied to each participant, two of them to be used as controls, and the other two to be exposed by the participant in a polystyrene phantom. Upon their return, NBS will evaluate the dose received by the ferrous-sulfate solutions, using the G-value recommended by the American Association of Physicists in Medicine.

Flynn, D. R., O'Hagan, M. E., **Measurements of the thermal conductivity and electrical resistivity of platinum from 100 to 900 °C,** *Engelhard Indust. Tech. Bull.* **8,** *No. 4, 117–147 (Mar. 1968).*

Key words: Conductivity; electrical conductivity; electrical resistivity; heat conductivity; Lorenz function; platinum; reference material; resistivity; standard; thermal conductivity.

Measurements have been made of the thermal conductivity and the electrical resistivity of commercial grade platinum (99.98% pure) in the temperature range 100 to 900 °C. The measurements have been made with a view to providing accurate data on the thermal conductivity of platinum to serve as a basis for establishing platinum as a thermal conductivity standard reference material. Two methods of measuring the thermal conductivity have been employed, one an electrical method and the other a non-electrical method. In the electrical method, a direct current passed through a necked-down portion of the specimen and the thermal conductivity was determined in terms of the temperature and electrical potential distribution in the necked-down region. The second method was of the absolute guarded longitudinal heat flow type. The experiment was designed to permit measurements by both methods in the same apparatus and on the same specimen thereby providing as direct a comparison as possible between the methods. The data given by the two methods agree within experimental error and show the thermal conductivity of platinum to be a smoothly increasing function of temperature in the measured range. Additional measurements on samples of differing purities are necessary before platinum could be adopted as a thermal conductivity reference material.

Flynn, D. R., Watson, T. W., **High temperature thermal conductivity of soils,** *(Proc. 8th Conf. Thermal Conductivity, Purdue University, West Lafayette, Ind., Oct. 7–10, 1968), Chapter in Thermal Conductivity, pp. 913–939 (Plenum Press Inc., New York, N. Y., Apr. 1969).*

Key words: Conductance; conductivity; heat transfer; nuclear safety; soils; temperature; thermal conductance; thermal conductivity.

A description is given of an apparatus which has been used to measure the thermal conductivity of soil samples at hot-side temperatures to 1600 °C. The method utilizes radial heat flow in a hollow cylinder 1.3 cm inside diameter, 7.6 outside diameter, and 43 cm long. The outside of the sample is maintained near room temperature while the inside is heated to the desired temperature by means of a specially designed heater. The mathmatical analysis of the method is given. Thermal conductivity values are given for nine natural or artificial soils which are representative of most of the subsoils found on earth.
The method used shows considerable promise as a means of rapid and cheap generation of engineering data on the thermal conductivity of loose-fill materials.

Flynn, D. R., Watson T. W., **Measurement of the thermal conductivity of soils to high temperature,** *Atomic Energy Report SC–CR–69–3059 (Apr. 1969).*

Key words: Conductance; conductivity; heat transfer; nuclear safety; soils; temperature; thermal conductance; thermal conductivity.

An apparatus is described which has been designed and built to enable measurement of the thermal conductance of soils at hot face temperatures approaching 1700 °C. The method utilizes radial heat flow through a hollow cylinder of soil contained between a central ceramic core and an outer water-cooled metal shell. Thermal conductivity values are reported for nine natural or artificial soils

representative of subsoils found on most of the earth's surface. For each of these soils, measurements have been completed on two different specimens under particular but reproducible conditions of preparation.

Franklin, A. D., Editor, **ARPA-NBS program of research on high temperature materials, Period covered, July 1 to December 31, 1968,** *Nat. Bur. Stand. (U.S.), Tech. Note 494, 28 pages (Sept. 1969), 35 cents.*

Key words: Copper; creep; crystal growth; diffusion; enthalpy; evaporation; fracture; glass band structure; high temperature materials; mass transport; materials properties; mechanical relaxation and polymers; oxides; pyrolytic graphite; transition metal borides.

Brief reviews are given of work performed during the period July 1 to December 31, 1968, on a number of projects concerning High Temperature Materials. Topics include the optical constants of titanium, diffusion of oxygen in oxides, growth of Al_2O_3 bicrystals by chemical vapor deposition, high temperature creep in copper, fracture in glass, the electronic structure of transition metal borides and related compounds, the enthalpy of pyrolytic graphite at high temperatures, the mechanism of volatilization of polymers, and the interaction between mechanical relaxation and annealing in polymers.

Frederick, N. Y., **A new high-frequency current standard,** *IEEE Trans. Instr. Meas.* **IM–17,** *No. 4, 285–290 (Dec. 1968).*

Key words: Ammeter; electrodynamometer; high frequency current; short-circuited ring; torsion balance.

A short-circuited-ring electrodynamic ammeter is described. The short-circuited-ring is supported by a fine quartz fiber and is suspended midway between the inner and outer conductors of a coaxial transmission line. The current on the line is measured by measuring the torque exerted against the ring by the current on the coaxial line. A new technique is given for determining the relationship between the torque on the ring and the current on the transmission line and is compared with the technique which has been used in the past. The new method is an application of the resonator action theorem used by A. L. Cullen for calibrating a torque operated microwave wattmeter. The major weakness in the previous evaluations of the torque current relation is discussed. The ammeter is useful for measuring current from one to one hundred amperes over the frequency range 1 MHz to 1 GHz with an uncertainty of the order of 0.5%.

Frederikse, H. P. R., Hosler, W. R., Casella, R. C., **Piezoresistive effects in semiconducting strontium titanate,** *Proc. Ninth Intern. Conf. Physics of Semiconductors, Moscow, USSR, July 23–29, 1968, pp. 1175–1180 (NAUKA, Leningrad, USSR, 1968).*

Key words: Piezoresistive effects; semiconductors; strontium titanate.

Piezoresistive effects in doped $SrTiO_3$ measured at 300, 77, and 4 K are interpreted in terms of a many-valleyed energy band model [spheroids along <100> direction]. Low temperature saturation is explained by assuming domain flipping under stress.

Frisch, R. C., Forman, R. A., **Nuclear magnetic resonance of Ti in Ti-H systems,** *J. Chem. Phys.* **48,** *No. 11, 5187–5190 (June 1, 1968).*

Key words: Hydrides; hydrogen; nuclear magnetic resonance; titanium.

The nuclear magnetic resonance spectrum of ^{47,49}Ti in powder samples of metallic titanium hydride TiH_x has been studied over the range of hydrogen concentrations corresponding to $1.7 \leq x \leq 2.0$. For TiH_2 the Knight shift is found to be $+ 0.26 \pm .04\%$, and there is no change in the Knight shift as a function of hydrogen concentration over the range studied. The titanium resonance in all samples was quite broad, 20 Oe, so that the lines from the two isotopes were not resolved. As a function of hydrogen concentration, lineshape was found to remain constant, but a rapid decrease of line intensity was noted.

In order to investigate the possibility of magnetic ordering suggested by earlier studies of the magnetic susceptibility of Ti_2, studies of the magnetic field dependence and temperature dependence of the resonance were also performed. No dependence of Knight shift or lineshape on magnetic field was observed over the range of 9.0 to 15.0 k0e. No changes in Knight shift or lineshape were observed in the temperature region from 170°K to 525°K, thoroughly encompassing the region of the magnetic susceptibility maximum at approximately 300°K. These results strongly suggest that the cause of the maximum in the magnetic susceptibility is not magnetic ordering.

Results on hydrogen and deuterium resonances in these samples are also reported.

Garfinkel, S. B., Mann, W. B., **A method for obtaining large numbers of measured time intervals in radioactive decay,** *Intern. J. Appl. Radiation Isotopes* **19,** *No. 9, 707–709 (Sept. 1968).*

Key words: Multichannel multiscaler analyzer; Poisson distribution; radioactive decay.

A method is described for the acquisition of large numbers of measured time intervals between consecutive alpha-particle emissions in radioactive decay. A multichannel multiscaler analyzer was used in a modified multiscaler mode. The data are to be analyzed to see if they conform to a Poisson distribution.

Gatterer, L. E., Bottone, P. W., Morgan, A. H., **Worldwide clock synchronization using a synchronous satellite,** *IEEE Trans. Instr. Meas.* **IM–17,** *No. 4, 372–378 (Dec. 1968).*

Key words: Atomic clocks; clock synchronization; geodesy; ionospheric propagation; navigation; satellite tracking; VHF satellite transponder.

An experiment performed in late 1967 is reported in which the synchronization of widely separated atomic clocks was investigated. One-way VHF radio transmissions from the reference clock were relayed to remote clocks using a geo-stationary satellite transponder. This is in contrast to experiments described in the literature [1,2,3,4] where two-way satellite communications were used. The problem of measuring the time difference between a remote clock and a reference clock using one-way radio transmissions reduces to the problem of predicting the propagation delay experienced by the radio wave. For example, the accuracy with which a user's clock can be set using WWV is limited by the predictability of the propagation delay from WWV to the user's receiver. The principal advantage of using a geo-stationary satellite transponder is that the radio path is predominately a free space, line-of-sight path, which is predictable. Those portions of the path for which radio refractive index is variable constitute only a small percentage of the total path. In this experiment predicted values of propagation delay were compared to measured values. The accuracy of predictability, and hence of clock synchronization, was 10 μsec. or 60 μsec., depending on the prediction method used. The technique may offer an alternative to transporting atomic standards to geodetic and tracking stations around the world fulfilling their clock synchronization requirements. Several methods were used to check the time differences between the station clocks. These included transported atomic clocks, a satellite technique using two-way communications, and a one-way microwave link using the moon as a passive reflector.

Ginnings, D. C., **Introduction in Experimental Thermodynamics,** J. P. McCullough and D. W. Scott, Eds., *Vol. I, Calorimetry of Non-reacting Systems, Chapt. 1, 1–13 (Butterworth & Co., London, England, 1968).*

Key words: Definitions; heat units and constants; methods of calorimetry; standard reference substances; symbols; terminology.

Ginnings, D. C., Stimson, H. F., **Calorimetry of saturated fluids including determination of enthalpies of vaporization,** *Chapter in Experimental Thermodynamics,* J. P. McCullough and D. W. Scott, Eds., *Vol. I, Calorimetry of Non-reacting Systems, Chapt. 11, 395–420 (Butterworth & Co., London, England, 1968).*

Key words: Adiabatic calorimetry; heat capacity; heats of vaporization.

Ginnings, D. C., West, E. D., **Principles of calorimetric design,** *Chapter in Experimental Thermodynamics*, J. P. McCullough and D. W. Scott, Eds., *Vol I, Calorimetry of Non-reacting Systems, Chapt. 4, 85–131 (Butterworth & Co., London, England, 1968).*

Key words: Design principles; heat leak errors; heat transfer; temperature gradients in calorimeters; tempering of leads.

Greenfeld, S. H., **A study of the variables involved in the saturating of roofing felts,** *Nat. Bur. Stand. (U.S.), Bldg. Sci. Ser.* **19,** *18 pages (June 1969), 30 cents.*

Key words: Absorption; asphalts; felts, moisture; roofing; saturation.

The degree of saturation of a #27 felt with a typical roll saturant and a #55 felt with roll, mixed, and shingle saturants varied with saturation time and pressure, saturant temperature and viscosity, felt conditions, and press roll pressure and clearance. Optimum temperature and viscosity ranges were determined for each asphalt-felt combination. Both pressure and vacuum increased the completeness of saturation under optimum conditions, but frequently shortened the working temperature range in which optimum saturation could be produced.
Rate and degree of moisture and liquid water absorption decreased with increasing saturation. Air permeability decreased with increasing saturation. The consequences of some of these findings are discussed.

Greenfeld S. H., **Hail resistance of roofing products,** *Nat. Bur. Stand. (U.S.), Bldg. Sci. Ser.* **23,** *11 pages (Aug. 1969), 25 cents.*

Key words: Asphalt shingles; built-up roofing; hail; roofing; shingles; storm damage.

A test was developed for evaluating the hail resistance of roofings, in which synthetic hailstones (ice spheres) of various sizes were shot at roof assemblies at their free-fall terminal velocities. Indentations, granule loss and roofing fracture were observed. The following conclusions have been made from these results:

(a) All roofing materials have some resistance to hail damage, but as the size of the hail increases, a level of impact energy is reached at which damage occurs. This level lies in the range of 1½ to 2 inch (3.8–5.1 cm) hailstones for most prepared roofings.

(b) Because of the ways in which prepared roofings are applied, most products have areas of different vulnerability.

(c) The solidly supported areas of roofing tend to be the most resistant to hail damage.

(d) Heavier shingles tend to be more hail-resistant than Type 235 shingles.

(e) Weathering tends to lower the hail resistance of asphalt shingles.

(f) Built-up roofs on dense substrates tend to resist hail better than those on soft substrates.

(g) Built-up roofs made with inorganic felts tend to be more hail resistant than those made with organic felts.

(h) Coarse aggregate surfacing tends to increase the hail resistance of roofing.

Grenley, D. G., **Study of the effect of certain modified mortars on compressive and flexural strength of masonry,** *(Proc. Intern. Conf. Masonry Structural Systems, University of Texas, Austin, Texas, Nov. 30–Dec. 2, 1967), Chapter in Designing Engineering and Constructing with Masonry Products, F. B. Johnson, Ed., Paper 5, pp. 28–33 (Gulf Publ. Co., Houston, Texas, May 1969).*

Key words: Flexural strength of clay masonry; high strength mortars; improved mortars; modified mortars; strength of clay masonry.

The use of high strength mortars materially improves the flexural and compressive strength of small masonry assemblages. This is found to be true with a variety of brick although there is indication that low quality brick will not experience a great degree of improvement in their structure strength. Brick and mortar strength are shown to be important factors in determining structure strength, however these variables alone will not permit a quantitative prediction of structure performance.

Grenley, D. G., Cattaneo, L. E., Pfrang, E. O., **Effect of edge load on flexural strength of clay masonry systems utilizing improved mortars,** *(Proc. Intern. Conf. Masonry Structural Systems, University of Texas, Austin, Texas, Nov. 30–Dec. 2, 1967), Chapter in Designing Engineering and Constructing with Masonry Products, F. B. Johnson, Ed., Paper 17, pp. 119–128 (Gulf Publ. Co., Houston, Texas, May 1969).*

Key words: Compressive and flexural interaction in walls; compressive strength of walls; flexural strength of walls; high bond strength mortars; improved mortars; masonry walls.

This paper proposes a theoretical interaction diagram for the effect of edge load and flexural load on the ultimate strength of masonry wall panels. Four experimental systems show good agreement with the theory and suggest a new approach to the rational design of masonry systems. The paper also indicates that substantial improvement in the strengths of masonry systems can be realized by improving the mortars used in their construction.

Hanley, H. J. M., Childs, G. E., **Dilute gas viscosities at low temperatures,** *J. Chem. Phys.* **50,** *No. 10, 4600–4601 (May 5, 1969).*

Key words: Argon; correlation; dilute gas viscosity; kinetic theory; potential functions.

We recently reported that the tabulated and generally accepted viscosity coefficients for simple gases could be systematically in error at high temperatures (>300 K). We have extended our work to cover viscosity data at low temperatures. We again find factors indicating possible errors in experimental data (although not as great as before) which reinforce our opinion that the whole subject of dilute gas viscosities needs careful reexamination.

Hein, R. A., Cox, J. E., Blaugher, R. D., Waterstrat, R. M., **Superconducting behavior of A–15 compounds,** *Solid State Commun.* **7,** *381–384 (1969).*

Key words: A–15 type phases; atomic ordering; beta-tungsten compounds; critical magnetic fields; critical temperatures; superconductors.

Superconductivity has been discovered in the A15 type compounds $V_{1-x}Ni_x$ V_3Pd and Ta_{85} Pt_{15} and a new feature has been observed in the T_c versus e/a correlation for these compounds. Evidence is presented to show that the anomalously low value of T_c for V_3Pd probably results from magnetic interactions which tend to depress T_c. Differences in the behavior of 3*d* compounds as compared with 4*d* compounds can be explained by the theory of McMillan.

Heinrich, K. F. J., **Common sources of error in electron probe microanalysis,** *Advan. X-ray Anal.* **11,** *40–55 (1968).*

Key words: Absorption correction; atomic number correction; electron probe microanalysis; fluorescence correction; quantitative analysis.

In order to reduce the error of quantitative electron probe microanalysis, error sources in the preparation and measurement of specimens and standards must be miminized. These sources of error are described, and literature references for detailed study are given. A critical analysis is made of 150 analytical measurements of binary specimens previously discussed by Poole and Thomas. It is shown that the cases of serious errors reported by these authors are mainly due to poorly characterized or measured specimens and in some cases to the omission of characteristic fluorescence corrections. If these sources of error are eliminated, a much more favorable error distribution can be obtained through relatively simple correction calculations. Further progress in quantitative microprobe analysis is dependent upon measurements using well-controlled conditions and standard materials of experimentally proven micro-homogeneity and reliably determined composition.

Henderson, M. M., **Introductory remarks and summary of discussion for symposium on critical reviews,** *J. Chem. Doc.* **8,** *231 and 245 (Nov. 1968).*

Key words: Galvanic cells; gas analysis; gas analysis using electrochemical oxygen determination; oxygen determination; trace gas analysis; trace oxygen determination.

A method has been developed for the absolute determination of oxygen in inert gases over the range from about 1 to 1000 ppm oxygen. The gas to be analyzed is caused to flow through a series of galvanic cells similar to the type developed by Hersch. Under the conditions used, most of the oxygen in a stream of gas is removed in the first cell; subsequent cells reduce oxygen concentrations to virtually zero in the effluent gas. Measurement of the increase in all cell current outputs when the gas flow rate is increased by a known increment allows calculation of the absolute oxygen concentration.

Heydemann, P. L. M., Houck, J. C., **Self-consistent ultrasonic method for the determination of the equation of state of liquids at very high pressures,** *J. Appl. Phys.* **40,** *No. 4, 1609–1613 (Mar. 15, 1969).*

Key words: Bulk modulus; density; equation of state; high pressure; velocity of sound; water.

Ultrasonic measurements on liquids at very high pressures and an accurate self-consistent ultrasonic method for the determination of the equation of state of liquids at very high pressures are described. The liquid sample is contained in a polyethylene-lined piston and cylinder device. The method described requires only the measurement of the transit time of an ultrasonic pulse through the liquid as a function of pressure. The difficulties and errors connected with a direct volumetric determination are thus avoided and a high accuracy is achieved. A computation of the uncertainties in the determination of the bulk moduli, the density and the velocity of sound is presented. Experimental results are given for water at 22°C and pressures up to 12.6 kbar. Data for the density of water reported by P. W. Bridgman and by L. H. Adams, and for the velocity of sound reported by Holton, et al., are found to be in good agreement with the present work.

Hoer, C. A., Smith, W. L., **A 1-MHz binary inductive voltage divider with ratios of 2^n to 1 or $6n$ dB,** *IEEE Trans. Instr. Meas.* **IM–17,** *No. 4, 278–284 (Dec. 1968).*

Key words: Attenuator; binary divider; inductive voltage divider; ratio transformer; voltage comparator; and voltage divider.

A voltage divider with ratios of 2^n:1 or $6n$ dB is obtained by cascading n binary dividers, each having a voltage ratio of 2:1. A theoretical analysis results in an expression for the ratio error. Several techniques are given for reducing this error. A voltage comparator is described for eliminating errors due to external loading of the divider. An experimental cascaded binary divider with a total of 42 dB in seven 6 dB steps is described. The attenuation of the divider was measured with a precision waveguide below-cutoff attenuator at 1 MHz. The divider and attenuator values agree within the uncertainty of the attenuator and measuring system at 1 MHz.

Hogben, D., **The distribution of the sample variance from a two-point binomial population,** *Am. Stat.* **32,** *No. 5, 30 (Dec. 1968).*

Key words: Distribution; parameter; probabilities; random sample; two-point binomial; variance.

In a random sample of size n the sample variance is

$S^2 = \sum_{i=1}^{n}(X_i-\overline{X})^2/(n\text{-}1)$. For the two-point binomial distribution, it is shown that for $c=i(n\text{-}i)/n(n\text{-}1)$ and $i=0, 1, \ldots, (n/2]$,

$$\Pr\,(S^2=c)=\binom{n}{i}p^iq^i\,(p^{n-2i}+q^{n-2i}),\ i<n/2,$$

$$=\binom{n}{n/2}p^{n/2}\,q^{n/2},\ n \text{ even and } i=n/2.$$

Two examples are given.

Horn, L., **Thermal gradient effects on thirteen flush mounted pressure transducers,** *Nat. Bur. Stand. (U.S.), Tech. Note 409, 23 pages (Aug. 1969), 30 cents.*

Key words: Pressure measurement errors; pressure transducers; response; temperature; thermal gradients; zero shift.

Thirteen different flush mounted pressure transducers of seven manufacturers were tested by creating a thermal gradient in them and recording the resultant zero shifts. Photographs of typical outputs are shown and the results are compared. A typical recording shows these general characteristics: (1) a very rapid change in output reaching a peak in a second or less, (2) a more gradual shift which reaches a peak in a time which may be a few seconds or more than a minute, and (3) a shift in reading which remains as long as the gradient is maintained. Examples were found in which each of these were positive or negative. The magnitude in a few cases was small, in many was a large fraction of its range, and in one case well in excess of the full scale range.

Hubbell, J. H., **Photon cross sections, attenuation coefficients, and energy absorption coefficients from 10 keV to 100 GeV,** *Nat. Stand. Ref. Data Ser., Nat. Bur. Stand. (U.S.),* **29,** *85 pages (Aug. 1969), 75 cents.*

Key words: Attenuation coefficient; Compton scattering; cross section; energy absorption coefficient; gamma rays; pair production; photoelectric absorption photons; x rays.

This report updates and extends previous NBS tabulations. Section 1 contains the information of most immediate practical use: (a) a tabulation of the attenuation coefficient for 23 elements ($_1$H to $_{92}$U) between 10 keV and 100 GeV and (b) a tabulation of the energy absorption coefficient for air, water, and 18 elements between 10 keV and 10 MeV, and for air, water, and 7 elements up to 100 MeV. Section 2 contains detailed information on the predominant processes (photoelectric absorption, Compton scattering and pair production) and a brief discussion of other processes which combine to give the attenuation coefficient. Theoretical and experimental data are reviewed, and auxiliary tables and approximation formulas are given. Section 3 contains tabulations of cross sections for the predominant processes between 10 keV and 100 GeV for 23 elements and for 13 compounds and mixtures.

Hudson, R. P., **The CMN temperature scale,** *Proc. XI Conf. Low Temperature Physics, St. Andrews, Scotland, Aug. 21–28, 1968, I, 501–504, Paper D1.8 (University of St. Andrews, Scotland, 1968).*

Key words: Adiabatic demagnetization; cerous magnesium nitrate; low temperature scales.

A re-examination of adiabatic demagnetization results for cerous magnesium nitrate (CMN) shows them to agree with Van Vleck's theory of dipole-dipole interaction for the region above 0.01 K. To pursue the examination to lower temperatures, one requires fourth order and higher terms in the $1/T$ expansion, which are not yet available. They have therefore been obtained by least squares fitting and so provide a polynomial formula for the entropy which may be used to calculate the heat capacity. The latter is of interest in comparing magnetic temperature scales for CMN obtained by different methods.

Hust, J. G., Powell, R. L., **Thermal conductivity of aerospace alloys at cryogenic temperatures,** *(Proc. 8th Conf. Thermal Conductivity, Purdue University, West Lafayette, Ind., Oct. 7–10, 1968), Chapter in Thermal Conductivity, C. Y. Ho and R. E. Taylor, Eds., pp. 197–208 (Plenum Press Inc., New York, N. Y., 1969).*

Key words: Aluminum alloy; electrical resistivity; Lorenz ratio; nickel alloy; thermal conductivity; thermopower; titanium alloy.

The apparatus described at the last Thermal Conductivity Conference has been used to determine the thermal conductivity, electrical resistivity, Lorenz ratio, and thermopower of several aerospace alloys between 4 and 300 K: titanium A-110 AT, Inconel 718*, Hastelloy X*, and aluminum 7039. These data are presented graphically. By utilizing detailed numerical and theoretical

analyses, we have been able to separate the electronic and lattice contributions to the total thermal conductivity. Various scattering mechanisms have also been resolved for both types of conduction. The first three alloys are predominately lattice conductors at low temperatures, with total Lorenz numbers as high as $15V^2/K^2$ near 20K.

Janz, G. J., Dijkhuis, Chr. G. M., **Molten salts: Volume 2, Section 1. Electrochemistry of molten salts: Gibbs free energies and excess free energies from equilibrium-type cells,** *Natl. Stand. Ref. Data Ser., Nat. Bur. Stand. (U.S.),* **28,** *116 pages (Aug. 1969).*

Key words: Critically evaluated data; equilibrium electrochemical cells; excess entropies; excess Gibbs free energies; Gibbs free energies; molten salt mixtures; molten salts; surface tension; thermodynamics of molten salts.

The critical evaluation of excess free energies of binary molten salt mixtures with a common ion from equilibrium-type electrochemical cells is described in this report. For this purpose calculations using the original emf data were systematically undertaken to establish comparisons of free energy values of various workers that would be significant. The reversibility of electrodes is investigated by comparing the electromotive force of cells with a single molten salt as liquid electrolyte with thermochemical data.

Janz, G. J., Lakahminarayanan, G. R., Tomkins, R. P. T., Wong, J., **Molten salts: Volume 2, Section 2. Surface tension data,** *Nat. Stand. Ref. Data Ser., Nzt. Bur. Stand. (U.S.),* **28,** *116 pages (Aug. 1969).*

Key words: Critically evaluated data; equilibrium electrochemical cells; excess entropies; excess Gibbs free energies; Gibbs free energies; molten salt mixtures; molten salts; surface tension; thermodynamics of molten salts.

Data on the surface tensions of single salt melts have been systematically collected and evaluated. Results are given for 106 inorganic compounds over a range of temperatures where available.

Jones, E., Yelon, W. B., Edelman, S., **Piezoelectric shakers for wide-frequency calibration of vibration pickups,** *J. Acoust. Soc. Am.* **45,** *No. 6, 1556–1559 (June 1969).*

Key words: Calibration damped resonant cylinders; damping; piezoelectric shaker; stagger-tuned; vibration; vibration pickup.

This paper describes a piezoelectric shaker consisting of a combination of damped resonant cylindrical elements. Material characteristics and design parameters are chosen so that the resonances of the combined elements overlap to provide "good" motion over a wide frequency range. Data from three shakers are presented to show how a suitable set of shakers can be used for calibration of vibration pickups at frequencies up to 100 kHz.

Jones, M. C., Giarratano, P. H., Simpson, A. U., **Flow and heat transfer characteristics of sub-triple-point cryogens in heated tubes,** *Proc. Second Intern. Cryogenic Engineering Conf., Brighton, England, May 7–10, 1968, pp. 83–88 (Iliffe Sci. and Technol. Publ., Ltd., Guilford, Surrey, England, 1968).*

Key words: Flow; hydrogen; nitrogen; solid-vapor mixture; solid plug; sub-triple point; tubes.

When liquids are expanded to pressures below their triple point pressures they form two-phase, solid-vapor mixtures. The continuous discharge of such mixtures through tubes is important in a variety of situations in space vehicles, but this can only be assured if the tubes are heated. By studying heat transfer some insight has been gained into the mechanism of particle-wall interaction, which leads eventually, at low heat input, to a tube completely plugged with solid. A similarity criterion is proposed by which minimum adequate heating conditions might be correlated. Experimental values are given.

Jones, M. C., Palmer, D. C., **A technique for the measurement of spectral reflectances at low temperatures in the infrared and far infrared,** *(Proc. AIAA Third Thermophysics Conf., Los Angeles, Calif., June 24–26, 1968), Chapter in Progress in Astronautics and Aeronautics. Vol.* **21,** *Thermal Design Principles of Spacecraft and Entry Bodies, pp. 543–557 (Academic Press Inc., New York, N. Y., 1969).*

Key words: Infrared; low-temperature; measurement; spectral reflectance; stainless steel; technique.

An experimental technique is described for the measurement of normal, spectral, specular reflectance of materials at temperatures from room temperature down to a few degrees above liquid helium temperature. The reflectance of samples is measured by comparison with reference samples of ultra-high-vacuum deposited gold on glass substrates. The difficulty of maintaining sufficient parallelism between sample and reference has been overcome; so-too the problem of excessive delay between recording sample and reference has been reduced. Experimental details are given and, in illustration of the technique, the reflectance of electro-polished stainless steel is presented for the wavelength range 3 μm to 300 μm at 297K, 77K, and 10.5K

Kasen, M. B., **A method for producing small grain size in super-purity aluminum,** *Trans. Met. Soc. AIME* **245,** *No. 7, 1660–1661 (July 1969).*

Key words: Aluminum; grain size; metals; recrystallization; super-purity.

A method has been developed for recrystallizing super-purity aluminum to produce a very small, uniformly distributed grain size. The method involves (a) introducing a very large amount of cold work at 76K, (b) a very short time exposure in a salt bath operating at 400°C, and (c) a water quench. Grain sizes of 30 microns mean diameter may be reproducibly obtained in aluminum having a resistivity ratio, ρ_{293K}/ρ_{4K}, in excess of 16,000.

Kuehner, E. C., Freeman, D. H., **Containers for pure substances,** *Chapter in Purification of Inorganic and Organic Materials,* M. Yief, *Ed., pp. 297–306 (Marcel Dekker, Inc., New York, N. Y., 1969).*

Key words: Container impurities; pure containers.

This is a brief discussion and summary of criteria used in the selection of a pure container for pure chemical substances. The various sources of contamination are classified according to container purity, container stability, and container inertness. A brief discussion of container cleaning is included. A tabular summary of various container materials is presented according to the relevant sources of container imperfection or failure.

Kulin, G., Editor, **Hydraulic research in the United States 1968,** *Nat. Bur. Stand. (U.S.), Spec. Publ.* **316,** *331 pages (June 1969), $2.50.*

Key words: Hydraulics; hydraulic research; hydraulic engineering; hydrodynamics; project summaries.

Current and recently concluded research projects in hydraulics and hydrodynamics for the years 1967–1968 are summarized. Projects from more than 200 university, industrial, state and federal government laboratories in the United States and Canada are reported.

Kuriyama, M., Miyakawa, T., **Theory of x-ray diffraction by a vibrating crystal,** *J. Appl. Phys.* **40,** *No. 4, 1697–1702 (Mar. 15, 1969).*

Key words: Dynamical diffraction; extinction; kinematical diffraction; piezoelectricity; theory; thickness vibration; vibrational modes; x-ray diffraction.

The scattering amplitude for x-ray diffraction by a vibrating crystal is obtained. The Bragg diffracted propagators for the perfect crystal are replaced by new propagators in which the Fourier transform of the polarizability of the crystal is multiplied by $J_o(\underset{\sim}{H} \bullet \underset{\sim}{A}_q)$ for the vibrational amplitude $\underset{\sim}{A}_q$, as is corrected by the Debye-Waller factor in the thermal problem. The scattering amplitude

contains not only dynamical scattering but kinematical scattering. The case of ideal thickness vibration is studied in detail. The real part of the perturbed scattering amplitude is proportional to sin $H \bullet A_q$ multiplied by the H-th Fourier transform of the polarizability. The transient process from dynamical to kinematical scattering, that is, a decrease in extinction, is clearly demonstrated in terms of the vibrational amplitude.

Kusuda, T., **Proposed procedures for determining building heating and cooling loads for energy calculations,** *ASHRAE Symposium Bulletin, pp. 1–75 (1969).*

Key words: Building heating and cooling loads; energy requirements; heating; thermal environment.

Hour by hour calculations of heating and cooling load are essential for the accurate evaluation of annual energy requirements needed to maintain a desired thermal environment within a building. There is a need for rigorous computer algorithms in calculating the transient thermal behavior of building structures under fluctuating climatic conditions. This paper describes most up-to-date computational algorithms for solar heat gain through fenestration, transient wall-heat conduction, psychrometrics, shadow movement, and others, which are recommended for the computer calculations of hourly heating and cooling loads.

Kusuda, T., **Thermal response factors for multi-layer structures of various heat condition systems,** *ASHRAE Trans,* **75,** *No. 1, V.3.1–V.3.25 (1969).*

Key words: Cylinder and sphere; multi-layer structures; response factors; transient heat conduction.

The thermal response factor method for calculating transient heat conduction through multi-layer slabs is generalized to include the solutions for many other important engineering heat transfer problems. Response factor formulas for multi-layer structures of cylindrical and spherical objects (hollow as well as solid), plane and curved surface walls adjacent to infinitely thick heat conduction medium, such as ground, and plane slabs are presented in this paper. Numerical evaluation of these formulas are carried out for selected multi-layer structures and the results are tabulated.

LaFleur, P. D., **Activation Analysis Section at the National Bureau of Standards, Washington, D. C., U.S.A., Laboratory of the Issue,** *J. Radioanalytical Chem.* **3,** *No. 1–2, 127–133 (July 1969).*

Key words: Activation analysis; Cockcroft-Walton neutron generator; LINAC, radiochemical separations; reactor; Standard Reference Material.

The history and facilities of the Activation Analysis Section, Analytical Chemistry Division of the National Bureau of Standards are described. The Section is divided into three projects, each having application to a specific irradiation source and a project in radiochemical separations. Several examples of work in progress and of past accomplishments are included, as well as planned activities in the future.

Lamb, V. A., **Electroplating with current pulses in the microsecond range,** *Plating* **56,** *No. 8, 909–913 (Aug. 1969).*

Key words: Electroplating with current in microsecond pulses; pulse plating.

Exploratory experiments were carried out on electrodeposition of copper and silver by use of pulsed direct current, with pulse periods from 0.1 to 50 microsecond and with very high current density. The microstructure and hardness of copper deposits made under these conditions were not significantly different than those of deposits plated under conventional conditions. Possible reasons are discussed. Current efficiency of copper deposition was low with the shortest pulses, but remained high for deposition of silver. Two experiments relating pulse duration to "reaction time" for the electrode reactions are described.

Lederer, P. S., **Pressure,** *ISA Transducer Compendium, 2nd Ed., Chapt. 1, Part 1, pp. 5–8 (1969).*

Key words: Evaluation; measurement; performance; pressure; test method; transducer calibration.

A chapter for the "ISA Transducer Compendium" briefly introducing the reader to the field of pressure and its measurement by means of electrical output transducers. The purpose of this chapter is to assist the reader to select the transducer most suitable for his application from those listed in the compendium.

Lippincott, E. R., Stromberg, R. R., Grant, W. H., Cessac, G. L., **Polywater,** *Science* **164,** *1482–1487 (June 27, 1969).*

Key words: Anomalous water; infrared spectrum of polywater; polywater; Raman spectrum of polywater; water.

The infrared and Raman spectra of a form of water prepared in quartz capillaries and previously designated as "anomalous" water have been obtained. The spectra appear to be unique with the apparent absence of the O-H stretching bands prominent in normal water spectra, and the appearance of new bands near 1600 and 1400 cm^{-1}. The interpretation is that new and previously unreported strong symmetric O-H-O bonds are formed, isoelectronic with FHF^-. The approximate bond distances are given as 2.3Å for O • • • O, and 1.5Å for H-O. These bonds are regarded as responsible for the remarkable properties of the material and have considerable covalent character. These bonds are so strong that they cannot be considered as normal O • • • H hydrogen bonds. Extensive electron delocalization could occur in structures which involve oxygen atoms in three equivalent bonds. The bond energy per O-H-O unit is given as approximately 30–50 kcal/mole, and an energy of 60–100 kcal per H_2O structural unit. Several structures are proposed which are consistent with the spectral data and the remarkable properties and stability of the material. It is concluded that the material is a true polymer of and therefore named polywater.

McCamy, C. S., **Photographic image structure evaluation,** *Chapter in Ultra-Microminiaturization Precision Photography for Electronic Circuitry, pp. 130–140 (Society of Photographic Science and Engineers, Washington, D. C., 1968).*

Key words: Photochemical fabrication; photographic image structure.

Photographic images are usually evaluated with respect to visual applications. Photochemical fabrication can benefit from the accumulated experience in this field, but introduces its own complications. The kind of optical density to be used or measured must be precisely known. The nature of light limits the amount of detail that can be reproduced. Photographic materials are limited with respect to resolving power, acutance, and granularity. These quantities can be useful in evaluating photochemical fabrication systems. Although modulation transfer theory has been applied to photographic systems, nonlinearities raise problems which may require more rigorous treatment.

Margoshes, M., Rasberry, S. D., **Fitting of analytical functions with digital computers in spectrochemical analysis,** *Anal. Chem.* **41,** *1163–1172 (Aug. 1969).*

Key words: Analytical curves; analytical functions; emission spectrometry; spectrochemical analysis; x-ray fluorescence spectrometry.

Two procedures are described for fitting spectrometric analytical functions on a digital computer and conversion of instrument readings to element concentrations. The first procedure is intended for computers giving rapid response, and particularly those which can operate in the conversational mode. During the running of the program the user decides on the equation to be used and whether data for any standards are to be rejected. The second procedure is intended for use on batch-loading computers; these decisions are incorporated in the program. Results are given of the use of both procedures. The occasional failures of the procedures are discussed, and methods are described for detecting such failures. A discussion is given of a method for including an estimate of the uncertainty of the analytical function in the estimated analytical error.

Marinenko, G., Champion, C. E., **Difference between the inflection point and the equivalence point in coulometric titra-**

tions of weak acids, *Anal. Chem.* **41,** *No. 10, 1208–1211 (Aug. 1969).*

Key words: Boric acid; equivalence point; inflection point; Roller equation.

Mannitoboric acids of varying pK_a were successfully used to test independently the validity of the Roller equation for evaluation of the error due to noncoincidence of the inflection point and the equivalence point of acid base titration. The use of mannitoboric acid in media of different mannitol concentrations has provided the first test of the Roller equation under conditions where both parameters, c and K_a, are varied for a single acid of known stoichiometry. Moreover, the applicability of the Roller equation to complex systems such as boric acid-mannitol has not been established prior to this investigation.

Menis, O., Rains, T. C., **Determination of arsenic by atomic absorption spectrometry with an electrodeless discharge lamp as a source of radiation,** *Anal. Chem.* **41,** *No. 7, 952–954 (June* 1969).

Key words: Arsenic; atomic absorption; electrodeless; extraction-displacement reaction; 4-methyl and selenium 726; reaction; standard reference materials.

The determination of arsenic in cast iron and high-purity selenium metal by atomic absorption spectrometry was facilitated by the extraction of the arsenic with diethylammonium diethyldithiocarbamate (DDDC) followed by a stripping process from the organic phase by displacement reaction. In addition, the high background absorption of arsenic radiation encountered in various oxidant-fuel systems was overcome with an argon(entrained air)-hydrogen flame. The electrodeless discharge lamp was found to be an excellent high intensity source of radiation for use in atomic absorption in the far ultraviolet region. The detection limits for arsenic in an aqueous medium free of interfering cations was 0.1 μg/ml.

Milton, J. B., **Standard time and frequency: Its generation, control, and dissemination from the National Bureau of Standards Time and Frequency Division,** *Nat. Bur. Stand. (U.S.), Tech. Note 379, 27 pages (Aug. 1969), 35 cents.*

Key words: Clock synchronization; frequency and time dissemination; primary frequency standard; standard frequency broadcasts; time interval; time scales.

The Time and Frequency Division of the National Bureau of Standards produces the NBS time scales, AT(NBS), SAT(NBS), and UTC(NBS). These time scales are developed by utilizing the properties of the NBS frequency standard, NBS-III. The main by-product of these time scales is the operational clock systems. These operational clock systems are used, among other things, to calibrate the clocks and secondary standards necessary for the operation of the NBS radio stations, WWV, WWVB, WWVL, and WWVH. These stations transmit SAT(NBS), UTC(NBS), and various tones, alerts, and corrections for time-of-day information.

Mopsik, F. I., **Dielectric constant and loss,** *Digest of Literature on Dielectrics* **31,** *56–79 (1969).*

Key words: Dielectric literature; dielectric literature in 1967; dielectric properties; digest of literature on dielectrics; Literature compilation; survey of dielectric literature.

A compilation has been made of the literature appearing in 1967 on the subject of dielectric properties of materials. A summary of the highlights is included.

Mopsik, F. I., **The effect of pressure, volume and temperature on the dielectric constant of simple organic liquids,** *Proc. 1967 Annual Report Conf. Electrical Insulation and Dielectric Phenomena, Buck Hill Falls, Pa., Sept. 18–20, 1967, pp. 66–69 (Natl. Acad. Sci.-Natl. Res. Council, Washington, D. C., 1968).*

Key words: Carbon tetrachloride; carbon disulfide; *N*-hexane; density; dielectric constant; polarizability; pressure.

Measurements have been made on carbon tetrachloride, carbon disulfide and hexane over a wide range of temperature and pressure for both density and dielectric constant. For all liquids there is a general decrease in the polarizability with an increase in density. *N*-hexane alone has shown a temperature dependence of its dielectric constant consistent with a dipole moment.

Mullen, L. O., Sullivan, D. B., **Fabrication of tunnel junctions on niobium films,** *J. Appl. Phys.* **40,** *No. 5, 2115–2117 (April 1969).*

Key words: Josephson effect; niobium; thin films; tunnel junctions; super conducting device; thin films.

High background currents, often observed in tunnel junctions when the barrier is formed by oxidizing niobium, probably stem from the fact that one oxide of niobium (NbO) is not an insulator. The fabrication process described in this paper uses an active layer of gas absorbed on the niobium surface that reacts with the upper film (e.g., lead) and forms the junction barrier. This technique avoids the problem above and results in tunnel junctions with low background currents.

Nargolwalla, S. S., Przybylowicz, E. P., Suddueth, J. E., Birkhead, S. L., **Solution of blank problems in 14-MeV neutron activation analysis for trace oxygen,** *Anal. Chem.* **41,** *No. 1, 168–170 (Jan. 1969).*

Key words: Blank; Cockcroft-Walton neutron generator; flow through container; geometrical correction gamma-attenuation; 14-MeV neutron activation analysis; neutron attenuation; systematic error analysis; trace.

A major difficulty in the analysis for trace oxygen by 14-MeV neutron activation analysis is the accurate determination of the oxygen contribution from the blank. If the count from the oxygen in the container is merely subtracted from the total sample-in-container count, errors greater than 100% in the oxygen content of the sample may result.
This work describes a procedure for accurately establishing the blank contribution. The method takes into consideration the attenuation of the activity produced in the polyethylene container by the sample during irradiation and counting. A proposed model permits corrections for the sample-in-container geometries with respect to the neutron source and detector system for different rod diameters. For metal rods, a "flow through" container propelled with nitrogen in the pneumatic transfer system was used to eliminate oxygen contribution from the container void volume. Within the precision of measurement, the experimental results agree with those predicted from theory.

NBS frequency and time broadcast services. Radio stations WWV, WWVH, WWVB, and WWVL, *Nat. Bur. Stand. (U.S.), Spec. Publ.* **236,** *16 pages (1969), (Supercedes NBS Special Publication 236, 1968 edition), 25 cents.*

Key words: Broadcast of standard frequencies; high frequency; low frequency standard frequencies; time signals; very low frequency.

Detailed descriptions are given of the technical services provided by the National Bureau of Standards radio stations WWV, WWVH, WWVB, and WWVL. These services are: 1. Standard radio frequencies; 2. Standard audio frequencies; 3. Standard musical pitch; 4. Standard time intervals; 5. Time signals; 6. UT2 corrections; 7. Radio propagation forecasts; and 8. Geophysical alerts. In order to provide users with the best possible services, occasional changes in broadcasting schedules are required. This publication shows the schedules in effect on January 1, 1969. Annual revisions will be made. Current data relating to standard frequencies and time signals are available monthly in the Time and Frequency Services Bulletin. Advance notices of changes occurring between revisions will be sent to users of NBS broadcast services who request such notice on the basis of need.

Newman, N., **Considerations in computing the useful frequency range of piezoelectric accelerometers,** *Nat. Bur. Stand. (U.S.), Tech. Note 487, 20 pages (July 1969), 30 cents.*

Key words: Electrical excitation; lowest resonant frequency; mechanical excitation; piezoelectric accelerometer; usable frequency range.

This paper analyzes two lumped-parameter models for computing the usable frequency range of piezoelectric accelerometers. The analyses indicate why application of an electrical excitation to the piezoelectric element of a mounted pickup does not, in general, give the same result as application of a mechanical acceleration to the structure on which the pickup is mounted. Tabular results of the computations for various sets of parameters indicate those cases for which the electrical drive will give resonant frequency values within 2% of those for the pickup mounted on a vibrating structure. For these parameter sets, the electrical drive can be used as a reliable substitute.

Newton, C. J., Ruff, A. W., Jr., **X-ray studies of plastically deformed silver alloys-effects due to oxygen, hydrogen, and tin solutes,** *Advan. X-Ray Anal.* **12,** *316–328 (1969).*

Key words: Domains; hydrogen; oxygen; silver alloys; stacking fault; strains; x-ray diffraction.

Solid specimens of silver were charged at different temperatures in atmospheres of oxygen and of hydrogen. X-ray diffraction line profiles were obtained using powders filed from the treated specimens. Fourier analysis of the diffraction lines was conducted following the method of Warren. The effective particle sizes and root-mean-square strains were obtained from the line shape analysis. Stacking fault and twin fault probabilities were determined from peak-position and center-of-gravity displacements, respectively. For the purpose of comparison, two vacuum-melted silver samples and two different silver-tin alloys (4 at.% and 10.3 at.% tin) were studied. The stacking fault and twin fault probabilities were observed to be nearly unaffected by charging in either oxygen or hydrogen. These results are consistent with recent direct determinations of the effect of oxygen on the stacking fault energy of silver. In contrast, the rms strains and particle sizes changed significantly after charging in oxygen. A decrease in the root-mean-square strain and a corresponding increase in the particle size was found. These effects were opposite to those obtained by adding substitutional solute to silver, confirmed in the present study of two silver-tin alloys. These findings are interpreted to indicate the effect of oxygen clustered with impurities on the dislocations and stacking faults in silver.

Nimeroff, I., Schleter, J. C., **Professor Harry J. Keegan: colorimetrist's spectrophotometrist,** *J. Appl. Opt.* **8,** *No. 4, 757–761 (Apr. 1969).*

Key words: Colorimetry; Keegan, Harry J.; photointerpretation; safety color codes, spectrophotometry; standards for spectrophotometers.

A tribute to Professor Harry J. Keegan (October 11, 1903 to April 19, 1968), prepared by two of his close associates at the National Bureau of Standards. The significance of his scientific and academic careers is reviewed and a substantially complete collection of references to his works is presented.

Odom, J. V., **Problems of metric conversion,** *ASTME Vectors* **4,** *No. 4, 17–19 (July/Aug. 1969).*

Key words: International system of units; measurement systems; metric system; metric system study.

The increasing worldwide use of the metric system is causing problems for manufacturers of hardware items. These problems and the law that was recently enacted by Congress to study these problems and seek sensible solutions are discussed, and the background that caused the law to be enacted is reviewed.

Parks, E. J., Linning, F. J., **An evaluation of certain methods for the chemical analysis of styrene-butadiene rubber,** *Nat. Bur. Stand. (U. S.), Tech. Note 485, 27 pages (July 1969), 35 cents.*

Key words: Bound styrene; carbon black; chemical analysis; latexes; oil; organic acid; serums; soap; stabilizer; styrene-butadiene rubber (SBR); washes.

The applicability of available methods for the analysis of unvulcanized styrene-butadiene rubber (SBR, formerly GR-S) for organic acid and soap is influenced by the type of coagulation (alum or salt-acid), the type of acid present (fatty acid, rosin acid, or mixed acids), and the presence of carbon black or oil. No single method is universally applicable for the analysis of organic acid and soap, but reasonably unbiased results can be attained by proper selection of the available procedures.
The complete-solution procedure for alum-coagulated (AC) SBR has given reasonably good results for organic acid in samples containing mixed acids, while the extraction procedure using aqueous isopropanol-toluene azeotrope (ITA) gives good results for AC samples containing fatty acid only.
The complete-solution procedure for SBR coagulated with salt and acid gives less biased results for organic acid and soap than the aqueous ITA extraction procedure, but the latter should be used for all SBR containing carbon black and for estimating oil in oil-rubber masterbatches. Both complete-solution procedures and the ITA extraction procedure can be adapted for the determination of stabilizer and bound styrene. The present ASTM extraction procedure using ethanol-toluene azeotrope is less satisfactory than the other procedures.

Pella, P. A., DeVoe, J. R., Snediker, D. K., **Problems in using Mössbauer spectrometry for quantitative analysis: application to tin,** *Anal. Chem.* **41,** *No. 1, 46–50 (Jan. 1969).*

Key words: High resolution detector; Mössbauer; quantitative analysis; source-sample-detector geometry; tin compounds; use of filters.

Initial studies for the application of Mössbauer spectroscopy to the quantitative analysis of tin compounds are described. The effect of variables such as drift in detector response, sample thickness, and sample concentration on the spectral parameters was studied using Pd_3Sn^{119m} as a source and synthetic samples of SnO_2 in an Al_2O_3 matrix. Under controlled conditions, the reproducibility of the spectral parameters were studied for sample sizes from 3 to 122 mg of SnO_2 with a relative standard deviation (of a single measurement) for 3 replicates of 0.5 to 5% over this range of sample size. The data were well approximated by an exponential absorption law. Such factors as source-sample-detector geometry, use of filters, and a high resolution detector were considered, in an effort to optimize the ratio of the resonant absorption intensity to the total transmitted intensity.

Pfeiffer, E. R., Schooley, J. F., **Superconducting transition temperatures of Nb-doped $SrTiO_3$,** *Phys. Letters,* **29A,** *No. 10, 589–590 (Aug. 11, 1969).*

Key words: Charge carrier density; Nb-doped $SrTiO_3$; superconductivity; transition temperatures; transition temperature maximum.

We have observed superconducting transitions in Nb-doped $SrTiO_3$ over the range of charge carrier densities $n = 0.13 - 2.2 \times 10^{20}$ cm^{-3}. A T_c maximum is observed similar to those previously observed in reduced $SrTiO_3$ specimens.

Powers, R. S., Snyder, W. F., Editors, **Radio-frequency measurements in the NBS Institute for Basic Standards,** *Nat. Bur. Stand. (U.S.), Tech. Note 373, 116 pages (June 1969), $1.00.*

Key words: Accuracy; calibration services; measurements; measurement techniques; radio frequency; uncertainties of measurement.

This volume is a collection of diagrams, tables, and text material, which has been assembled to show the interrelationships between various radio frequency measurements made by the Institute for Basic Standards (IBS). In particular, the measurements are those which lead to services provided to the public or to other government agencies. These services include not only calibrations made for fees, but the broadcast services of the four NBS radio stations. Measurements made as part of the IBS research and development program are not included.
The information included is designed to give the users and potential users of the radio frequency services a clearer understanding of the origins of the measurement output of IBS in this field.

Przybylowicz, E. P., Smith, G. W., Suddueth, J. E., Nargolwalla, S. S., **Activation analysis of halogens in photographic emulsions using a neutron generator,** *Anal. Chem.* **41,** *No. 6, 819–823 (May 1969).*

Key words: Chloride; iodide; 14.7-MeV neutrons; non-destructive neutron activation analysis; photographic emulsions; silver bromidem-2.8-MeV neutrons.

A non-destructive neutron activation technique for the analysis of chloride and iodide in a silver bromide matrix is described. Chlorine was measured after activation with 14.7-MeV neutrons. The 3.1-MeV gamma rays from ^{37}S were measured without interference. Calibrations were carried out using photographic emulsions containing 10 to 200 milligrams of chlorine. The relative standard deviation of a single determination at the 10 milligram level is 5%; at the 200 milligram level it approaches 1%. Iodine was measured via ^{128}I produced by (n, γ) activation with 2.8-MeV neutrons. A straight line curve was established for 2 to 420 milligrams of iodine. The relative standard deviation of a single determination at these two levels was 20% and 1% respectively. The method offers an attractive alternate to existing chemical and instrumental methods for the determination of iodide and chloride in silver halide mixtures since it has the potential for providing rapid analyses with reasonably good precision. With an order of magnitude increase in neutron flux, the method would be unquestionably superior to other instrumental methods for the halides.

Radford, H. E., **Scanning microwave echo box spectrometer,** *Rev. Sci. Instr.,* **39,** *No. 11, 1687–1691 (Nov. 1968).*

Key words: Cavity spectrometer; echo box; free radicals; hydroxyl radical; microwave absorption.

A resonant cavity microwave spectrometer for wavelengths between 3 and 30 cm, which uses radar echo boxes as absorption cells, is described. The minimum detectable absorption coefficient at 10 cm wavelength is 10^{-10} cm^{-1}, and this sensitivity is maintained during frequency scans by automatic feedback tuning of the echo box. The spectrometer is well suited to studies of gaseous chemical reactions, and some preliminary observations are reported, including the negative results of a search for the 10 cm spectrum of CH, and measurements of OH spectra at 4.7 and 6.0 GHz.

Rains, T. C., Menis, O., **High-precision flame emission spectrometry,** *Spectroscopy Letters* **2,** *No. 1, 1–7 (1969).*

Key words: Differential flame emission; precision; phase shifter and attenuator; synchronous detector.

A new technique for differential flame emission spectrometry is described. The application of this method permits the determination of lithium as a major component in a glass matrix with a precision of one part per thousand.

Reeve, G. R., **A heterodyne near-zone field-strength meter,** *IEEE Trans. Instr. Meas.* **IM–18,** *No. 1, 32–37 (Mar. 1969).*

Key words: Electric field strength; field; line; medium field strength; near zone electromagnetic; semiconducting plastic transmission.

This paper describes a tunable field strength meter covering the 12 to 30 MHz range which can be used to measure electric intensities from 0.1 to 1000 volts/meter in the near zone of an antenna with an estimated uncertainty of ± 2 dB.
The use of high-conducting plastic telemetry lines enables the field to be probed without disturbance, while a novel detector circuit and meter enable a 40 dB display with minimal reading error. Laboratory and field test data on the device are presented.

Risley, E. W., **Discontinuity capacitance of a coaxial line terminated in a circular waveguide,** *IEEE Trans. Microwave Theory and Tech.* **MTT–17,** *No. 2, 86–92 (Feb. 1969).*

Key words: Discontinuity capacitance; open circuited coaxial line; Rayleigh-Ritz variational method; solid center conductor.

This calculation evaluates the discontinuity capacitance of a coaxial line terminated in a circular waveguide using the Rayleigh-Ritz variational technique. A 50 ohm, ¾ inch, coaxial line termination with solid center conductor was fabricated with center and outer conductor dimensions of 0.32568 ± 0.00002 and 0.74995 ± 0.00002 inches respectively. The measured value of capacitance of this termination at 1000 Hz was 2.164×10^{-13} farads as compared with the calculated value of 2.177093×10^{-13} farads. Calculated values of capacitance for other line sizes were also compared with measured values and in each case the calculated value agreed with the measured value to within the experimental error of the measured value.

Rothwell, C. J., **The performance concept: A basis for standards development,** *ASTME Vectors* **1969/2,** *23–25 (Mar.–Apr. 1969).*

Key words: Engineering standards; performance concept; performance standards.

Technological measurements and standards are use-related and at the interface between science and its application in industry and government. They extend the principles of good measurement to the engineering world and to the complex needs of today's society. But it is increasingly important that such measurements and standards do not hamper the introduction of new technologies or innovations for accomplishing society's objectives. One way to avoid such restrictions is suggested by the concept of using performance requirements as the basis for standards. This concept includes a concern for subjective factors which of necessity enter measurement problems as soon as man becomes part of the system to be measured.

Ruff, A. W., Jr., Ives, L. K., **Stacking fault energy determinations in HCP silver-tin alloys,** *Acta Met.* **17,** *1045–1055 (Aug. 1969).*

Key words: Dislocation double ribbons; dislocation nodes; HCP alloys; silver-tin alloys; stacking fault energy.

Measurements of the intrinsic stacking fault energy as a function of tin solute concentration are reported through the range of the intermediate hexagonal ξ-phase. Four different alloy compositions in the range 12 to 17 atomic percent tin were studied. Extended dislocation nodes and dislocation double ribbons were observed and measured in order to determine the stacking fault energy. The stacking fault energy values obtained from measurements on these two configurations were in good agreement and indicated that the magnitude of the stacking fault energy increased linearly with solute concentration in the hcp phase. These results are compared with those of the cubic α-phase alloys. The dislocation configurations in the hexagonal alloys are briefly described.

Ryan, J. V., **Federal government's role and activities in consumer safety. The role of the Fabric Flammability Section,** *Proc. Spring Workshop, Home Conf., 5 pages. National Safety Council, General Session, Washington, D. C., May 26, 1969.*

Key words: Fabrics, flammability; flammable fabrics act, rugs, textiles, wearing apparel.

A review is given of consumer safety programs at the National Bureau of Standards, particularly those in response to legislation. The provisions of the Flammable Fabrics Act are listed, and the chief items of implementation are discussed. Procedures for the development of standards have been published in the Federal Register. The initial step under the Procedures, a notice of finding that there may be need for new or amended flammability standards, has been taken for wearing apparel, carpets, and rugs. Test method development in support of these findings is in progress. Research has been initiated in the flammability of materials. The National Advisory Committee for the Flammable Fabrics Act has been appointed and has met.

Ryan, J. V., **The flammable fabrics act and its implementation,** *Proc. Second Annual Meeting Information Council on Fabric Flammability, New York, N. Y., Dec. 3, 1968, pp. 231–237 (Information Council on Fabric Flammability, New York, N. Y., 1968).*

Key words: Carpets; fabrics; flammable fabrics act; National advisory committee; regulations' textiles; wearing apparel.

The 1967 Amendments to the Flammable Fabrics Act delegated authority for establishment of regulations, research, investigations and test method development, and called for a National Advisory Committee with which the Secretary of Commerce must consult. The National Bureau of Standards has been coordinating with Public Health Service in studying burn cases, and has established a Fabric Flammability Section to carry out the research responsibilities, the coordination, data analysis, and the formulation or recommendations for new or amended standards and regulations. Research will start with basic consideration of what happens in fires that represent hazards to life and property. Data will be considered from any competent source, in or out of government. Consumers Union has provided data on carpets and blankets. The Department has published Procedures for developing standards, and findings that there may be need for standards for wearing apparel and for rugs and carpets. Announcement of the membership of the National Advisory Committee is expected in the near future.

Saylor, C. P., **The freezing staircase method,** *Chapter 11 in Purification of Inorganic and Organic Materials,* M. Zief, Ed., *pp. 125–138 (Marcel Dekker, Inc., New York, N. Y., 1969).*

Key words: Crystallization; entrapment; impurity; phase equilibrium; purification; purity; solid solution.

In the freezing staircase method of purification, frozen portions of the material being purified are attached to the walls of the vessel. They move slowly with the rotating apparatus, transporting matter in that direction. An equal mass of liquid flows in the opposite direction. The solid portions are maintained in a crystalline state by stationary coolers outside the containers. Since the growing front and the melting surfaces of each solid portion remain stationary, the solid is caused to grow on one side and melt on the other until, under good conditions, it becomes monocrystalline. By this means there is a close approach to theoretical distribution coefficient of impurity between the liquid and solid phases except at locations in the apparatus where the concentration of solid insoluble impurities is at a high level (>5%). During the greater part of any run under good conditions, there is no spontaneous nucleation. Encapsulation and entrapment are nearly or entirely eliminated. There is no back mixing of rejected impurities. Purification factors can easily be achieved in each stage which are clearly in excess of one thousand.

Sengers, J. V., **Transport properties of compressed gases,** *Chapter in Recent Advances in Engineering Science,* A. C. Eringen, Ed., *III, 153–196 (Gordon and Breach, Inc., New York, N. Y., 1968).*

Kev words: Compressed gas; thermal conductivity; transport properties; viscosity.

This paper reviews the experimental information on the viscosity and thermal conductivity of compressed one-component gases. The common features in the pressure and density dependence of these transport coefficients observed for various simple gases are summarized. An assessment is made of some methods used to predict the transport coefficients of a compressed gas and the relation between experiment and theory is discussed. A survey is included of the behavior of viscosity and thermal conductivity in the critical region and of the anomalous behavior of the dimensionless Rayleigh and Prandtl number, frequently encountered in the description of certain heat transfer processes. A new method to study transport processes by observing the spectrum of scattered light is discussed and some applications are indicated.

Sher, A. H., **Lithium-ion drift mobility in germanium,** *J. Appl. Phys.* **40,** *No. 6, 2600–2607 (May 1969).*

Key words: Germanium; lithium ion mobility; radiation detectors.

The mobility of lithium in germanium has been determined at several temperatures between 23.8 and 61.2°C by measuring the change of the capacitance with time of a reverse-biased p-i-n diode. The mobilities of lithium thus obtained (at the specified temperatures) were: 3.04×10^{-10} cm²/V-s (23.8°C), 5.30×10^{-10} cm²/V-s (36.2°C), 7.96×10^{-10} cm²/V-s (46.2°C), and 16.86×10^{-10} cm²/V-s (61.2°C). These values are higher than those which are obtained by the extrapolation of the results of others determined at higher temperatures into this temperature range. The results also suggest that at least three distinct field configurations exist during the early stages of the lithium drifting process rather than the two normally considered.

Simpson, J. A., **Electron impact spectrometry for gas phase chemical analysis,** *Mater. Res. Stand.* **9,** *No. 8, 13–16 (Aug. 1969).*

Key words: CO in air; electron impact spectrometer; gas analysis.

Electron impact spectrometry provides a new tool for gas phase chemical analysis. The data obtained is directly related to ultraviolet optical absorption but is easier to obtain and interpret. The instrument is briefly described and its performance demonstrated on CO in air at 15 ppm.

Smith, R. V., **Review of heat transfer to helium I,** *Proc. 1968 Summer Study on Superconducting Devices and Accelerators, Brookhaven National Laboratory, Upton, N. Y., June 10–July 19, 1968, Part I, BNL 50155 (C–55), pp. 249–292 (Clearinghouse for Federal Scientific and Technical Information, Springfield, Va., Apr. 1969, $3.00).*

Key words: Boiling, convection; critical, heat transfer; helium I; supercritical.

This paper reviews heat transfer to Helium I. The data were collected, compiled, and the results discussed. Recommendations are made for expressions for use in design studies and for further work required to produce needed information.

Spinner, S., Barton, F. W., **Some problems in measuring tread wear of tires,** *Nat. Bur. Stand. (U. S.), Tech. Not 486, 27 pages (Aug. 1969), 35 cents.*

Key words: Tires; tread wear testing; statistics.

Some problems in tread wear testing of tires are discussed and methods for dealing with these problems are presented. Experimental data are shown to illustrate these methods. Finally some recommendations are made, based primarily on this information, in order to achieve greater uniformity and a statistically valid approach to tread wear testing.

Stephens, R. E., Sutton, L. E., **Diffraction image of a point in the focal plane and several out-of-focus planes,** *J. Opt. Soc. Am.* **58,** *No. 1001–1002 (July 1968).*

Key words: Diffraction image; image evaluation; lens analysis.

For the case of an aberration-free lens system with circular aperture, a table is presented which gives the fraction of maximum irradiance in the diffraction image of a point. The columns of the table correspond to variations in location of the focal plane; the rows to variations in the distance from the center of a diffraction pattern. These values were obtained, to an accuracy of five decimal places, through Gaussian integration of the required Bessel function expressions, the calculations being performed on a digital computer.

Stevens, M. E., **Automatic analysis, Encyclopedia of Library and Information Science,** A. Kent and H. Lancour, Eds., **2,** *144–184 (Marcel Dekker Inc., New York, N. Y., 1969).*

Key words: Automatic character recognition; automatic classification; automatic content analysis; automatic indexing; automatic pattern recognition; keyword indexing; linguistic data processing; question-answering; statistical association.

Progress in techniques and applications of automatic analysis are discussed in terms of library and information science interests. Topics discussed include automatic pattern recognition, machine indexing by extraction of keywords, automatic indexing and classification, statistical association techniques, linguistic data processing, automatic content analysis and question-answering systems.

Stiehler, R. D., **History of measurement and the SI units,** *Mater. Res. Std.* **9,** *No. 6, 14–18 (June 1969).*

Key words: Ancient measures; history; measurement; SI units; units of measurement.

The evolution of the units of measurement from ancient Babylonia and Egypt to the present is briefly described. The so-called English units did not originate in England; they descended from antiquity. The confusion caused by the multiplicity of ancient units that were in use in Europe during the Renaissance was the stimulus that led to the development of the metric units. Similarly, the multiplicity of metric units for the same quantity that have arisen since 1800 led to the development of the rational and coherent International System of Units (SI) which were adopted in 1960 by the General Conference on Weights and Measures. The advantages and weaknesses of SI are discussed.

Stiehler, R. D., Parks, E. J., Linning, F. J., **Stiffening of elastomers by organic fillers,** *Appl. Poly. Symp. No. 7, 143–153 (1968).*

Key words: Anisotropic; beta-naphthyl group; block polymers; bonds; crystallization; elastomers; expansivity; forces; phenyl-beta-naphthylamine; stiffening; x-ray diffraction.

Elastomers can be stiffened in various ways. Self-stiffening occurs in elastomers that crystallize or in block copolymers composed of one block in the elastomeric state and two or more blocks in the glassy or crystalline state. Fillers also cause stiffening. Some crystalline organic compounds which contain a beta-naphthyl group are particularly effective. The conditions under which the crystals form in the elastomer affect the degree of stiffening. Under favorable conditions, about 3% crystalline phenyl-beta-naphthylamine (PBNA) stiffens rubber to about the same degree as 40 phr carbon black. Since the crystals can be extracted with organic solvents, the stiffening effect is reversible. Studies with PBNA and results in the literature suggest that (1) stiffening of elastomers by fillers is primarily a physical phenomenon, (2) the effectiveness of a filler is determined by both surface area and interfacial forces between the filler and elastomer, (3) surface area is determined by the geometry of the particles, (4) interfacial forces depend on the number of atoms per unit surface area that are sufficiently close to atoms in the elastomer molecule to develop a substantial force, (5) interfacial forces are maximized when the atoms in the surface layer of the filler have a geometric structure similar to the atoms in the elastomer, and (6) the elastomer molecule or segments of it must have sufficient mobility to permit alignment with the filler surface to achieve attraction at as many points as possible.

Straty, G. C., **Bellows-sealed valve for reactive gases at moderately high pressures,** *Rev. Sci. Instr.* **40,** *No. 2, 378–379 (Feb. 1969).*

Key words: Bellows; fluorine; high pressure; packless; reactive; valve.

A relatively simple and inexpensive laboratory size bellows sealed valve for use at pressures in excess of 3000 psi is described. The valve is a modification of one of several commercially available, small high pressure valves and uses a number of standard components.

Strobridge, T. R., **Refrigeration at 4 °K,** *Proc. 1968 Summer Study on Superconducting Devices and Accelerators, Brookhaven National Laboratory, Upton, N. Y., June 10–July 19, 1968, Part I, BNL 50155 (C–55), pp. 193–204 (Clearinghouse for Federal Scientific and Technical Information, Springfield, Va., Apr. 1969, $3.00).*

Key words: Claude; cryogenics; Gifford-McMahon; helium; Joule-Thomson; liquid; power; Simon; size; Stirling.

Superconducting accelerators and support elements are being considered for the next generation of particle accelerators. Until practical materials with higher transition temperatures become a reality, refrigeration in the neighborhood of 4 K will be required for these superconducting devices. This paper summarizes a lecture given on 4 K refrigeration covering evaporating liquid helium baths, the Simon process, the Joule-Thomson, Brayton, Claude, Stirling, and Gifford-McMahon cycles. Also included were examples of analysis and descriptions of modern refrigerators and their components.

Strobridge, T. R., **Refrigeration for superconducting and cryogenic systems,** *(Proc. 1969 Particle Acceleration Conf., Washington, D. C., March 5–7, 1969), IEEE Trans. Nuclear Sci.* **NS–16,** *Part I, No. 3, 1104–1108 (June 1969).*

Key words: Cost; cryogenic; efficiency; mass; 1.8 to 90 K; refrigeration; volume.

Cryogenics and high energy physics have been intimately associated for many years. The liquid hydrogen bubble chamber remains a primary detector for particle interactions and the recent successful development of superconducting RF cavities will vastly improve the duty cycle of linear accelerators. Aside from target and detection devices, it is not clear what role low temperature environments will play in the particle accelerators now being conceived. The amount of cooling required and the refrigeration temperatures may vary widely from concept to concept. To assist in planning, this survey of modern cryogenic refrigerators, covering refrigeration temperatures from about 1.8 K to 90 K, gathers together performance, physical characteristic and typical cost information from industry, academic, and government sources both in the U.S. and abroad. Whenever possible, data on liquefiers are converted to an equivalent refrigeration capacity. The capacities discussed range from about one watt to kilowatts.

Strobridge, T. R., **Review of the cryogenics session second week of the Brookhaven summer study on superconducting devices and accelerators,** *Proc. 1968 Summer Study on Superconducting Devices and Accelerators, Brookhaven National Laboratory, Upton, N. Y., June 10–July 19, 1968, Part I, BNL 50155 (C–55), pp. 368–375 (Clearinghouse for Federal Scientific and Technical Information, Springfield, Va., Apr. 1969, $3.00).*

Key words: Cryogenics; cryopump; cryostat; electrical lead; heat transfer; mechanical properties; refrigeration; safety; super conductivity; superfluid.

This paper reviews the lectures given during the cryogenics session at the Brookhaven Summer Study on Superconducting Devices and Accelerators. Lectures were given on the low temperature mechanical properties of both metallic and nonmetallic structural materials, cryostat design, cryopumping, electrical lead design, safety, superfluid helium, heat transfer to helium I and finally three talks were given on refrigeration. The experts' opinions are outlined and the areas which most urgently require further research and development are listed.

Swartzendruber, L. J., Bennett, L. H., Watson, R. E., **Dilute ^{57}Fe Mössbauer studies in Cu-Ni alloys,** *J. Appl. Phys. 40, No. 3, 1489–1490 (Mar. 1, 1969).*

Key words: Copper; invar effect; iron; magnetism; Mössbauer; nickel.

The ^{57}Fe Mössbauer effect has been used to study the properties of iron as a dilute impurity in Cu-Ni alloys. Using either 0.5 at.% Fe as an absorber or ^{57}Co as a source in Cu-Ni alloys, we find a small, partially resolved magnetic hyperfine field in what are normally considered non-magnetic alloys. Previously the hyperfine field at 4 K was reported as undergoing a rapid decrease in value near the equiatomic composition: from 243 dT (243 kG) at 55 at.% Ni to 0 dT (0 kG) at 45 at.% Ni (both alloys are ferromagnetic at 4 K). The present work extends this study and finds that the magnetic field drops instead to the small value of 10 dT (10 kG). This field is almost independent of Ni concentrations between 10 and 45% Ni (i.e. in both ferromagnetic and paramagnetic regions). It is temperature independent between 4.2 and 298 K, and is the same for either the source or absorber (0.5%). The Mössbauer results suggest an invar-type effect occurs in this alloy system.

Swanson, H. E., McMurdie, H. F., Morris, M. C., Evans, E. H., **Standard x-ray diffraction powder patterns,** *Nat. Bur. Stand. (U.S.), Monogr. 25, Section 7, 188 pages (Sept. 1969), $1.50.*

Key words: Crystal structure; integrated intensities; peak intensities; reference intensities; lattice constants; powder patterns; standard; x-ray diffraction.

Standard x-ray diffraction powder patterns are presented for 81 substances. Forty-five of these patterns represent experimental data and 36 are calculated. The experimental x-ray powder diffraction patterns were obtained with a Geiger or proportional counter x-ray diffractometer, using samples of high purity. All d-values were assigned Miller indices determined by comparison with computed interplanar spacings and from consideration of space group extinctions. The densities and lattice constants were calculated, and the refractive indices were measured whenever possible. The calculated x-ray powder diffraction patterns were computed from published crystal structure data. Both peak height and integrated intensities are reported for the calculated patterns.

Tate, D. R., **Gravity measurements and the standards laboratory,** *Nat. Bur. Stand. (U.S.), Tech. Note 491, 10 pages (Aug. 1969), 25 cents.*

Key words: Absolute gravity; deadweight; force; geodetic pendulum; gravity; gravity meter; Potsdam system; standard gravity; units of force.

The local value of the acceleration due to gravity is a fundamental datum for almost every standards laboratory as it, together with accurate standards of mass, is the basis for the standards involving force. Instruments used as standards in this area include precise deadweight piston gages, deadweight calibrators for force transducers, liquid manometers, and earth field accelerometer calibrators. The practical realization of the absolute ampere and the absolute volt require a knowledge of force. This paper presents the basic information about how gravity measurements are made and outlines procedures for obtaining a suitable value for a given location. It also gives a brief discussion of the background and meaning of the term "standard gravity", and its application in the computation of forces in units of the pound-force and the kilogram-force.

Taylor, J. K., **Modern electrochemistry,** *Ind. Res.* **10,** *No. 10, 68–74 (Oct. 1968).*

Key words: Chemical analysis; coulometry; electrochemical analysis; electrochemical instrumentation; ion-selective electrodes; polography.

Electrochemical methods of analysis are especially attractive because of the sensitivity and accuracy they provide. Methods based on measurement of resistance, current, and voltage singly or in combination provide a variety of techniques applicable from trace determinations to assays for major constituents. The methods are especially applicable to automation, process control, and remote-location monitoring situations. The recent advent of ion-selective electrodes promises to increase the scope of electroanalysis, especially for routine determination of moderate accuracy. The techniques most frequently used at the present time are described and discussed with reference to the areas of their greatest utility.

Thompson, B. A., LaFleur, P. D., **Rapid group radiochemical separations for activation analysis of steels,** *Anal. Chem.* **41,** *No. 6, 852–855 (May 1969).*

Key words: Activation analysis; group separations; radiochemical separations; steels.

Rapid group radiochemical separation procedures based on solvent extraction have been developed for the determination of W, Mo, Cu, Cr, As, Co, Sb, and Ga in steel and cast iron. The procedures have been applied to the analysis of NBS Standard Reference Material steels and give results in agreement with the NBS certified values. The precision obtained is routinely ±10% at the 95% confidence level and in favorable situations can be ±2%.

Torrance, K. E., Orloff, L., Rockett, J. A., **Experiments on natural convection in enclosures with localized heating from below,** *J. Fluid Mech.* **36,** *Part 1, 21–31 (1969).*

Key words: Enclosures; flow visualization; modeling; natural convection.

An experimental study was made of the steady state natural convection induced in enclosures by a small hot spot centrally located on the floor. Enclosures of rectangular and circular floor plan were employed, with height equal to major radius of the floor plan. The movement of air within the chambers was made visible by adding metaldehyde dust particles and illuminating with an intense light beam. The Grashof number (Gr) based on hot spot temperature and enclosure height ranged from 8×10^5 to 1×10^{10}. Laminar flows were observed for $Gr-1.2 \times 10^9$. The experimental flows in the circular chamber are compared in a companion paper with theoretically calculated flows (Torrance and Rockett (1968)). In the region of laminar flows the agreement was excellent. The present paper notes certain similarities in the flows in rectangular and circular geometries. The disturbing effect of a slight heating of one wall of the rectangular enclosure was also investigated. Measurements were made of heat transfer from the hot spot to the air in the chamber.

Torrance, K. E., Orloff, L., Rockett, J. A., **Numerical study of natural convection in an enclosure with localized heating from below—creeping flow to the onset of laminar instability,** *J. Fluid Mech.* **36,** *Part 1, 33–54 (1969).*

Key words: Circular cylinder; enclosures; natural convection; numerical.

An analytical study was made of the natural convection induced in an enclosure by a small hot spot centrally located on the floor. The enclosure was a circular cylinder, vertically oriented, with height equal to radius. A Prandtl number of 0.7 (air) was assumed; the Grashof number (Gr) was based on cylinder height and hot spot temperature. The equations of fluid flow in axisymmetric cylindrical coordinates were simplified with the Boussinesq approximation. The equations were solved numerically with a computationally stable, explicit method. The computation, starting from quiescent conditions, proceeded through the initial transient to the fully developed flow. Solutions were obtained for Gr from 4×10^4 to 4×10^{10}. The calculated flows were compared with the experimental flows presented in a companion paper, Torrance, Orloff and Rockett (1968). The experimental flows were laminar for $Gr \leq 1.2 \times 10^9$; turbulence was observed above this value. In the laminar flow region ($Gr \leq 1.2 \times 10^9$) agreement between the theoretical and experimental flow patterns was excellent. When extended into the experimentally observed turbulent range ($Gr = 4 \times 10^{10}$) the theoretical flow developed a periodic vortex shedding, suggestive of the onset of transition.

Veillon, C., Margoshes, M., **An evaluation of the induction-coupled, radio-frequency plasma torch for atomic emission and atomic absorption spectrometry,** *Spectrochim. Acta* **23B,** *503–512 (1968).*

A study has been made of the radio-frequency plasma torch as a source of atoms for emission and absorption spectrochemical analysis. The factors evaluated include sensitivity, limits of detection, inter-element effects, limitations, and general convenience. In agreement with other reports, the plasma torch was found to give useful emission signals for several elements which are difficult to excite in chemical flames, such as B, Ta, and Ti. The value of the source for atomic absorption spectrometry was found to depend on the availability of bright line sources. Pronounced inter-element effects were found, affecting particularly the emission signals. In most cases, these inter-element effects were enhancements of the emission, although in one case a suppression was observed. Except for a few refractory elements, the plasma torch does not appear to be a suitable replacement for the chemical flame.

Key words: Atomic absorption spectrometry; atomic emission spectrometry; detection limits; inter-element effects; plasma torch; radio frequency; spectrochemical analysis.

Veillon, C., Margoshes, M., **A pneumatic solution nebulization system producing dry aerosol for spectroscopy,** *Spectrochim. Acta* **23B,** *553–555 (1968).*

Key words: Atomizer; nebulizer; pneumatic aspirator; sample introduction; solvent removal; spray.

An efficient sample introduction system was developed for aqueous solutions. It is made up of a pneumatic nebulizer, a heated chamber for solvent evaporation, and a chilled condenser for solvent

removal. Features include low gas flow rate, high efficiency, and elimination of the solvent. Overall efficiency is 35%.

Viezbicke, P. P., Jr., **Interactions between nested receiving rhombic antennas,** *IEEE Trans. Ant. Prop.* **AP–17,** *No. 1, 16–23 (Jan. 1969).*

Key words: Antenna; comparison; co-planar; gain; interactions; mutuals; nested patterns; planar proximity; rhombic; spacing.

In order to install as many radiating circuits as possible in a given area, consideration has to be given to the operation of antennas in close proximity to one another. Therefore, mutual coupling between two nested rhombics and the effect of one rhombic on the radiation pattern of the other were measured.

For a ratio of antenna sizes of 2 to 1, the presence of either a coplanar or non-coplanar antenna had no influence on the gain and radiation pattern of the reference rhombic. To determine the minimum acceptable separation, measurements were extended to include rhombics almost equal in size and as close as practicable to each other. For wire separations of 0.5λ, the gain of the reference rhombic was reduced by 0.5 db. For 0.2λ separation the gain was reduced by 1 db, and for 0.04λ, by approximately 4 db. Except for very close spacings, the radiation patterns remained substantially unchanged.
Mutual coupling, expressed as transmission loss between the antennas in db, varied between −23 and −41 db.

Waddell, W. J., Bates, R. G., **Intracellular pH,** *Physiol. Rev.* **49,** *No. 2, 289–329 (1969).*

Key words: Acidity; cell acidity; extracellular pH; glass electrode; intracellular pH.

Intracellular and extracellular pH are defined and methods for their determination are outlined. The literature on pH measurements in cells of the human body is summarized.

Wagman, D. D., **Elements of chemical thermodynamics: Introduction to thermal methods,** *Chapter 86 in Treatise on Analytical Chemistry, Part I, Theory and Practice, I. M. Kolthoff, P. J. Elving, and E. B. Sandell, Eds., 8, 4909–4936 (Interscience Publ. Inc., New York, N. Y., 1968).*

Key words: Equilibria; freezing point equation; ideal solution laws; thermal analyses; thermodynamic laws.

The chapter presents a short introductory statement of the principles of chemical thermodynamics, with special relevance to the laws used in the application of temperature and heat measurement to determinations of purity and extent of chemical reaction.

Waterstrat, R. M., **Evaluation of a gallium-palladium-tin alloy for restorative dentistry,** *J. Am. Dental Assoc.* **78,** *No. 3, 536–541 (Mar. 1969).*

Key words: Dental amalgam; dental materials; gallium alloy; palladium alloy; restorative dentistry.

A gallium-palladium-tin alloy has been developed which may possibly be used for restorative dentistry. The alloy is handled using techniques very similar to those used with conventional dental amalgams. The gallium alloy, however, has a higher strength and a much greater resistance to flow or creep under an applied load. In addition the gallium alloy wets tooth structure and has a thermal expansion coefficient which is fairly close to that of human teeth. Much more clinical and biological testing will be needed before the alloy can be recommended for general use.

Watson, R. E., Bennett, L. H., Freeman, A. J., **Comments on "Origin of solvent Knight shifts in alloys",** *Phys. Rev.* **179,** *590–592 (Mar. 10, 1969).*

Key words: Alloys; charge impurity screening; hyperfine fields; Knight shift; noble metals; orthogonalized plane waves.

Objections, based on considerations of changes in electronic specific heat, to our proposal on the source of the changes in solvent Knight shift upon alloying, are examined and rejected.

Weiss, B-Z., Meyerson, M. R., **Effect of chromium diffusion coatings on fatigue in iron,** *Trans. Met. Soc.* **AIME 245,** *1633–1643 (July 1969).*

Key words: Armco Iron; chromium diffusion coatings; crack formation; crack propagation; fatigue.

Chromium diffusion coatings on commercial Armco Iron lead to structural, compositional, and stress distributional changes in the outer layers. These changes affect the mechanism of fatigue crack formation. In chromized samples, the crack initiates below the Cr-rich zone after only a limited portion of the total lifetime (5% to 10%). The crack formation was observed at the grain boundaries, where precipitated Cr-carbides were found. Residual tensile stresses and a stress concentration caused by the carbides are considered as accelerating factors. In uncoated samples, the cracks form at slip boundaries after 40% to 50% of total lifetime. The propagation process in coated samples is slower than in uncoated samples, as a result of the moderate rate of propagation until such time as the crack proceeds completely through the coating. At best, the Cr-diffusion causes little if any increase in fatigue life, and in certain cases a severe deterioration in fatigue life is observed.

Weissberg, S. G., Brown, J. E., **Osmometry of polymers,** *Encyclopedia of Polymer Science and Technology* **9,** *659–668 (Interscience Publs., New York, N. Y., 1969).*

Key words: High speed osmometer; number-average molecular weight; osmometer; osmotic pressure; semipermeable membranes.

Brief summary of principles and methods of measurement of osmotic pressures of polymer solutions, with survey of modern high speed instruments.

Wexler, A., **Calibration of humidity-measuring instruments at the National Bureau of Standards,** *ISA Trans.* **7,** *No. 4, 356–362 (1968).*

Key words: Calibration accuracies; gravimetric hygrometer; hygrometry; humidity calibration; humidity generator.

The National Bureau of Standards provides a service to Government agencies and the public for the calibration of humidity measuring instruments. The equipment and procedures employed in making these calibrations and the available ranges and accuracies are described. Calibrations are performed by subjecting the instrument under test to atmosphere of known moisture content produced by the NBS two-pressure humidity generator. The most accurate calibrations are made with the NBS standard hygrometer, a device based on the gravimetric method. With the latter, a measurement can be made with an estimated uncertainty (estimated systematic error plus three times the standard deviation) of 13 parts in 10^4.

Yakowitz, H., Michaelis, R. E., Vieth, D. L., **Homogeneity characterization of NBS spectrometric standards. IV: Preparation and microprobe characterization of W − 20% Mo alloy fabricated by powder metallurgical methods,** *(Proc. 17th Annual Conf., Applications of X-ray Analysis, Estes Park, Colo., Aug. 21–23, 1968), Chapter in Advances in X-ray Analysis, C. S. Barett, G. R. Mallett, and J. B. Newkirk, Eds., 12, 418–438 (Plenum Press Inc., New York, N. Y., 1969).*

Key words: Homogeneity testing; metallography; microprobe analysis; NBS standards; powder metallurgy; tungsten-molybdenum alloys.

A significant problem of the National Bureau of Standards Standard Reference Materials program is the provision of standards suitable in homogeneity for use with microanalytical techniques such as the spark source mass spectrograph and the electron probe microanalyzer. An interim approach to the problem has been the extended homogeneity characterization of selected existing standards. This paper describes the preparation and evaluation of the first NBS standard tested specifically from the beginning for application to electron probe microanalyzers. The standard designated SRM 480 is a tungsten-20 weight percent molybdenum alloy prepared by a powder metallurgy process. Based on the results of about 1500 determinations for both tungsten and molybdenum by electron probe microanalysis, the material was found to be of high

homogeneity at about the micrometer level of spatial resolution. The coefficient of variation for molybdenum was 2.5% and that for tungsten 1.5%. Correction of relative intensity ratios to obtain concentrations is discussed in terms of input parameter uncertainties such as mass absorption coefficients, and electron backscatter factors. The result of studies for atomic number correction and effects on operating voltage on the microprobe absorption correction, will be given. It is concluded that SRM 480 should be a valuable addition to any microprobe laboratory doing quantitative analyses.

Yonemura, G. T., Kasuya, M., **Color discrimination under reduced angular subtense and luminance,** *J. Opt. Soc. Am.* **59,** *No. 2, 131–135 (Feb. 1969).*

Key words: Color discrimination; signal lights; vision.

Under reduced visual conditions, small area and low luminance, color discrimination for normal eyes deteriorates in a manner similar to that observed for tritanopic vision. The purpose of this study was to investigate and quantify the reciprocal relation between area and luminance for conditions where this loss in color discrimination occurs for people with normal vision. Quadratic equations, $\ln s = a(\ln F)^2 + b(\ln F) + C$, were obtained from the empirical data to describe the relationship between chromaticity discriminatibility, with luminous flux F; where s = the standard deviation of color matches and $F = \omega^{3/4}L$ (target solid angular subtense ω, and luminance). The constants a, b, and c are different for the red-green and blue-yellow directions on the chromaticity diagram. The results of this study find their most obvious application in the field of signal lights.

Young, D. S., Mears, T. W., **Measurement and standard reference materials in clinical chemistry,** *Clin. Chem* **.14,** *No. 10, 929–943 (Oct. 1968).*

Key words: Clinical; measurement; medicine; standard reference materials.

The concept of the measurement system based upon the four parameters—length (meter), mass (kilogram), time (second), and temperature (Kelvin)—is developed. The proper daily operation of an analytical laboratory depend on these basic measurements, and several derived from them, e.g., the liter. An additional component of chemical measurement which directly influences accuracy is the purity of the standards and reagents employed. The Standard Reference Materials program of the National Bureau of Standards provides a central source of guaranteed high-purity reference materials which are available to all. The reliability of chemical measurements wil increase as new Standard Reference Materials such as cholesterol, uric acid, urea, and creatinine are utilized to standardize methods and instruments in the clinical laboratories of this country.

Other NBS Publications

J. Res. Nat. Bur. Stand. (U.S.), 74A (Phys. and Chem)., No. 1 (Jan.-Feb. 1970), SD Catalog No. C13.22/sec. A:74/1. $

Standardization of cesium-137 gamma-ray sources in terms of exposure units (Roentgens). T. P. Loftus.

Calculations of Zn II $3d^9 4s5s$ and Ag I $4d^9 5s6s$, and some new levels in these spectra. W. C. M. and J. Sugar.

New vacuum ultraviolet wavelengths and revised energy levels in the second spectrum of zinc (Zn II). W. C. Martin and V. Kaufman.

CIE. 1960 UCS diagram and the Müller theory of color vision. D. B. Judd and G. T. Yonemura.

Blemish formation in processed microfilm.II. C. I. Pope.

Positive and negative ion sublimation from transition metal surfaces: A review of some recent results. M. D. Scheer.

Generation of controlled low pressures of nitrogen by means of dissociation equilibria. R. H. Orcutt.

Temperature coefficient of the bismuth I-II transition pressure. J. C. Houck.

Isothermal diffusion in the dilute range of the system $Ca(OH)_2$–H_3PO_4–H_2O—Theory. E. C. Moreno, P. R. Patel, and W. E. Brown.

High-speed (subsecond) measurement of heat capacity, electrical resistivity, and thermal radiation properties of molybdenum in the range 1900 to 2800 K. A. Cezairliyan, M. S. Morse, H. A. Berman, and C. W. Beckett.

P-V-T, Thermodynamic and related properties of oxygen from the triple point to 300 K at pressures to 33 MN/m². L. A. Weber.

J. Res. Nat. Bur. Stand. (U.S.), 74A (Phys. and Chem.) No. 2 (March-April, 1970), SD Catalog No. C13.22/sec. A: 74/2. $

A theoretical investigation of the configurations $(3d+4s)^4 4p$ in neutral vanadium (V I). C. Roth.

A theoretical investigation of the configurations $(3d+4s)^5 4p$ in neutral chromium (Cr I). C. Roth.

A theoretical investigation of the configurations $(3d+4s)^7 4p$ in neutral iron. C. Roth.

The intensity as a function of temperature of the low-angle x-ray diffraction maxima of the *n*-paraffins: hexatriacontane, tetratetracontane, and tetranonacontane. P. K. Sullivan and J. J. Weeks.

Photoelastic constants of ruby. R. M. Waxler and E. N. Farabaugh.

Estimation of critical constants T_c, ρ_c from the $\rho(T)$ and $T(\rho)$ relations at coexistence. Robert D. Goodwin.

Synthesis and growth of fresnoite ($Ba_2TiSi_2O_8$) from a TiO_2 flux and its relation to the system $BaTiO_3$–SiO_2. C. R. Robbins.

Photoionization study of $Fe(CO)_5$ and $Ni(CO)_4$. G. Distefano.

Papers presented at the Conference, Electronic Density of States, National Bureau of Standards, Gaithersburg, Maryland November 3–6, 1969

The band structure problem. J. M. Ziman.

Optical properties and electronic density of states. M. Cardona.

Excitonic effects in x-ray transitions in metals. G. D. Mahan.

Soft x-ray band spectra and their relationship to the density of states. G. A. Rooke.

The electronic structure of disordered alloys. J. L. Beeby.

Summary of the conference on electronic density of states. H. Ehrenreich.

J. Res. Nat. Bur. Stand. (U.S.), 74B (Math, Sci.) No. 1, (Jan.-Mar. 1970), SD Catalog No. C13.22/sec. B: 74/1. $1.25.

Partitions—a survey. H. Gupta.

A relation between the coefficients and roots of two equations and its application to diophantine problems. T. N. Sinha.

An enumeration problem for a congruence equation. Richard A. Brualdi and M. Newman.

Orthogonal decompositions of tensor spaces. S. Pierce.

Partitioned hermitian matrices. R. Merris.

Bounds on a polynomial. T. J. Rivlin.

Entire functions of exponential type. F. Gross.

Abramowitz, S., Levin, I. W., Raman spectrum of ONF_3, J. Chem. Phys. **51,** No. 1, 463–464 (July 1, 1969).

Ahearn, A. J., Paulsen, P. J., Workshop on mass spectrometric analysis of solids at the National Bureau of Standards in Gaithersburg, Md., Nov. 18 and 19, 1968, Anal. Chem. **41,** No. 2, 79A–81A (Feb. 1969).

Ausloos, P., Rebbert, R. E., Lias, S. G., Gas-phase photolysis of cyclohexane in the photoionization region, J. Phys. Chem. **72,** No. 11, 3904–3914 (Oct. 1968).

Beatty, R. W., Yates, B. C., A graph of return loss versus frequency for quarter-wavelength short-circuited waveguide impedance standards, IEEE Trans. Microwave Theory Tech. **MTT-17,** No. 5, 282–284 (May 1969).

Bender, P. L., Optical orientation experiments at Princeton, Chapter in Polarisation Matiere et Rayonnement, Volume Jubilaire en L'Honneur D'Alfred Kastler, pp. 436–441 (Presses Universitaires de France, Paris, 1969).

Bennett, H. S., Magnet scattering of neutrons from Heisenberg antiferromagnets, J. Appl. Phys. **40,** No. 3, 1552–1553 (Mar. 1, 1969).

Bennett, H. S., Ultrasonic attenuation in Heisenberg magnets, Phys. Rev. **181,** No. 2, 978 (May 10, 1969).

Boyd, M. E., Larsen, S. Y., Kilpatrick, J. E. Quantum mechanical second virial coefficient of a Lennard-Jones Gas. Helium, J. Chem. Phys. **50,** No. 9, 4034–4055 (May 1, 1969).

Bowen, R. L., Mullineaux, A. L., Adhesive restorative materials, Dental Abstr. **14,** No. 80, 80–82 (Feb. 1969).

Bur, A. J., Roberts, D. E., Rodlike and random-coil behavior of poly(*n*-butyl isocyanate) in dilute solution, J. Chem. Phys. **51,** No. 1, 406–420 (July 1, 1969); Proc. 1968 Annual Report Conf. Electrical Insulation and Dielectric Phenomena, Buck Hill Falls, Pa., pp. 80–84 (Natl. Acad. Sci.—Natl. Res. Council, Washington, D. C., 1969).

Butterfield, M. A., OCR standards today, Chapter 37 in Optical Character Recognition and the Years Ahead, pp. 318–335 (Business Press, Elmhurst, Ill., July 1969).

Cahill, K. E., Pure states and the *P* representation, Phys. Rev. **180,** No. 5, 1239–1243 (Apr. 25, 1969).

Cahill, K. E., Regularization of the *P* representation, Phys. Rev. **180,** No. 5, 1244–1255 (Apr. 25, 1969).

Carter, R. S., Rush, J. J., Editors, Molecular dynamics and structure of solids. Proceedings of 2nd Material Research Symposium held at the National Bureau of Standards, Gaithersburg, Md., Oct. 16–19, 1967, Nat. Bur. Stand. (U.S.), Spec. Publ. 301, 571 pages (June 1969), $4.00.

Casella, R. C., Time reversal and the K^0 meson decays. II, Phys. Rev. Letters **22,** No. 11, 554–556 (Mar. 17, 1969).

Cassel, J. M., Gallagher, J., Reynolds, J. A., Steinhardt, J., The Role of transport ion binding studies of serum albumin, Biochemistry **8,** No. 4, 1706–1713 (Apr. 1969).

Cassel, J. M., Steinhardt, J., Limitations inherent in the ΔpH method of determining binding isotherms of bovine serum albumin, Biochemistry **8,** No. 6, 2603–2609 (June 1969).

Champion, C. E., Marinenko, G., Errors in coulometric chloride titrations due to photodecomposition of silver chloride, Anal. Chem. **41,** No. 1, 205–207 (Jan. 1969).

Chung, K., Danos, M., Huber, M. G., Microscopic description of the absorption of bound π-mesons, Physics Letters **29B,** No. 5, 265–267 (May 26, 1969).

Colwell, J. H., Mangum, B. W., Utton, D. B., The low temperature magnetic properties of some hexagonal rare-earth trihalides, Phys. Rev. **181,** No. 2, 842–854 (May 10, 1969).

Cook, A. R., Matarrese, L. M., Zero-field EPR of Fe^{3+} in quartz, J. Chem. Phys. **50,** No. 6, 2361–2364 (Mar. 15, 1969).

Cooper, M. J., Point transformation of classical hard-core potential, J. Math. Phys. **9,** No. 4, 571–578 (Apr. 1968).

Cooper, M. J., Green, M. S., Generalized scaling and the critical eigenvector in ideal Bose condensation, Phys. Rev. **176,** No. 1, 302–309 (Dec. 5, 1968).

Coxon, B., P. M. R. evidence for the conformations of 1, 2-0-benzylidene-α-D-glucofuranose derivatives, Carbohydrate Res. **8,** 125–134 (1968).

Crawford, B. H., Nimeroff, I., Radiation sources and their power supplies, Chapter in Techniques of Photostimulation in Biology, (North-Holland Publ. Co., Amsterdam, The Netherlands) pp. 19–48 (1968).

Crissman, J. M., Mechanical relaxation in polypropylene as a function of polymorphism and degree of lamellar orientation, J. Poly. Sci. **7,** Part A2, 389–404 (1969).

Cushen, W. E., Systems analysis activities at the Technical Analysis Division of the National Bureau of Standards, C-E Newsletter **4,** No. 3, 4–5 (June 1969).

Czyz, W., Maximon, L. C., High energy scattering of strongly interacting composite particles, Physics Letters **27B,** No. 6, 354–357 (Aug. 19, 1968).

Dehl, R. E., Hoeve, C. A. J., Broadline NMR study of H_2O and D_2O in collagen fibers, J. Chem. Phys. **50,** No. 8, 3245–3251 (1969).

Dibeler, V. H., Liston, S. K., Mass-spectrometric study of photoionization, XI. Hydrogen sulfide and sulfur diozide, J. Chem. Phys. **49,** No. 2 ,482–485 (July 15, 1968).

Dibeler, V. H., Walker, J. A., Mass spectrometric study of photoionization. XIV. Nitrogen trifluoride and trifluoramine oxide, Inorg. Chem. **8,** 1728–1733 (1969).

Dodd, J. N., Enemark, E., Gallagher, A., Quenching of cesium resonance radiation by helium, J. Chem. Phys. **50,** No. 11, 4838–4842 (June 1, 1969).

Duerst, R. W., Baum, S. J., Kokoszka, G. F., Exchange coupling in two dimeric copper adenine complexes, Nature **222,** 665–666 (May 17, 1969).

Edmonds, J., Matroid partition, Chapter in Mathematics of the Decision Sciences, American Mathematical Society Lectures in Applied Mathematics **11,** 335–345 (American Mathematical Society, Providence, R. I., 1968).

Eicke, W. G., The zener diode, a working D-C voltage standard, 1968 IEEE Intern. Convention Digest, page 71 (Mar. 1968).

Ernst, M. H., Transport coefficients from time correlation functions, Lectures Theoret. Phys. IX C-Kinetic Theory, 417–441 (Gordon and Breach, Science Publ. Inc., New York, N. Y., 1967).

Farrar, T. C., Johannesen, R. B., Coyle, T. D., Magnetic nonequivalence in the high-resolution NMR spectra of diborane, J. Chem. Phys. **49,** No. 1, 281–285 (July 1, 1968).

Fraction, G. F., Walker, J. C., Tauber, S. J., Connection tables from Wiswesser line notation: A partial algorithm, (Proc. Wiswesser Line Notation Meeting, Army Chemical Information and Data Systems Program, Edgewood Arsenal, Aberdeen, Md., Oct. 6–7, 1966, Spec. Publ. 400–8), AD665397, pp. 139–195 (Clearinghouse for Federal Scientific and Technical Information, Springfield, Va., Jan. 1968, $3.00).

Freeman, D. H., Paulson, R. A., Chemical microstandards from ion exchange resin, Nature **218,** 563 (1968).

Gallagher, A., Excitation transfer in nearly adiabatic thermal collisions, Phys. Rev. **179,** No. 1, 105–110 (Mar. 5, 1969).

Harber, S., Osgood, C. F., On a theorem of Piatetsky-Shapiro and approximation of multiple integrals, Math. Comput. **23,** No. 105, 165–168 (Jan. 1969).

Hanley, H. J. M., Klein, M., Selection of the intermolecular potential function, III. From the isotopic thermal diffusion factor, J. Chem. Phys. **50,** No. II, 4675–4770 (June 1, 1969).

Harris, W. P., Roberts, D. E., New standard reference dielectric specimens at NBS, Proc. 1968 Annual Report Conf. Electrical Insulation and Dielectric Pheonomena, Oct. 21–23, 1968, Buck Hill Falls, Pa., pp. 80–84 (Natl. Acad. Sci.—Natl. Res. Council, Washington, D. C., 1969).

Herron, J. T., Huie, R. E., Rates of reaction of atomic oxygen (O^3P). Experimental method and results for some C_1 to C_3 chloroalkanes and bromoalkanes, J. Phys. Chem. **75,** No. 5, 1326–1335 (May 1969).

Hiza, M. J., Duncan, A. G., Comments on "Intermolecular forces: thermal diffusion and diffusion in He-Kr and H_2-Kr", Phys. Fluids **12,** No. 7, 1531–1532 (July 1969).

Hoffman, J. D., Lauritzen, J. I., Jr., Passaglia, E., Ross, G. S., Frolen, L. J., Weeks, J. J., Kinetics of polymer crystallization from solution and the melt, Kolloid-Z. Polymere **231,** 564 (1969).

Hubbell, J. H., Gamma-ray cross-section evaluation and compilation, Proc. Special Sessions on Gamma-Ray Production and Transport and on Civil Defense Shielding, Winter Meeting of the American Nuclear Society, Nov. 5–9, 1967, Chicago, Ill., A. E. Straker, ed., ANS-SD-7, AEC TID-4500 Series, pp. 71–77, 82–100 (Aug. 1969).

Huget, E. F., Brauer, G. M., Kumpula, J. W., Civjan, S., A filled cold-curing acrylic resin as a splinting material, J. Am. Dent. Assoc. **79,** 645–648 (Sept. 1969).

Hutchinson, J. M. R., Mann, W. B., Smith, C. N., Whittaker, J. K., The half lives of two excited states in ^{239}Np, Intern. J. Appl. Radiation Isotopes **20,** No. 7, 493–498 (July 1969).

Ives, J. M., Hughes, E. E., Taylor, J. K., Absolute determination of low concentrations of oxygen in inert gases by means of galvanic cells, Anal. Chem. **40,** No. 12, 1853–1856 (Oct. 1968).

Jackson, J. L., Lifson, S., Coriell, S. R., Association times of counterions to polyelectrolytes in solution, J. Chem. Phys. **50,** No. 11, 5045 (June 1, 1969).

Jacox, M. E., Milligan, D. E., Matrix-isolation study of the vacuum-ultraviolet photolysis of methyl fluoride. The infrared spectra of the free radicals CF, HCF, and H_2CF, J. Chem. Phys. **50,** No. 8, 3252–3262 (Apr. 15, 1969).

Keller, R. A., Intersystem crossing from excited triplet states into the singlet manifold, (Proc. Intern. Conf. Molecular Luminescence, Loyola Univ., Chicago, Ill., Aug. 20–23, 1968), Chapter in Molecular Luminescence, E. C. Lim, ed., pp. 453–468 (W. A. Benjamin Inc., New York, N. Y., 1969).

Keller, R. A., Dolby, L. J., Intramolecular energy transfer between triplet states of weakly interacting chromophores. III. Compounds in which the chromophores are separated by a rigid steroid bridge, J. Am. Chem. Soc. **91,** 1293–1299 (1969).

Kelley, R. D., Klein, R., Scheer, M. D., The *cis-trans* effect in the H-atom addition to olefins, J. Phys. Chem. **73,** 1169–1170 (1969).

Kirchhoff, W. H., The microwave spectrum, structures, and dipole moment of *cis*-thionylimide, J. Am. Chem. Soc. **91,** 2437–2442 (1969).

Klein, R., Scheer, M. D., Reaction of $O(^3P)$ with 2-methyl-2-pentene at low temperatures and its implication for the transition state, J. Phys. Chem. **73,** 1598–1599 (1969).

Klose, J. Z., Experimental lifetimes of the $5p$ levels in argon I, J. Opt. Soc. Am. **58,** No. 11, 1509–1512 (Nov. 1968).

Klose, J. Z., Transition probabilities and mean lives of the $2S_2$ laser level in neon I, J. Quant. Spec. Rad. Trans. **9,** No. 6, 881–883 (June 1969).

Koonce, C. S., Tunneling into low carrier density superconductors, Phys. Rev. **182,** No. 2, 5407 (June 10, 1969).

Kraft, R., An unusual mixed initial boundary problem in two independent variables, J. Math. Anal. Appl. **25,** No. 2, 233–249 (Feb. 1969).

Ku, H. H., Kullback, S., Approximating discrete probability distributions, IEEE Trans. Info, Theory **IT–15,** No. 4, 444–447 (July 1969).

Laufer, A. H., Photolysis of ketene. Mechanism of hydrogen production and the reaction of methylene with methane, J. Phys. Chem. **73,** 959–963 (1969).

Lehner, J., Newman, M., On Reimann surfaces with maximal automorphism groups, Glasgow Math. J. **8,** Part 2, 102–112 (July 1967).

Leiss, J. E., Penner, S., Rose, J. E., Broberg, J. B., Transient beam loading in electron linear accelerators, (Proc. 1969 Particle Accelerator Conf., Washington, D. C., March 5–7, 1969), IEEE Trans. Nucl. Sci. **NS–16,** Part I, No. 3, 1027–1030 (June 1969).

Levin, I. W., Abramowitz, S., Vibrational spectra and force field for ruthenium tetroxide, J. Chem. Phys. **50,** No. 11, 4860 (June 1, 1969).

Lide, D. R., Jr., Structure of the alkali hydroxides. IV. Interpretation of vibration-rotation interactions in CsOH and RbOH and refinement of structures, J. Chem. Phys. **50,** No. 7, 3080–3086 (Apr. 1, 1969).

Linzer, M., Line parameters of Lorentzian curves containing arbitrary mixtures of absorption and dispersion, J. Appl. Phys. **40,** No. 1, 372–376 (Jan. 1969).

Lipkin, H. J., Meshkov, S., The importance of the $\eta\pi$ decay mode in the split A_2 decay, Phys. Rev. Letters **22,** No. 5, 212–213 (Feb. 3, 1969).

Lutz, G. J., Calculation of sensitivities in photon activation analysis, Anal. Chem. **41,** No. 3, 424–427 (Mar. 1969).

McCamy, C. S., Units for logarithmic scales, Phys. Today **22,** No. 4, 42–44 (Apr. 1969).

McNesby, J. R., The photochemistry of Jupiter above 1200 Å, J. Atmospheric Sci. **26,** No. 3, 594–599 (May 1969).

McNesby, J. R., Kelley, R. V., High temperature vacuum ultraviolet photolysis of *n*-butane, J. Phys. Chem. **73,** No. 4, 789–793 (1969).

Madey, T. E., Yates, J. T., Jr., The measurement of sticking coefficients at high temperature using the isotopic mixing method, (Proc. Sixth Intern. Symp. Rarefied Gas Dynamics, Cambridge, Mass., July 22–26, 1968), Chapter in The Measurement of Sticking Coefficients at High Temperatures Using the Isotopic Mixing Method II, 1345–1348 (Academic Press Inc., New York, N. Y., 1969).

Mangum, B. W., Soulen, R. J., Utton, D. B., Magnetic ordering in cerium trichloride at low temperatures, Proc. XI Conf. Low Temperature Physics, St. Andrews, Scotland, Aug. 21–28, 1968, 2, 1361–1363, Paper C10.9 (University of St. Andrews, Scotland, 1968).

Mangum, B. W., Thornton, D. D., Nuclear relaxation measurements of ^{35}Cl in $PrCl_3$, Phys. Rev. Letters **22,** No. 21, 1105–1107 (May 26, 1969).

Marcus, M., Newman, M., Doubly stochastic associated matrices, Duke Math. J. **34,** No. 3, 591–598 (Sept. 1967).

Marinenko, G., Taylor, J. K., Electrochemical equivalents of benzoic and oxalic acid, Anal. Chem. **40,** No. 11, 1645–1651 (Sept. 1968).

Martin, W. C., Techt, J. L., Wilson, M., Note on the $3p^54s3d$ configuration in neutral potassium (K I), Phys. Rev. **181,** No. 1, 66–69 (May 5, 1969).

Matarrese, L. M., Wells, J. S., Peterson, R. L., EPR spectrum of Fe^{3+} in synthetic brown quartz, J. Chem. Phys. **50,** No. 6, 2350–2360 (Mar. 15, 1969).

May, L., Spijkerman, J. J., On the relationship between Mössbauer spectroscopy and the nuclear magnetic resonance of organotin compounds, J. Chem. Phys. Letter to the Editor **46,** No. 8, 3272–3273 (Apr. 15, 1967).

Melmed, A. J., Single-specimen FEM-LEED studies: carbon on tungsten, J. Appl. Phys. **40,** No. 5, 2330–2334 (Apr. 1969).

Menke, J. L., Beam monitoring at the NBS linac-energy, positioning, current, charge, (Proc. 1969 Particle Accelerator Conf., Washington, D. C., March 5–7, 1969), IEEE Trans. Nucl. Sci. **NS–16,** Part I, No. 3, 921–922 (June 1969).

Mighell, A. D., Reimann, C. W., Santoro, A., The crystal and molecular structure of dibromotetrapyrazolenickel (II), $Ni(C_3H_4N_2)_4Br_2$, Acta Cryst. **B25,** Part 3, 595–599 (Mar. 1969).

Mighell, A. D., Smith, J. P., Brown, W. E., The crystal structure of phosphoric acid hemihydrate, $H_3PO_4\ 1/^2H_2O$, Acta Cryst **25,** 776 (1969).

Miller, K. J., Mielczarek, S. R., Krauss, M., Energy surface and generalized oscillator strength of the $^1A''$ Rydberg state of H_2O, J. Chem. Phys. **51,** No. 1, 26–32 (July 1969).

Moore, C. E., Bibliography on the analyses of optical atomic spectra. Section 3. ^{42}Mo-^{57}La and ^{72}Hf-^{89}Ac, Nat. Bur. Stand. (U.S.), Spec. Publ. 306–3, 37 pages (May 1969), 50 cents.

Mopsik, F. I., Dielectric properties of slightly polar organic liquids as a function of pressure, volume, and temperature, J. Chem. Phys. **50,** No. 6, 2559–2569 (Mar. 15, 1969).

Mountain, R. D., Deutch, J. M., Light scattering from binary solutions, J. Chem. Phys. **50,** No. 3, 1103–1108 (Feb. 1, 1969).

Newman, M., A diophantine equation, J. London Math. Soc. **43,** 105–107 (1968).

Newman, M., Some results on roots of unity, with an application to a diophantine problem, Aequat. Math. **2,** No. 2/3, 163–166 (Nov. 28, 1967).

O'Connell, J., An isospin sum rule for photonuclear reactions, Phys. Rev. Letters **22,** No. 24, 1314–1316 (June 16, 1969).

Peterson, R. L., Matarrese, L. M., Wells, J. S., Mathematical techniques for EPR analysis of $S = 5/2$ ions in C_2 symmetry. Application to FE^{3+} in quartz, Nat. Bur. Stand. (U. S.), Tech. Note 372, 23 pages (June 1969), 35 cents.

Pong, W., Photoemission from Al-Al_2O_3 films in the vacuum ultraviolet region, J. Appl. Phys. **40,** 1733–1739 (1969).

Powell, C. J., Analysis of optican- and inelastic-electron-scattering data. Parametric calculations, J. Opt. Soc. Am. **59,** No. 6, 738–743 (June 1969).

Powell, R. L., Clark, A. F., Fickett, F. R., Longitudinal magnetoresistance of pure copper, (Proc. Conf. Electron Mean Free Paths in Metals, Zurich, Switzerland. Sept. 3–5, 1968), Phys. kondens. Materie **9,** 104–112 (Lange and Springer, Berlin, West Germany, 1969).

Radziemski, L. J., Jr., Kaufman, V., Wavelengths, energy levels, and analysis of neutral atomic chlorine (Cl I), J. Opt. Soc. Am. **59,** No. 4, 424–443 (Apr. 1969).

Rains, T. C., Chemical aspects of atomic absorption, Am. Soc. Testing Mater. Spec. Tech. Publ. 443, 19–36 (1969).

Rains, T. C., Chemical interferences in condensed phase, Chapter 12 in Flame Emission and Atomic Absorption Spectometry, J. A. Dean and T. C. Rains, Eds., 1, 349–379 (Marcel Dekker Inc., New York, N. Y., June 1969).

Rebbert, R. E., Ausloos, P., The photolysis of methane at 584 Å, J. Am. Chem. Soc. **90,** 7370–7371 (1968).

Roach, F. E., Diffuse galactic light, Chapter in Modern Astrophysics: A Memorial to Otto Struve, M. Hack., Ed., pp. 49–66 (Gordon and Breach, New York, N. Y., 1967).

Robbins, R. F., Weitzel, D. H., An automated resilience apparatus for polymer studies from −196 to +180 °C, Rev. Sci. Instr. **40,** No. 8, 1014–1017 (Aug. 1969).

Rossmassler, S. A., Modification of dissemination channels for scientific information, J. Chem. Doc. **9,** No. 1, 17–19 (Feb. 1969).

Rubin, R. J., Transmission properties of an isotopically disordered one-dimensional harmonic crystal, J. Math. Phys. **9,** No. 12, 2252–2266 (Dec. 1968).

Santone, L. C., Application of systems analysis to urban problems, International City Management Association, The Municipal Yearbook, pp. 225–232 (1969).

Santoro, A., Mighell, A. D., Zocchi, M., Reimann, C. W., The crystal and molecular structure of hexakis (imidazole)Ni(II)-nitrate, Acta Cryst. **B25,** No. 3, 842 (Apr. 1969).

Scala, A. A., Ausloos, P., Gas-phase photolysis and radiolysis of cyclopropane, J. Chem. Phys. **49,** No. 5, 2282–2290 (Sept. 1,1968).

Schafer, G. E., Precision microwave measurements—today and tommorrow, Microwave J. **12,** No. 6, 25 (June 1969).

Scheer, M. D., Fine, J., The desorption kinetics of Cl^- and I^- on Mo and Ta as determined by the pulsed-beam method, (Proc. Sixth Intern. Symp. Rarefied Gas Dynamics, Cambridge, Mass., July 22–26, 1968), Chapter in The Measurement of Sticking Coefficients at High Temperatures Using the Isotopic Mixing Method II, 1469–1477 (Academic Press Inc., New York, N. Y., 1969).

Scheer, M. D., Fine, J., The electron affinity of lithium, J. Chem. Phys. **50,** No. 10, 4343–4347 (May 15, 1969).
Scheer, M. D., Fine, J., The reaction of carbon monoxide with a tantalum surface heated above °K, Surface Sci. **12,** 102–107 (1968).
Scheer, M. D., Klein, R., Low-temperature oxygen atom addition to olefins. III. Transition state and the reaction with *cis-* and *trans-*2–butenes, J. Phys. Chem. **73,** 597–601 (1969).
Seidel, G. P., Neutron radiation hardening of polycrystalline iron, Radiation Effects **1,** 177–190 (1969).
Shirk, J. S., Bass, A. M., Matrix-isolation spectra of discharge "sputtered" metals, J. Chem. Phys. **49,** No. 11, 5156–5160 (Dec. 1, 1968).
Shirley, J. H., Validity of the semiclassical approximation in maser theory, Phys. Rev. **181,** No. 2, 600–609 (May 10, 1969).
Simmons, J. D., Bass, A. M., Tilford, S. G., The fourth positive system of carbon monoxide observed in absorption at high resolution in the vacuum ultraviolet region, Astrophys. J. **155,** 345–358 (Jan. 1969).
Sitterly, C. M., Forbidden transitions in atoms: catalogs and identifications, Mem. Soc. Roy. Sci. Liege **V,** No. 16, 17–29 (1969).
Stromberg, R. R., Polymer adsorption on substrates (Proc. Symp. Interface conversion Polymer Coatings, General Motors Research Laboratories, Detroit, Mich., Oct. 1967), Chapter in Interface Conversion for Polymer Coatings, P. Weiss and G. D. Cheever, Eds., pp. 321–337 (American Elsevier Publ. Co., Inc., New York, N. Y. 1969).
Swartzendruber, L. J., Variable temperature Mössbauer effect spectrometer with provision for longitudinal external fields, Nucl. Instr. Methods **69,** 101–105 (1969).
Tate, E. L., Variations on a theme: government and library cooperation, D. C. Libraries **39,** No. 3, 53–55 (1968).
Tipson, R. S., Cohen, A., Reaction of some sulfonic esters of D-mannitol with methoxide; synthesis of 2,3:4,5-dianydro-D-iditol, Carbohydrate Res. **7,** 232–243 (1968).
Tipson, R. S., West, B. F., Brady, R. F., Acid-catalyzed hydrolysis of isopropylidene acetals of some 2-pentuloses and 2-hexuloses, Carbohydrate Res. **10,** 181–183 (1969).
Tsang, T., Self-consistent correlation function approximation in ising ferromagnets, Physica **42,** 1–11 (1969).
Tsang, T., Farrar, T. C., Nuclear magnetic relaxation studies of internal rotations and phase transitions in borohydrides of lithium, sodium, and potassium, J. Chem. Phys. **50,** No. 8, 3498–3502 (Apr. 15, 1969).
Tsang, W., Thermal decomposition of 3,4-dimethylpentene-1, 2, 3, 3-trimethylpentane, 3, 3-dimethylpentane, and isobutylbenzene in a single pulse shock tube, Intern. J. Chem. Kinetics **1,** 245–278 (1969).
Verdier, P. H., A simulation model for the study of the motion of randomcoil polymer chains, J. Computational Phys. **4,** No. 2, 204–210 (1969).
Vincentini-Missoni, M., Levelt Sengers, J. M. H., Green, M. S., Thermodynamic anomalies of CO_2, Xe, and He^4 in the critical region, Phys. Rev. Letters **22,** No. 9, 389–393 (Mar. 3, 1969).
Wacker, P. F., Cord, M. S., Burkhard, D. G., Petersen, J. D., Kukol, R. F., Microwave spectral tables. Polyatomic molecules with internal rotation, Nat. Bur. Stand. (U.S.), Mono. 70, Volume III, 275 pages (June 1969), $4.25.
Waterstrat, R. M., Crystal structure transformations in VPt produced by plastic deformation at room temperature, Trans. Met. Soc. AIME **245,** 1360–1361 (June 1969).
Weir, C. E., Piermarini, G. J., Block, S., Single crystal x-ray diffraction at high pressure, Proc. American Crystallographic Association High Pressure X-ray Diffraction Symposium, Seattle, Washington, Mar. 23–29, 1969, 5, 105–111 (1969).
Weisman, I. D., Bennett, L. H., Quadrupolar echoes in solids, Phys. Rev. **181,** No. 3, 1341–1350 (May 15, 1969).
Wolcott, N. M., Falge, R. L., Bennett, L. H., Magnetic behavior of intermetallic compounds of beryllium, J. Appl. Phys. **40,** No. 3, 1377–1378 (Mar. 1, 1969).
Woo, S. B., Branscomb, L. M., Beaty, E. C., Sunlight photodetachment rate of ground state O_2^-, J. Geophys. Res. Space Physics **74,** No. 11, 2933–2940 (June 1, 1969).

** Publications for which a price is indicated are available by purchase from the Superintendent of Documents, U.S. Government Printing Office, Washington, D.C. 20402 (foreign postage, one-fourth additional). The NBS non-periodical series are also available from the Clearinghouse for Federal Scientific and Technical Information, Springfield, Va. 22151. Reprints from outside journals and the NBS Journal of Research may often be obtained directly from the authors.*

☆ U.S. GOVERNMENT PRINTING OFFICE: 1970 O—388-122

SURC JUNE 46129
UNIVERSITY MICROFILMS INC
SERIALS SECTION
300 NORTH ZEEB ROAD
ANN ARBOR MICHIGAN 48106

UNITED STAT
GOVERNMENT PRINTING OFFICE
DIVISION OF PUBLIC DOCUMENTS
WASHINGTON, D.C. 20402

OFFICIAL BUSINESS

PENALTY FOR PRIVATE USE $300

POSTAGE AND FEES PAID
U.S. GOVERNMENT PRINTING OFFICE

JOURNAL OF RESEARCH of the National Bureau of Standards
C. Engineering and Instrumentation

Vol. 74C, Nos. 1 and 2 Jan.–June 1970

Page

Production of near-perfect interferograms of variable visibility. J. B. Saunders. 1

Locked nuclear quadrupole resonance spectrometer for pressure measurements. Ronald C. Frisch and David L. VanderHart. 3

Precise continuous optical attenuator. G. Ruffino. 9

An A–C resistance thermometer bridge. Robert D. Cutkosky. 15

On the flow induced by a Maxwell-Chartoff rheometer. Elliot A. Kearsley. 19

Mechanical compliance measurements of single-edge-notch tension specimens. Mary Jane Orloski. 21

Effect of notch geometry and temperature on the creep-rupture behavior of a titanium alloy. William D. Jenkins and William A. Willard. 29

Publications of the National Bureau of Standards. 41

Library of Congress Catalog Number: 62–3900

For sale by the Superintendent of Documents, U.S. Government Printing Office, Washington, D.C. 20402. (Order by SD Catalog No. C 13.22/sec. C:74/1&2. Price $1.25 (single copy). Subscription price: $5.00 a year; $1.25 additional for foreign mailing.
UNITED STATES GOVERNMENT PRINTING OFFICE, WASHINGTON: 1970